

This is the peer reviewed version of the following article:

Destabilizers of the thymidylate synthase homodimer accelerate its proteasomal degradation and inhibit cancer growth / Costantino, Luca; Ferrari, Stefania; Santucci, Matteo; MH Salo-Ahen, Outi; Carosati, Emanuele; Franchini, Silvia; Lauriola, Angela; Pozzi, Cecilia; Trande, Matteo; Gozzi, Gaia; Saxena, Puneet; Cannazza, Giuseppe; Losi, Lorena; Cardinale, Daniela; Venturelli, Alberto; Quotadamo, Antonio; Linciano, Pasquale; Tagliazucchi, Lorenzo; Moschella, Maria Gaetana; Guerrini, Remo; Pacifico, Salvatore; Luciani, Rosaria; Genovese, Filippo; Henrich, Stefan; Alboni, Silvia; Santarem, Nuno; Cordeiro Da Silva, Anabela; Giovannetti, Elisa; J Peters, Godefridus; Pinton, Paolo; Rimessi, Alessandro; Cruciani, Gabriele; M Stroud, Robert; C Wade, Rebecca; Mangani, Stefano; Marverti, Gaetano; D'Arca, Domenico; Ponterini, Glauco; Costi, Maria Paola. - In: ELIFE. - ISSN 2050-084X. - 11:(2022), pp. 1-104. [10.7554/eLife.73862]

Terms of use:

The terms and conditions for the reuse of this version of the manuscript are specified in the publishing policy. For all terms of use and more information see the publisher's website.

19/12/2025 07:11

Destabilizers of the thymidylate synthase homodimer accelerate its proteasomal degradation and inhibit cancer growth.

Authors: Luca Costantino^{1‡}, Stefania Ferrari^{1‡}, Matteo Santucci^{1‡}, Outi M. H. Salo-Ahen^{3&}, Emanuele Carosati^{4,x}, Silvia Franchini¹, Angela Lauriola^{2±}, Cecilia Pozzi⁵, Matteo Trande^{1±}, Gaia Gozzi¹, Puneet Saxena^{1#}, Giuseppe Cannazza¹, Lorena Losi¹, Daniela Cardinale⁶, Alberto Venturelli¹, Antonio Quotadamo¹, Pasquale Linciano¹, Lorenzo Tagliazucchi¹, Maria Gaetana Moschella¹, Remo Guerrini⁷, Salvatore Pacifico⁷, Rosaria Luciani¹, Filippo Genovese¹, Stefan Henrich³, Silvia Alboni¹, Nuno Santarem⁸, Anabela da Silva Cordeiro^{8,9}, Elisa Giovannetti^{10,11}, Godefridus J Peters^{10^}, Paolo Pinton¹², Alessandro Rimessi¹², Gabriele Cruciani⁴, Robert M. Stroud^{13,†}, Rebecca C. Wade^{3,14,15,†}, Stefano Mangani^{5†}, Gaetano Marverti², Domenico D'Arca^{2*}, Glauco Ponterini^{1*} & Maria Paola Costi^{1*}.

Affiliations:

¹ Department of Life Sciences, University of Modena and Reggio Emilia, 41125 Modena, Italy.

² Department of Biomedical, Metabolic and Neural Sciences, University of Modena and Reggio Emilia, 41125 Modena, Italy.

³ Molecular and Cellular Modeling Group, Heidelberg Institute for Theoretical Studies, 69118 Heidelberg, Germany.

⁴ Department of Chemistry, Biology and Biotechnology, University of Perugia, 06123, Perugia, Italy.

⁵ Department of Biotechnology, Chemistry and Pharmacy, University of Siena, 53100 Siena, Italy.

25 ⁶ Respiratory, Critical Care & Anesthesia UCL Great Ormond Street Institute of Child Health
 26 London, U.K.

27 ⁷ Department of Chemical and Pharmaceutical Science, University of Ferrara, 41121 Ferrara,
 28 Italy.

29 ⁸ IBMC I3S, 4200-135 Porto, Portugal.

30 ⁹ Department of Biological Sciences, Faculty of Pharmacy, University of Porto, Portugal

31 ¹⁰ Department of Medical Oncology, Amsterdam University Medical Center, Cancer Center
 32 Amsterdam, 1081HV, Vrije Universiteit Amsterdam, The Netherlands.

33 ¹¹ CancerPharmacology Lab, Fondazione Pisana per la Scienza, 56017 Pisa, Italy.

34 ¹² Dept. of Medical Sciences and Laboratory for Technologies of Advanced Therapies (LTTA),
 35 University of Ferrara, 44121 Ferrara, Italy.

36 ¹³ Biochemistry and Biophysics Department, University of California San Francisco, San
 37 Francisco, CA 94158, USA.

38 ¹⁴ Interdisciplinary Center for Scientific Computing (IWR), Heidelberg University, 69120
 39 Heidelberg, Germany.

40 ¹⁵ Center for Molecular Biology (ZMBH), DKFZ-ZMBH Alliance, Heidelberg University, 69120
 41 Heidelberg, Germany.

42

43 [&]current address: Pharmaceutical Sciences Laboratory/Structural Bioinformatics Laboratory,
 44 Faculty of Science and Engineering, Pharmacy/Biochemistry, ÅboAkademi University,
 45 Tykistökatu 6A, FIN-20520 Turku, Finland.

46 ^x Current address: AbocaS.p.A, loc. Aboca, 52037, Sansepolcro (AR), Italy.

47 [±]current address: Department of Biotechnology, University of Verona, 37134 Verona.

[#]current address: Excelra Knowledge Solutions, Plot No. 79, IDA Mallapur, Nacharam,
Hyderabad-500076 India.

[^] second affiliation Department of Biochemistry, Medical University of Gdansk, Gdansk, Poland

^{*} To whom correspondence should be addressed: Maria Paola Costi,
mariapaola.costi@unimore.it,

Glauco Ponterini, glauco.ponterini@unimore.it, Domenico D'Arca domenico.darca@unimore.it.

[†]These authors contributed equally to this work as senior authors.

[‡] These authors contributed equally to this work as first authors.

Abstract: Drugs that target human thymidylate synthase (hTS), a dimeric enzyme, are widely used in anti-cancer therapy. However, treatment with classical substrate-site-directed TS inhibitors induces over-expression of this protein and development of drug resistance. We thus pursued an alternative strategy that led us to the discovery of TS-dimer destabilizers. These compounds bind at the monomer-monomer interface and shift the dimerization equilibrium of both the recombinant and the intracellular protein toward the inactive monomers. A structural, spectroscopic, and kinetic investigation has provided evidence and quantitative information on the effects of the interaction of these small molecules with hTS. Focusing on the best among them, **E7**, we have shown that it inhibits hTS in cancer cells and accelerates its proteasomal degradation, thus causing a decrease in the enzyme intracellular level. **E7** also showed a superior anticancer profile to fluorouracil in a mouse model of human pancreatic and ovarian cancer. Thus, over sixty years after the discovery of the first TS prodrug inhibitor, fluorouracil, **E7** breaks the link between TS inhibition and enhanced expression in response, providing a strategy to fight drug-resistant cancers.

Introduction

Small molecule able to bind at specific pockets of the monomer/monomer interface of a dimeric protein may perturb the dimeric assembly to the limit of disrupting it, and thus alter metabolic pathways associated with the cellular functions of the monomeric and dimeric protein forms (Taddia et al., 2015). Such a drastic structural change of the protein may open the way to unexpected events, such as a higher liability to intracellular degradation of the protein monomers relative to the dimers.

Human thymidylate synthase (hTS) is an obligate, stable homodimer ($K_d = 80$ nM (Genovese et al., 2010)) with two active sites, each including residues from both monomers (Costi et al., 2005). As a dimeric enzyme, it provides the sole *de-novo* pathway to deoxythymidylate (dTMP) synthesis in human cells by catalyzing the reductive methylation of deoxyuridylate (dUMP) to dTMP using methylenetetrahydrofolate (mTHF) as the one-carbon methyl donor (Costi et al., 2005; Carreras and Santi, 1995). By interacting with its own and other mRNAs, this protein regulates its own levels and those of other proteins involved in apoptotic processes, including bcl2, c-myc, and p53 (Brunn et al., 2014; Jennings and Willis, 2015). Its inhibition is usually achieved with compounds that bind at the protein active-site, competing either with the dUMP substrate, such as 5-fluorodeoxyuridine 5'-monophosphate (FdUMP), or with the folate cofactor, such as raltitrexed (RTX) and pemetrexed (PMX) (Carreras and Santi, 1995; Jennings and Willis, 2015) (Figure 1A,B). However, these drugs induce cells to develop drug resistance

94 associated with increased hTS levels which eventually leads to therapy failure (Peters, 2018). A
95 drastic change of strategy, based on the design of new compounds with different mechanisms of
96 action, is thus necessary (Voeller et al., 2002; Cardinale et al., 2011). Here we report the
97 discovery of molecules that bind at the hTS monomer/monomer interface and, despite their small
98 size, markedly shift the monomer-dimer equilibrium of the enzyme towards the inactive
99 monomeric form. Acting as destabilizers of the hTS dimer, they not only inhibit the activity of
100 this obligate homodimeric enzyme but also favor its intracellular degradation and, hence,
101 decrease its level.

102 Using a tethering approach in which sulfhydryl-containing fragments were initially identified by
103 reaction with cysteine residues inserted by mutation around the target site, we identified
104 fragments anchored by disulfide bond formation at the interfacial mutant cysteine residues. We
105 then employed molecular modeling and medicinal chemistry to modify the fragments and
106 develop inhibitors able to bind WT hTS guided solely by their affinities for the interface region.
107 For these small molecules, we have developed a model able to quantitatively account both for the
108 dissociation of the hTS dimer, observed spectroscopically, and for the corresponding activity
109 inhibition. We have also shown that their ability to induce the TS-dimer dissociation in cells lies
110 below their efficacy in inhibiting growth of colon, ovarian and pancreatic cancer cells. One of
111 our hTS-dimer destabilizers, compound **E7**, induced apoptosis in cancer cells and a decrease of
112 hTS levels due to enhanced proteasomal degradation of the enzyme monomers with respect to
113 the dimers. Remarkably, in a mouse model of orthotopic pancreatic cancer, this dimer disrupter
114 caused a higher reduction of cancer growth and had lower toxicity than 5-fluorouracil (**5-FU**),
115 the prodrug of 5-FdUMP. Like what we observed *in vitro*, the molecular analysis of exported
116 treated cancer tissues demonstrated decreased hTS protein and mRNA levels. These findings

establish **E7** as a new lead with an hTS dimer-disruptive ability and link the dimer-to-monomer equilibrium shift of this protein to its faster intracellular degradation.

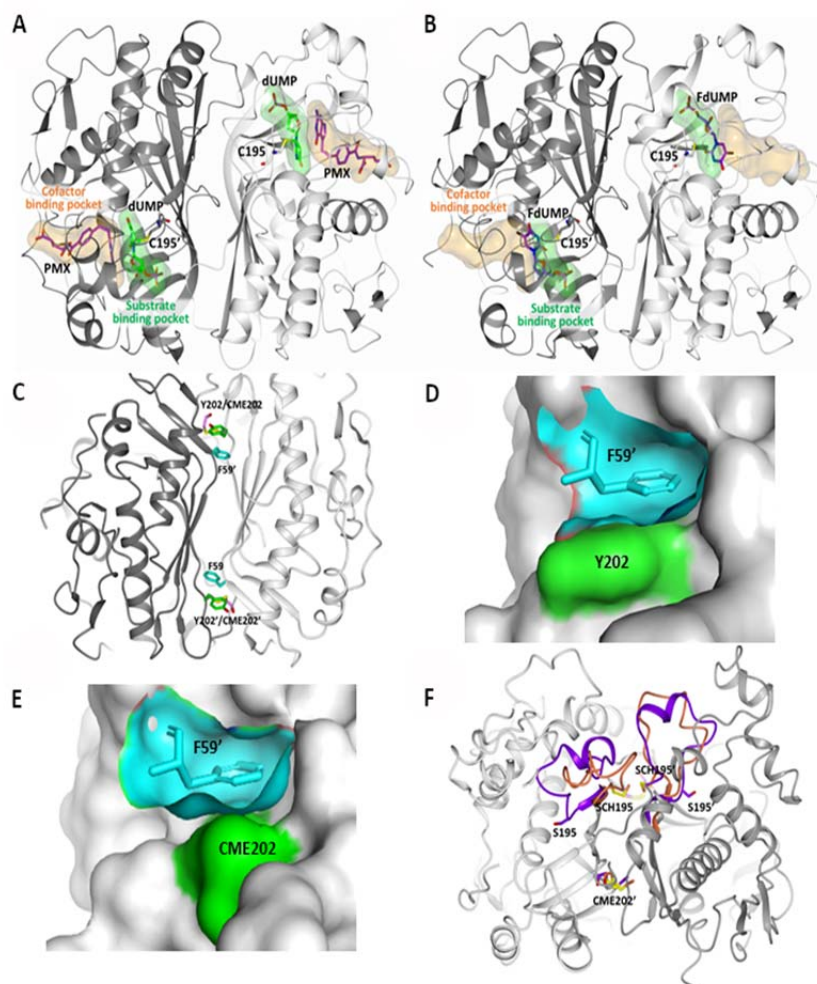


Figure 1. Drug target sites on hTS: the active-site (A,B) and the Y202 pocket (C-F). Drugs that are directed to the active site of hTS can mimic either the cofactor MTHF or the substrate dUMP and bind in their binding pockets. **A**, hTS (in cartoon with the A and B subunits colored white and grey, respectively) inhibited by the cofactor analogue pemetrexed (PMX, in sticks, purple carbons), which occupies the cofactor binding pocket by establishing a π - π interaction

with the dUMP substrate (in sticks, green carbons) (PDB ID: 1JU6). The substrate and cofactor binding sites are represented as green and orange surfaces, respectively. The catalytic cysteine, C195, is highlighted in sticks. **B**, The substrate analogue 5-fluoro-2'-deoxyuridine monophosphate (**FdUMP**) (in sticks, purple carbons) binds inside the catalytic cavity, mainly filling the substrate binding pocket (PDB ID: 3H9K, hTS variant R163K). **C**, Location of F59, Y202 and CME202 residues at the hTS dimer interface by superimposition of native hTS and hTS-C195S-Y202C double mutant structures (CME: S,S(2-hydroxyethyl)cysteine; PDB-ID: 3N5G, 4O1X). **D**, Surface of the Y202 pocket (cyan) filled by F59' from the opposite monomer (cyan sticks). The surface of Y202 is highlighted in green (PDB-ID: 3N5G). **E**, Surface of the C202 pocket (cyan) filled by F59' from the opposite monomer (cyan sticks) in the C195S-Y202C double mutant (PDB-ID: 4O1X). The surface of C202 (oxidized as CME) is highlighted in green. **F**, Superimposition of the hTS-C195S-Y202C and hTS-Y202C crystal structures with the catalytic loop in hTS-Y202C (inactive conformation, in orange) and in hTS-C195S-Y202C (active conformation, in violet); notice the different orientations of the catalytic residue couples S195/SCH195 and S195'/SCH195' (PDB-ID: 4O1X, 4O1U) (SCH: S-methyl-thio-cysteine). The one-letter code is used for the standard amino-acids, while for the chemically modified amino-acid, a conventional 3-letter code is used as described above.

Results

Choice of the ligand binding-site on the target protein surface.

To target the monomer-monomer interface and dissociate the hTS dimer, we applied the 'cysteine tethering' approach to fragment-based drug design (Erlanson et al., 2000). We investigated the crystal structures of the active and inactive hTS (PDB-IDs 1HVV and 1YPV,

respectively) and carried out molecular dynamics (MD) simulations of the monomeric and dimeric forms of the enzyme to explore the monomer-monomer interface of homodimeric hTS and identify targetable binding pockets and residues suitable to be mutated to cysteine for the tethering experiments (*Supplementary file 1*). We selected the ‘Y202 pocket’, which accommodates the side-chain of F59’ from the other monomer, as the most promising region to target (Figure 1C-F, Figure 2A-B, *Figure 1-figure supplement*) (Salo-Ahen et al., 2015).

In *Figure 1-figure supplement 1* in panel a-d shows Y202 and K47 pockets at the hTS monomer-monomer interface (PDB ID: 1HVV, A chain) are represented. **a**, Surface presentation of the hTS monomer, with residue F59’ (in orange, shown as sticks) from the opposite monomer binding in the Y202 pocket (PDB ID: 1HVV, chain A). Crystallographic water molecules found in the Y202 pocket region are shown as red spheres. **b**, Cartoon representation of the hTS monomer with F59’ (in orange, shown as sticks) from the opposite monomer binding in the Y202 pocket (PDB ID: 1HVV, chain A). Residues forming the Y202 pocket are shown in sticks. Atom colour code: carbon – grey/orange; nitrogen – blue; oxygen – red. **c**, Surface representation of the K47 pocket region in the hTS monomer (PDB ID: 1HVV, chain A), with residue Y202’ (in orange, shown as sticks) from the opposite monomer, binding in the K47 subpocket K47b (green) adjacent to the K47a subpocket (pink). **d**, Cartoon and sticks presentation of the K47 pocket region in the hTS monomer with residue Y202 (in orange, shown as sticks) from the opposite monomer, binding in the K47b subpocket (PDB ID: 1HVV, chain A). Residues K47, S57 and D254 form a dividing wall that is part of both sub-pockets K47a (pink) and K47b (green), (see also Table S1). Atom color code: carbon – grey/orange/green/pink; nitrogen – blue; oxygen – red.

This pocket lies in the perimeter space of the intermonomer interface and is accessible in the dimeric form of the protein. It is large enough (22 \AA^3) to accommodate a phenyl group and has several smaller crevices around it. During the MD simulations of monomeric hTS, the sidechain of Y202 moved away leaving a larger pocket and behaving like a gate. We therefore made the Y202C mutant and screened for compounds able to form a covalent disulfide bond with C202 from a library of organic disulfides. We also mutated the active site cysteine to serine to prevent

the selection of compounds that bound at the active site (C195S). We made mutants with single point mutations at C195S and Y202C to test their functional and structural properties (*Supplementary file 1, Figure 1-figure supplement 1*) as well as the double mutant, hTS C195S-Y202C. This was used for the ligand selection according to the above-described tethering approach. As expected from removal of the catalytic C195 residue, this double mutant was inactive, but X-ray crystallography showed that it takes the active conformation of hTS (*Figure 1F, Figure 2-figure supplement 1, Supplementary file 2A,B*).

Figure 2-figure supplement 1 shows the X-ray crystallographic structure of hTS-Y202C and hTS C195S-Y202C. **a-c**, Unbiased omit map (blue wired map contoured at 3.0 σ), showing the S,S(2-hydroxyethyl)cysteine (CME) chemical modification occurring at the mutated residue C202 (panel **a**), and the mutated residue S195 (panel **b**) in the hTS double mutant C195S-Y202C. Panel **c** reports the omit map (contoured at 3.0 σ) showing the S,S(2-hydroxyethyl)cysteine (CME) chemical modification occurring at the mutated residue C202 in the single hTS Y202C mutant. The mutated serine and the CME residues are represented as sticks. The hTS C195S-Y202C structure is drawn in violet whereas the single mutant structure is coloured in orange (cartoon representation). **d-e**, H-bond interactions (represented as dashed lines) involving the CME202 residue in hTS Y202C subunits A (panel **d**) and B (panel **e**). Interacting residues are represented as sticks and water molecules as red spheres. Residues belonging to the A subunit are coloured in yellow while those of the B subunit are coloured in orange. **f-g**, two views of the surface of the hTS Y202C dimer. The two symmetry-related subunits are shown in violet (subunit A) and orange (subunit B), while the CME and S-methyl-thio-cysteine (SCH) residues are represented as spheres. Only SCH43 (panel **f**), appears fully solvent accessible, with CME202, partially visible in its pocket, just below SCH43. Panel **g**, shows that SCH180 is partially solvent accessible, while SCH195, CME199 and C210 are buried to different extents below the hTS surface. **h-j**, surface representations showing the solvent accessibility of C180 residues in wt hTS and hTS double mutant (C195S-Y202C). The protein is shown in a transparent surface and the C180-C180' residues from two facing subunits are represented by labeled blue-violet spheres. **h**, wt hTS dimer in inactive conformation (PDB ID: 3N5G); **i**, wt hTS in active conformation (PDB ID: 2RDA); **j**, C195S-Y202C hTS mutant in active conformation (PDB ID: 4O1X). PISA server analysis indicates that C180-C180' are buried in all three structures. However, as it can be appreciated by comparing the three figures, the active conformation increases

the shielding of the facing C180-C180' residues from solvent as their buried surface goes from about 30 Å² (**h**) to 50-68 Å² (**i-j**). Also, the crevice between subunits is much larger in inactive vs. active conformation (from about 15 x 6 Å in inactive to about 5 x 5 Å in active conformation).

We employed the C195S-Y202C double mutant to capture compounds that, driven by some affinity for the region near residue 202, formed a covalent disulfide with C202 *Supplementary file 3A*. These compounds were selected by their stability towards reduction by β-mercaptoethanol (BME), and the C202-S-S-small-compound disulfides formed were identified by two mass spectrometric (MS) experiments, MALDI-TOF and ESI-QTOF (*Supplementary file 3B,C*).

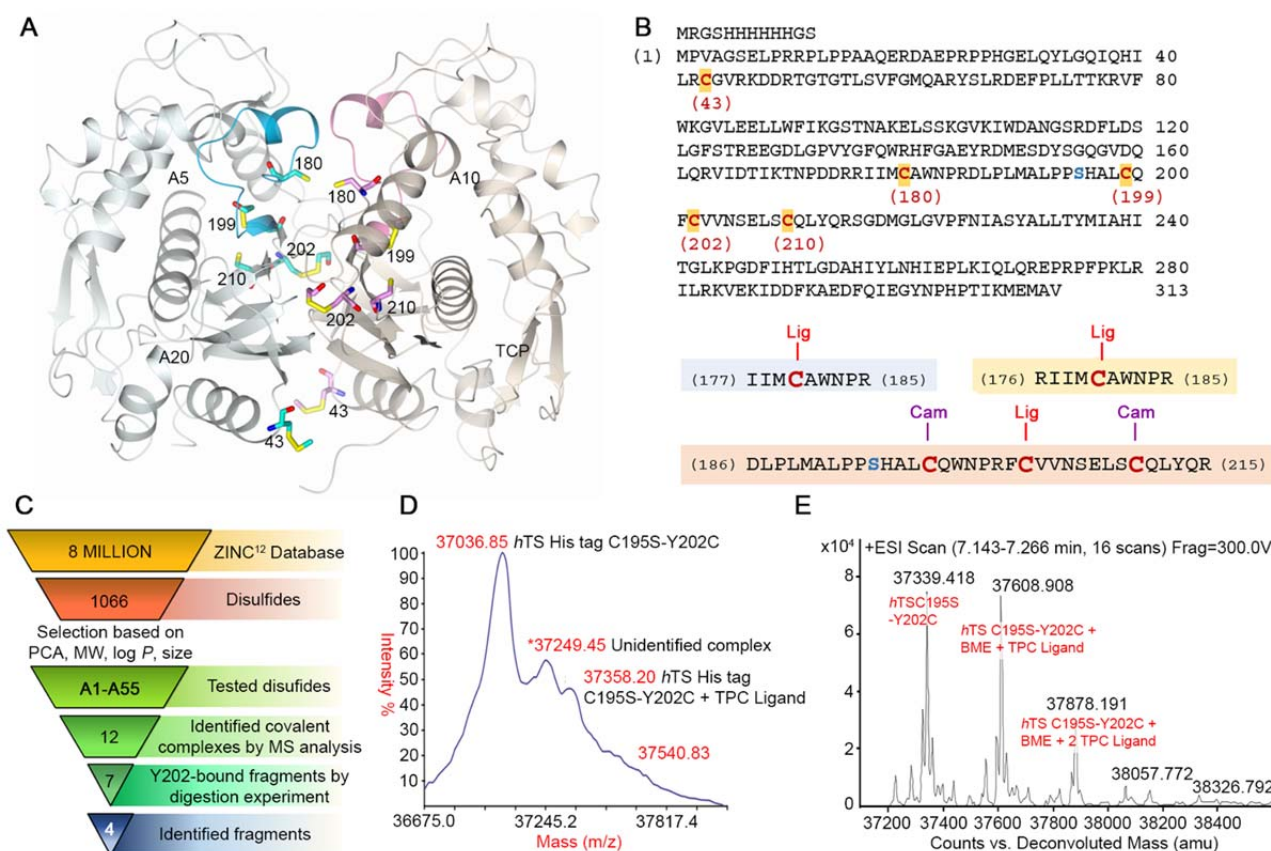


Figure 2. Disulfide library design and screening on the hTS C195S-Y202C variant.

A, Crystal structure of the hTS C195S-Y202C dimer (in the cartoon, the A and B subunits are colored pale blue and grey, respectively; the catalytic loops, in active conformation, are highlighted in cyan and pink, respectively) showing the positions of the cysteine residues (in sticks, carbon atoms are colored cyan and pink in subunits A and B, respectively. Compounds **A5**, **A10**, **A20** and the reference compound N-tosyl-D-prolinecysteamine (**TPC**) (Appendix 2-figure 1) were selected through the tethering experiments. They are indicated close to the peptide sequence found in the mass spectrometry identification process (*Supplementary file 3B,C*). Their chemical structures are reported in *Supplementary file 3A*. **B**, Sequence of the hTS C195S-Y202C variant and cysteine-containing peptides generated by trypsin digestion. Cysteine residues are displayed in red (the residue number is reported below each cysteine) and the mutated S195 (the catalytic residue) in blue. Three cysteine-containing peptides were generated by proteolytic cleavage of the hTS C195S-Y202C variant: peptide I177-R185 and peptide R176-R185 containing C180 and peptide D186-R215, containing C199, C202 and C210. Ligand (Lig)-bound cysteines and those alkylated as carbamidomethyl (Cam)-cysteines are displayed. **C**, Screening cascade from the 6 million compounds from the ZINC database (Irwin and Shoichet, 2005) to the final 4 fragments expected to bind in the Y202 pocket. **D**, **E**, Representative MS spectra in the hTS-binding evaluation step. Maldi (**D**) and ESI (**E**) MS spectra for the reference compound **TPC** (Erlanson et al., 2000). The three labeled peaks are due to hTS C195S-Y202C and to the protein bound to BME and one and two molecules of TPC.

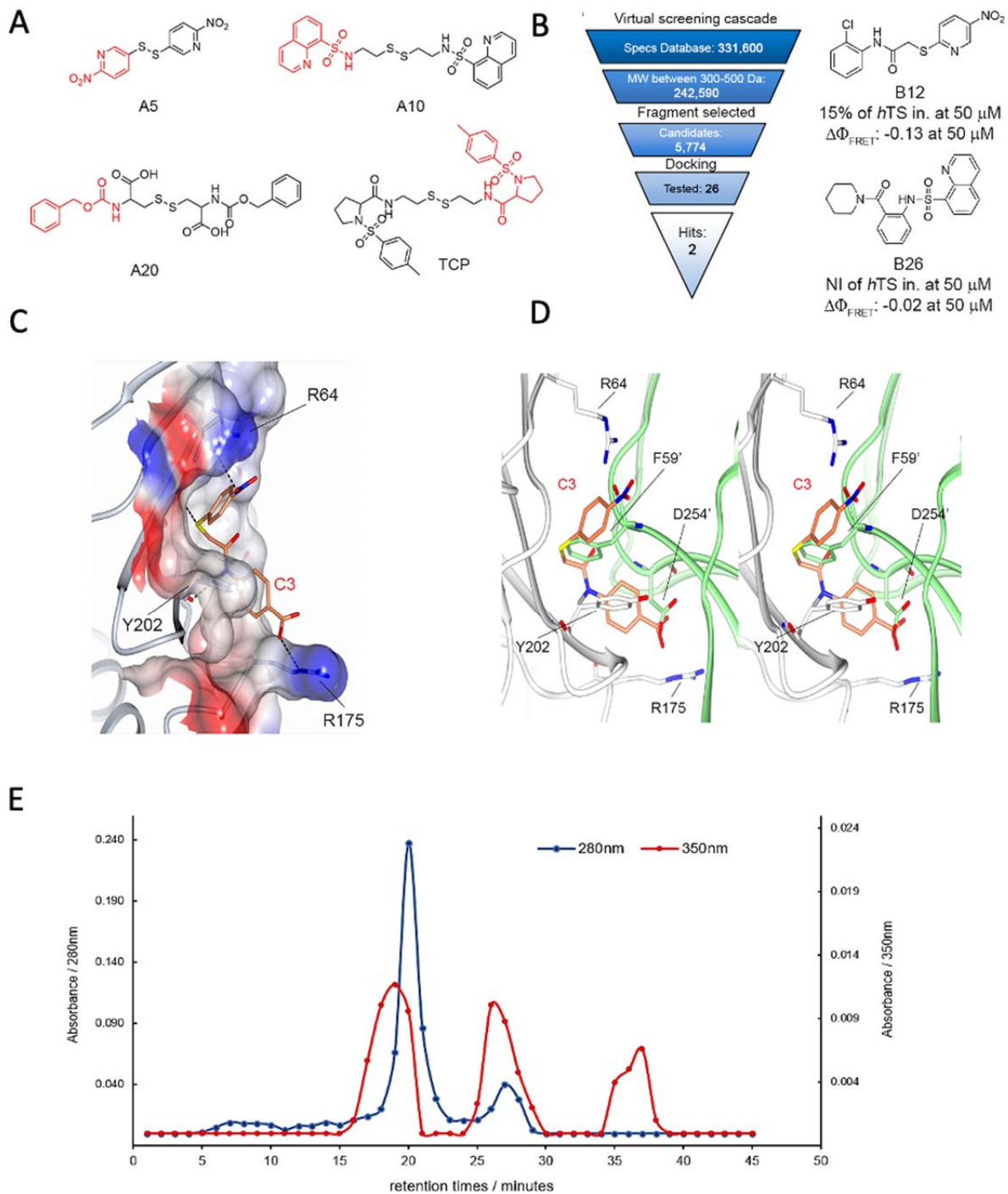
Mass-spectrometric ligand selection.

238 To identify molecules able to covalently bind near Y202, we designed a library of commercially
239 available compounds from the ZINC database (Irwin and Shoichet, 2005) (Figure 2C). We first
240 selected 1066 disulfide compounds that were either symmetric (RSSR) or asymmetric (R_1SSR_2)
241 and had drug-like or fragment-like properties. 1066 molecules were screened for their molecular
242 properties (PCA, MW, logP, size) and 55 were evaluated with the MS techniques. Thirteen out
243 of the 55 compounds were found to bind the protein according to the results of both MS
244 techniques (Figures 2D, 2E, *Appendix 1, Supplementary file 3A,B,C*). Among them, 7
245 compounds, **A5**, **A6**, **A10**, **A15**, **A20**, **A38** and **TPC**, were selected based on the feasibility of
246 their chemical modification and were further analyzed by a bottom-up MALDI-TOF and ESI-
247 QTOF MS proteomic analysis to identify the cysteine residues they had bound (*Supplementary*
248 *file 3C*). The 7 compounds bound either peptides (I177-R185) IIMCAWNPR (sequence A) or
249 (R176-R185) RIIMCAWNPR (sequence B), both containing the C180 residue of the digested
250 protein (*Supplementary file 3C*). Four molecules, **A5**, **A10**, **A20** and **TPC** also bound peptide
251 (D186-R215) DLPLMALPPSHALCQFCVVNSELSCLYQR (sequence C) (*Supplementary file*
252 *3C*), containing the engineered Y202C together with the native C199 and C210. In agreement
253 with the described computational and crystallographic data (see above), Y202C is the most
254 exposed of these three cysteines and is thus easily available for disulfide-bond formation with the
255 RS fragments, being therefore suitable for tethering experiments. Other reasons to select the
256 Y202 pocket are that Y202 is not predicted to be part of the mRNA binding region and has the
257 capability to interact with various functional groups. Hence, despite the difficulties in the
258 identification of the precise cysteine to which the fragments could bind, all the above arguments
259 support the choice of the Y202 pocket at the hTS interface as a suitable binding site for further

260 structure-based studies. Therefore, we considered the fragments **A5**, **A10**, **A20** and **TPC** for
261 further medicinal chemistry modifications (Figure 3A).

262

263



264

265

266

267 **Figure 3. From hits to dimer-destabilizing compounds.** **A**, Structures of the compounds
268 identified in MS studies (in red the fragments used for the virtual screening approach to the
269 design of the compound library without the disulfide bonds). **B**, Virtual screening cascade and
270 chemical structures of the identified compounds, **B12** and **B26**. **C**, Detail of the binding mode of
271 compound **C3** (orange sticks) with the hTS interface residues R64, Y202 and R175 (positive and
272 negative potential regions are colored in blue and red, respectively) obtained with docking
273 methods. **D**, Stereo view of the superimposition of the calculated binding mode of **C3** onto the
274 first monomer (white cartoon) with the opposite monomer overlapping (lime cartoon). Atom
275 color code: nitrogen – blue; oxygen – red; sulphur – yellow. **E**, Results of anion exchange
276 chromatography showing co-elution experiments of **C3** with hTS dimer and monomer through
277 anion exchange chromatography. Absorbances at 280 (blue) and 350 nm (red) of
278 chromatographic fractions obtained by loading a 50 μ M hTS and 4 μ M **C3** solution on an anion-
279 exchange AEX HiPrep Q HP 16/10mm column. (*Figure 3-figure supplement 1, Figure 3-figure*
280 *supplement 1-Source data 1*).

281 *Figure 3-figure supplement 1* reports the anion-exchange chromatograms obtained with a 280 nm detection (blue
282 traces) by loading on an AEX HiPrep Q HP 16/10mm, Cytiva, column. **A**: hTS 300 μ L, 50 μ M. **B** hTS + 250 μ M
283 dUMP and RTX. **C**: hTS +4 μ M **C3**. **D**: hTS +40 μ M **C3**. **E**: hTS + 80 μ M **C3**. Green traces: NaCl gradient (% of
284 buffer 'B'), red traces: conductivity (mS/cm). The insets are the UV-Vis spectra of the indicated species.

285

286 **From low-affinity compounds to TS homodimer destabilizers.**

Starting from the four fragments identified by tethering/MS (**TPC**, **A5**, **A10**, **A20**) (Figure 3A), we performed an analogue search that yielded a dataset of 331,600 commercially available compounds (Specs dataset, www.specs.net) potentially able to bind non-covalently at the Y202 pocket of the monomer/monomer interface. The initial dataset was progressively reduced to 5,774 candidates using MW, structural and chemical criteria (Figure 3B). These were then docked into the Y202 pocket with the software FLAP (Cross et al., 2010) using a receptor-based pharmacophore model built from the X-ray crystal structure of hTS (PDB: 1HVV). A final set of 26 molecules (**B1-B26**, *Supplementary file 4A*) was selected to be tested for their ability to inhibit recombinant hTS and destabilize its dimeric form using, respectively, a kinetic and a spectroscopic, FRET (Förster resonance energy transfer)-based assays (Ponterini et al., 2016). For the FRET-based assay (Genovese et al., 2010), we conjugate one protein monomer with red-emitting tetramethylrhodamine (T) and the other with green-emitting fluorescein (F). Only when the monomers are close to each other, i.e., combined to form a dimer, F-to-T excitation energy transfer occurs, a FRET signal is detected, and its efficiency determined. We can thus investigate the dimer/monomer equilibrium of hTS, characterize it by the corresponding dissociation equilibrium constant and evaluate the effect of a tested compound thereupon.

Among the 26 compounds selected by VS, **B12** and **B26** (Figure 3B, *Supplementary file 4A*), caused low but reproducible decreases in the efficiency of FRET ($\Delta\Phi_{\text{FRET}} = -0.13$ and $\Delta\Phi_{\text{FRET}} = -0.02$, respectively), thus indicating some ability to perturb the enzyme dimeric assembly. In the docked poses, interactions were established by **B12** with Y202 through the *o*-chloro-phenyl ring and with R175 through the *p*-nitro-pyridyl ring, and by **B26** with Y202 through the piperidin-1-yl ring and with R175 through the quinoline ring (Figure 3C, D).

Next, we designed and synthesized 4 sets of compounds (**C-F**) (*Supplementary file 4*) to develop **B26** into biologically active compounds that exhibited the ability to both disrupt the dimer and inhibit recombinant hTS (*Appendix 2-figure 2-7*). The most relevant compounds were **C2**, **C3** (Figure 3), **C4**, **E5**, **E6** and **E7** (*Supplementary file 4B-E*). The former three, differing only for the position of the carboxylic group on the phenyl ring, featured IC₅₀ values between 5.25 μM and 246 μM (*Supplementary file 4*) and were selected for a quantitative mechanistic analysis of FRET and inhibition data with recombinant hTS (see the next paragraph). It was however compounds **E5**, **E6** and **E7** that proved to be the most interesting to continue our study. They featured IC₅₀ values against recombinant hTS of 40, 10 and 7 μM respectively, and decreased FRET efficiency by -0.24 at 50μM (**E5**, **E6**) and -0.1 at 10 μM (**E7**, *Supplementary file 4*). Compound **E7**, that was the most active on cells, was determined to be a racemic mixture of two enantiomers that equilibrated with a half-life of 56 min (*Appendix 3, Appendix 3-figure 1, Appendix 3-figure 2*).

Appendix 3-Figure 1 shows the 2D structure of the **E7** enantiomers.

Additional evidence of the ability of compounds **C3** and **E5** to bind hTS and destabilize its dimers was provided by anion-exchange (AE) chromatographic experiments. Two bands, separated by ca. 2 minutes, both corresponding to fractions characterized by the absorption spectrum of hTS, were found in the AE chromatogram based on absorbance at 280 nm (*Figure 3-figure supplement 1A*). The relative area of the second band was only about 3.5% that of the first one and decreased further (*Figure 3-figure supplement 1B*) when the protein was loaded together with dUMP and Raltitrexed, both at 250 μM, a concentration more than one order of magnitude larger than their dissociation constants from hTS. Because binding of hTS to its

nucleotidic substrate stabilizes the active, dimeric form of the enzyme, and consistently with the expectations based on protein size and the correlated elution times, we attribute the two bands to the hTS dimers the first one, and monomers the second. In keeping with this assignment, when hTS was loaded on the AE column after a 1 h incubation with compound **C3** at three concentrations, namely 4, 40 and 80 μ M, the monomer band was delayed by additional 3-4 minutes relative to the dimer band in the chromatograms (*Figure 3-figure supplement 1A* and *Figure 3-figure supplement 1C-E*) and its relative area increased markedly, from 0.035 to 0.08, to 0.24 and to 1.09, respectively. Co-elution, hence stable non covalent binding of the **C3** inhibitor with hTS, was established by observing that the fractions containing the hTS dimers and monomers also exhibited absorption at 350 nm (*Figure 3E*), a wavelength at which no absorption comes from the protein. Accumulation of compound **C3** in these fractions was confirmed by identifying and quantifying it in the AE chromatographic fractions by high-resolution mass spectrometry (*Supplementary file 5, Figure 3-figure supplement 2, Figure 3-figure supplement 2-Source data 1*).

Figure 3-figure supplement 2 shows the profile of the variation in concentration of compound **C3** in the AE chromatographic fractions determined by high-resolution MS (UltiMate 3000 UHPLC tandem Orbitrap Q-Ex). Comparison with *Figure 3E* shows that most ligand is co-eluted with the hTS monomer, around a 25 min retention time. The much larger amount of compound **C3** in the protein monomer fractions (23-27 min) relative to the dimer containing fractions (18-22 min) possibly results from preferential co-precipitation of the ligand with the protein dimers relative to the monomers prior to injection into the mass spectrometer.

Absorbances at 350 nm in *Figure 3E* indicated similar concentrations of the compound in the fractions corresponding to the protein dimers and monomers, in spite of the fact that the 280 nm

dimer chromatographic band was much more intense than the monomer band. This finding suggests a somewhat larger affinity of the ligand for the latter. Consistently, parallel MS experiments in which 4 μ M **E5** was loaded on the AE column with hTS identified this ligand mainly in the fractions containing the protein monomers (see additional information in the *Supplementary file 5*. So, overall, the results synthesized here show that these small compounds co-elute with hTS, thus proving beyond doubt that they remain bound to it, possibly to the monomer more tightly than to the dimer, throughout the AE chromatographic runs. Also, they qualitatively show the ability of these ligands to de-stabilize the hTS dimers in favor of the monomers.

Mechanistic analysis of dissociative inhibition.

The nitrothiophenyl derivative, **C3** and its isomers, **C2** and **C4** (*Supplementary file 4B*), are structurally similar to compound **E7** (*Supplementary file 4D*) and are much more soluble in water. So, they were used for quantitatively investigating the molecular mechanistic basis of their ability to both inhibit recombinant hTS and disrupt its dimer. The three isomeric compounds showed different inhibitory potencies against 300 nM hTS, with IC₅₀ values of 5.25, 83 and 246 μ M, respectively. Consistently, **C3** caused the largest decrease in FRET efficiency ($\Delta\Phi_{\text{FRET}}$) at concentrations lower than 50 μ M (Figure 4A, Figure 4B, *Figure 4-Source data 1*).

The dependence of Φ_{FRET} , that in our conditions is a direct measure of the mole fraction of hTS dimers, on each inhibitor concentration (Figure 4B) was fitted according to the dimer-monomer equilibrium model sketched in Figure 4C. This was analyzed as reported in the *Appendix 3*. We searched for evidence of the disruptive character of compound **C3** by investigating the

dependence of its dose-effect curves on total protein concentration, E_T (Figure 4D, *Figure 4-Source data 1*).

As expected for a dissociative inhibition mechanism, the limit values of Φ_{FRET} at high **C3** concentrations were consistent with a 5-fold increase in the equilibrium dissociation constant for the protein bound to **C3** with respect to the free protein (Figure 4E, *Figure 4-Source data 1*).

From the common limit values of Φ_{FRET} at high concentrations (Figure 4B), we conclude that, when saturating hTS, compounds **C2-C4** have similar effects on the dimer stability. The five-fold increase in the protein-dimer dissociation equilibrium constant and the corresponding decrease in ΔG° for dimer disruption, from -40.5 to about -36.5 kJ mol⁻¹, $\Delta\Delta G^\circ = -4$ kJ mol⁻¹, are evidence of the dimer-destabilizing ability of compounds **C2-C4**. On the other hand, their different abilities to decrease the FRET efficiency at lower concentrations can be attributed to different affinities for the protein dimers, with K_I 's of 2.8×10^{-5} , 1×10^{-5} and 2×10^{-5} M, for **C2**, **C3** and **C4**, respectively. Thus, the observed overall effect of such an inhibitor result from a combination of affinity for the protein and ability to destabilize its dimeric assembly by impairing crucial attractive inter-monomer interactions.

Binding of compounds **C2-C4** at the Y202 pocket of the hTS monomer/monomer interface is supported by computational docking (Figure 3C, D). In the hTS dimer, the aromatic ring of the Y202 residue forms a π - π interaction with the phenyl ring of the F59' residue from the opposite subunit. Such a ring is replaced by the phenyl ring of the benzoic acid portions of **C2-C4** in their modeled complexes with hTS. Thus, these compounds mimic some of the residue side chains from the opposite monomer in the dimer, providing similar interactions in this region. This finding is supported by the higher affinities of the inhibitors for the hTS monomer ($K_I = 10^{-6}$ M) than for the dimer ($K_I' = 1.7 \times 10^{-5}$ M), as obtained by fitting of the FRET data in Figure 4B.

The reliability of our docking virtual experiments was strengthened by their ability to explain the observed higher affinity for hTS of compound **C3** relative to its isomers, **C2** and **C4**. While the nitro-groups of all these ligands can make head-to-head hydrogen-bonding interactions with R64 (Figure 3C-D), only the *para* carboxylic group of compound **C3** arranges properly to establish an additional H-bond with R175. Instead, the *meta* and *ortho* carboxylic groups of **C2** and **C4** do not have the correct orientations for interacting with this arginine residue.

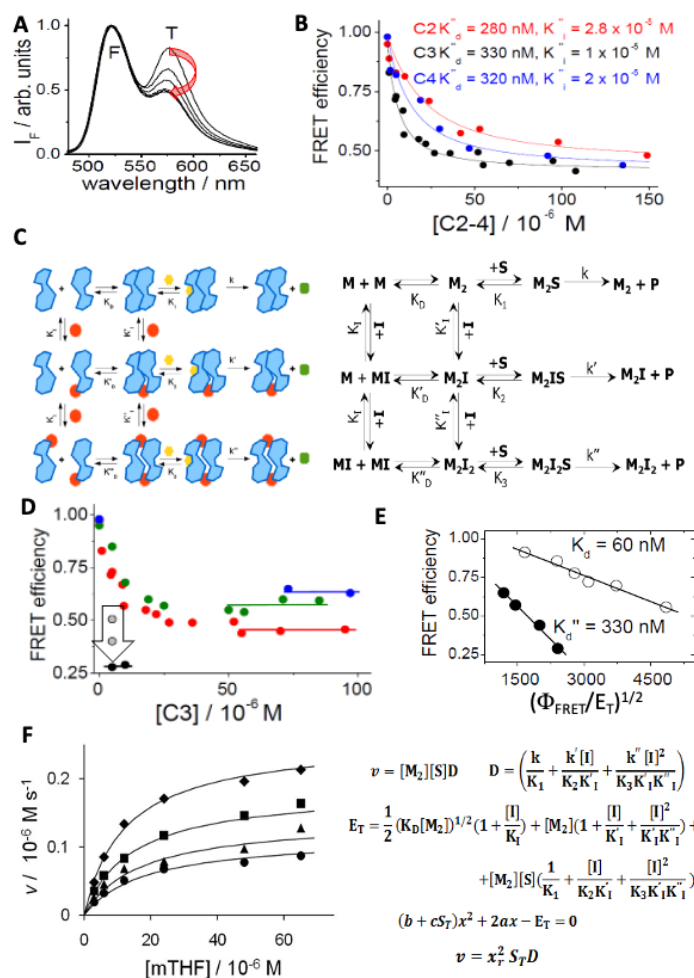


Figure 4. Spectroscopic and mechanistic analysis of hTS dissociative inhibition for compounds C2, C3 and C4. **A**, Emission spectra of fluorescein(F)- and tetramethylrhodamine (T)-labelled hTS ($\lambda_{exc} = 450$ nm): the decreasing emission contribution of T relative to F with

increasing concentrations of **C3** (0, 4.5, 9.5, 15, 25, 100 μM) parallels the decrease in the hTS
 dimer mole fraction. **B**, Dependence of the observed FRET efficiency on the concentrations of
 three inhibitors (**C3**, black; **C4**, blue; **C2**, red); the hTS dimer concentration was 100 nM. The
 lines represent the best fittings of the experimental results to Equation S3 in the *Appendix 4*. The
 most significant fitting parameters are reported. **C**, Cartoon, and standard chemical
 representations of the dissociative inhibition mechanism of hTS. Blue shapes represent enzyme
 monomers (M) in the active conformation bound to dUMP; red dots indicate a dissociative
 inhibitor (I), yellow hexagons, the folate substrate (S), green octagons, the product. **D**,
 Dependence of FRET efficiency on the concentration of **C3** with total protein concentrations
 (E_T) of 490 nM (blue circles), 250 nM (green circles), 100 nM (red circles) and 50 nM (black
 circles). The horizontal segments represent the values of the efficiency in the limit of high
 inhibitor concentration. At $E_T = 50$ nM and $I_T = 5$ μM the vertical arrow indicates the evolution
 of the measured value of the FRET efficiency 5, 7 and 12 minutes after inhibitor addition (grey
 and black circles). **E**, Analysis of the hTS monomer-dimer equilibrium according to eq. $\Phi_{\text{FRET}} =$
 $1 - 0.5(\Phi_{\text{FRET}}/E_T)^{1/2} K^{1/2}$ (Genovese et al., 2010) and corresponding equilibrium constants without
C3 (white circles, $K = K_D$) and at saturating **C3** concentrations (black circles, $K = K''_D$, $\Phi_{\text{FRET}} =$
 FRET efficiency). **F**, Dependence of the initial reaction rate (v) on mTHF concentration (free
 substrate, [S], and total, S_T) at four different **C3** concentrations (from top to bottom, [I] = 0, 12,
 24 and 36 μM). The fitting curves represent equation $v = x_r^2 S_T D$ derived in the *Appendix 4* and
 computed with E_T (total enzyme dimer concentration) = 300 nM, $k = k' = 0.9 \text{ s}^{-1}$, $k'' = 0.1 \text{ s}^{-1}$,
 $K_1 = K_2 = 10^{-5} \text{ M}$, $K_3 = 2 \times 10^{-5} \text{ M}$, $K_I = 10^{-6} \text{ M}$, $K_I' = K_I'' = 10^{-5} \text{ M}$, $x = [M_2]^{1/2}$ and using for x_r the
 only acceptable root of the quadratic equation in panel 4F (*Figure 4-Source data 2*).

438 As for the mechanism of inhibition of hTS enzyme activity by compounds **C2-C4**, we show that
 439 the scheme in Figure 4C can account for the dependence of the initial reaction rate (v) on the
 440 substrate concentration at different inhibitor concentrations with very reasonable fitting
 441 parameters (Figure 4F). Simple observation of the dependence of v on **[C3]** with total enzyme
 442 concentration (E_T) 300 nM (Figure 4F and *Figure 4-Source data 2*), indicates a regular decrease
 443 with increasing **[C3]** to a limiting rate that is about 1/5 the rate in the absence of inhibitor. On the
 444 other hand, the E_T -dependent limiting value of Φ_{FRET} was about half the full one (Figure 4B).
 445 This difference in the limit behaviors of v and Φ_{FRET} suggests that, when bound to the inhibitor,
 446 the dimeric enzyme is less catalytically active than when free. Or, in terms of the
 447 dissociative/noncompetitive model in Figure 4C, K_2 and K_3 are larger than K_1 , or k' and/or k''
 448 are smaller than k . The curves that go through the kinetic data in Figure 4F are plots of eq. $v =$
 449 $x_T^2 S_T D$ that was obtained by fast-equilibrium solution of the scheme in Figure 4C (for the
 450 derivation of the equation and the meanings of the symbols therein, see the *Appendix 4*).
 451 Remarkably, the fitting parameters, provided in the caption, are consistent with the results of the
 452 FRET-based analysis of the equilibria in Figure 4C and the limit behaviors of the initial rate and
 453 of Φ_{FRET} . More in detail: i) k'' is much smaller than k and k' , i.e., M_2I_2 is almost catalytically
 454 inactive, a feature typical of noncompetitive inhibition; ii) K_3 is larger than $K_{1,2}$, i.e., inhibitor
 455 binding reduces the enzyme affinity for MTHF; iii) K_I' and K_I'' remain one order of magnitude
 456 larger than K_I ; i.e., when saturated with dUMP, the enzyme dimer shows lower affinity for the
 457 inhibitor than the monomer; iv) using the relationships among the equilibrium constants, we
 458 estimate that $K_D'/K_D = K_I'/K_I \approx 10$ and $K_D''/K_D' = K_I''/K_I \approx 10$, i.e., the kinetic results confirm a
 459 progressive dissociation of the enzyme dimer to monomers upon subsequent additions of **C3**.

The latter is therefore confirmed to be both a dimer disrupter and a dissociative inhibitor, the two roles being intimately connected with each other.

The dimer destabilizers engage hTS in cancer cells.

To gain evidence that our hTS dimer destabilizers engage this enzyme in cells, we resorted to fluorescence microscopy. For this experiment, we selected compound **E5** to be incorporated in the final conjugated probe because its chemical precursor, **E3**, has a reactive carboxylic group (*Supplementary file 4D*) and is therefore suitable for probe conjugation chemistry. **E6** and **E7** do not have the same suitable precursors. Using a short ether linker, we conjugated it to fluorescein isothiocyanate (FITC), a green-emitting probe that favors cell internalization (*Appendix 2-figure 8-10*). The **E5-(O₂Oc)-CAM-FITC (E5-FITC)** conjugate is permeable to the cells. It proved slightly less active at inhibiting recombinant hTS than **E5** ($IC_{50S} = 40$ and $100 \mu M$, for **E5** and **E5-FITC**, respectively), likely because the probe tail caused some steric hindrance for its binding to the enzyme. For these experiments, we ectopically expressed in HT-29 cells either Wild Type (WT) hTS or a mutant with a tetracysteine motif (CCPGCC, TC) inserted near the N-terminus (TS-TC) (Ponterini et al., 2016). The tetracysteine motif tightly binds ReAsH, a rhodamine-based diarsenical probe. The ReAsH/TC-TS complex emits red fluorescence with much higher efficiency than the unbound probe. HT-29 cells (transfected with either WT TS or TC-TS) were treated with ReAsH and **E5-FITC**. In the ReAsH-TC-hTS/**E5-FITC** complex, fluorescein transferred excitation energy to rhodamine thus signaling formation of the complex with a FRET signal. Indeed, our image analysis (Figure 5) showed that cells expressing hTS-TC produced a significantly higher ($P < 0.0001$) average FRET signal (4222 ± 2128) than control

cells that expressed WT TS (1250 ± 1178), thus proving the occurrence of intracellular hTS/E5 engagement.

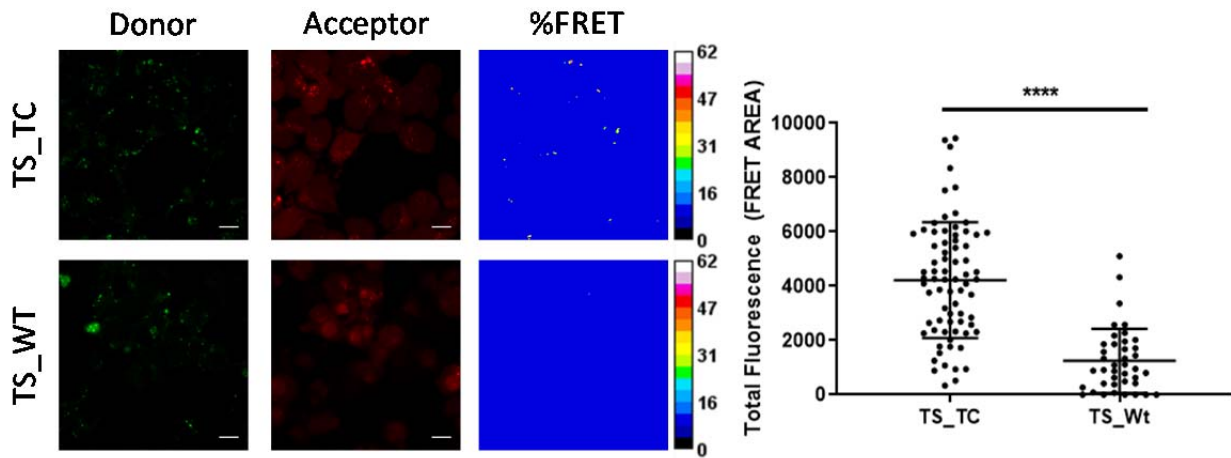


Figure 5. Fluorescence microscopy analysis of hTS dissociative inhibition. Representative fluorescence microscopy images of TS-TC- and WT-TS-expressing HT-29 cells stained with red-emitting ReAsH and incubated with green-emitting **E5-FITC**. From left to right: green-emission and red-emission channels, and FRET efficiencies depicted according to the colour scale (%) in the right bars. Right: comparison of the average FRET areas for cells overexpressing TS with (TS_TC) or without (TS_Wt) ReAsH binding sites, obtained using PixFRET within ImageJ. Each dot represents the total FRET area of an individual field with at least 10 cells. The statistical analysis was performed using unpaired two tailed t-test (P value >0,0001) using Prism 8 for windows (version 3.1.1).

Cancer cell growth inhibition by hTS dimer destabilizers.

The compounds that both inhibited recombinant hTS and decreased the FRET efficiency, i.e., **C2-C5, C9, C10, C13, D5-D9, D12, E1** and **E3-E7**, were selected to test cancer-cell growth inhibition. They were tested as racemates, employing **5-FU**, metabolized to **FdUMP** inside cells, as a reference compound. Tests were performed on several model cancer cell lines. Because **5-FU** is a key therapeutic in the pancreatic-cancer first-line regimen FOLFIRINOX, we chose three pancreatic adenocarcinoma primary cell cultures, PDAC-2, PDAC-5 and LPc167, which express low, intermediate and high TS levels, respectively (Funel et al., 2008, Firuzi et al., 2019). These cell lines showed a similar trend in the TS mRNA levels (3.93 ± 0.58 , 11.49 ± 1.39 , 49.02 ± 2.76 , respectively) (*Figure 6-figure supplement 1, Figure 6-figure supplement 1-Source data 1*). These cultures were obtained from radically-resected patients which reflected the histopathological and genomic features of human PDACs. Noteworthy, **E7** was almost as equally active against both PDAC2 and PDAC5 cells. Both were sensitive to **5-FU** (*Supplementary file 6A*). The LPc167 primary culture, which expressed high levels of TS was resistant to **5-FU** but still sensitive to **E7** (*Figure 6-figure supplement 2, Figure 6-figure supplement 2-Source data 1*).

Figure 6-figure supplement 2 shows the dose-response curve of Pancreatic cancer cells LPc167 growth inhibition for compounds E7, E5 and 5FU.

Other models used in our investigation were two ovarian cancer cell lines, IGROV1 and TOV112D, and two gynecological cancer cell lines that feature high hTS levels resulting from cross-resistance to cisplatin (C13*, A2780/CP) as well as the corresponding cisplatin-sensitive lines (2008, A2780) (Cardinale et al., 2011) (*Figure 6A, Figure 6 - figure supplement 3, Figure 6 - figure supplement 3-Source data 1, Supplementary file 6B*).

Figure 6 - figure supplement 3 shows the dose-response curves for the inhibition of ovarian cancer cells by E5, E6, E7 and 5FU and other compounds.

Since **5-FU** is always included in the treatment of colorectal cancer, we added three epithelial colorectal cancer cell lines, HCT116, HT29 and LoVo, which exhibit different sensitivities to **5-FU** (Bracht et al., 2010). We observed similar results in all tested cell lines. While most compounds produced weak effects, we could determine IC₅₀ values for compounds **E5-E7** (Figure 6-figure supplement 4, Figure 6-figure supplement 4-Source data 1. Supplementary file 6A).

Figure 6-figure supplement 4 shows the cell survival percentages as the mean ± S.E.M. of three separate experiments performed in duplicate. **a** is referred to HCT116 cells. **B** is referred to HT29 cells and **c** is referred to LoVo cells. Data indicate mean values and standard deviation from three experiments performed in duplicate. P values were calculated with two-sided Student's t-test and ANOVA followed by the Tukey's multiple comparison. * p < 0.05; ** p < 0.01; *** p < 0.001, n=3.

E7 was the most interesting among these compounds, being active on all the cancer cells tested with IC₅₀ values between 10 and 37 µM after 72 hours of exposure. It showed a lower or, in a few cases, comparable activity with respect to **5-FU**.

A crucial issue remains the intracellular mechanism of action of these dimer destabilizers. Among the classical active-site inhibitors of hTS, **5-FU** forms a stable ternary complex with the MTHF cofactor and the hTS protein and induces high expression of hTS by stabilizing the dimeric assembly, thereby impairing both the protein feed-back regulation and the proteasomal degradation (Chu et al., 1991; Berger et al., 2004; Peña et al., 2009). On the other hand, **PMX**, another TS active-site inhibitor with a folate-analog structure, binds at the MTHF binding site and forms a reversible non-covalent ternary complex with dUMP (Costi et al., 2005; Wilson et al., 2014). Our dimer destabilizers inhibit recombinant hTS with a different mechanism of action, i.e., by destabilizing its dimer. Thus, we expect them to act differently in cells too, and to

produce a different modulation of the intracellular hTS levels with respect to **5-FU** and **PMX**. These studies are reported in Figure 7.

The dimer destabilizers decrease the hTS levels and promote cell death.

To investigate the intracellular mechanism of action of compounds **E5** and **E7**, we first determined whether they induce apoptotic cell death both in cisplatin-sensitive A2780 cells and in cisplatin-resistant A2780/CP cells. As a control, we included cisplatin (cDDP) that, as expected, caused a higher rate of apoptotic cell death in sensitive than in resistant cells. Remarkably, **E7** induced apoptotic death in the two cell lines after a 48 hours treatment with a slightly higher efficiency than **PMX** (*Figure 7-figure supplement 1, Figure 7-figure supplement 1-Source data 1, Figure 7-figure supplement 2*).

Figure 7-figure supplement 1. Effect of cisplatin on cell death, effect of dimer destabilizers on hTS activity and hTS protein levels in cancer cells. **a**, flow cytometric analysis of apoptosis of A2780 and A2780/CP cells treated with cisplatin (13 μ M, 72h) (Annexin V-/PI-: live cells, Annexin V+/PI-: early apoptotic cells, Annexin V+/PI+: late apoptotic cells, Annexin V-/PI+: necrotic cells). **b**, quantification of Annexin V-positive cells (Q2+Q3) was performed using Annexin V/PI kit. **c**, effects of **E7** (different times) on hTS protein level in HT29 cells, and **on** A2780/CP cells. **e**, cellular extracts from A2780 and A2780/CP cell lines processed for TS activity after incubation with **E5** and **E7** at concentrations corresponding to IC₅₀ values (28.8 and 34.3 μ M for **E5**; 10.1 and 21.5 μ M for **E7**). **f**, cellular extracts from 2008 and C13* cell lines processed for TS activity after incubation with **E5** and **E7** at concentrations corresponding to IC₅₀ values (29.8 and 38.3 μ M for **E5**; 14.6 and 21.1 μ M for **E7**). All the results are the mean of three experiments performed in duplicate. Data indicate mean values and standard deviation. P values were calculated with two-sided Student's *t*-test and ANOVA followed by the Tukey's multiple comparison. * $p < 0.05$; ** $p < 0.01$; *** $p < 0.001$.

Figure 7-figure supplement 2 shows an example of gating strategy used for cell death analysis. Gating strategy (representative flow cytometry profiles) used to assess the percentage of apoptotic cells (Annexin V/PI) shown in

Fig. 6B in the main text. In panel **a**, the untreated (ctr) A2780 cells are reported. The left panel represents the Forward scatter (FSC-A) vs Side scatter (SSC-A). The right panel is the representative flow cytometry analysis plots of Annexin V/PI staining (Parameters: PI-PI-BL2-A vs ANNEXIN V-FITC-BL1-A; Gate: all events). In panel **b**, the cisplatin treated cells (13 μ M, 72hours) are shown. In the left panel, FSC-A vs SSC-A are reported. In the right panel, a representative flow cytometry analysis plots of Annexin V/PI staining is reported (Parameters: PI-PI-BL2-A vs ANNEXIN V-FITC-BL1-A; Gate: all events).

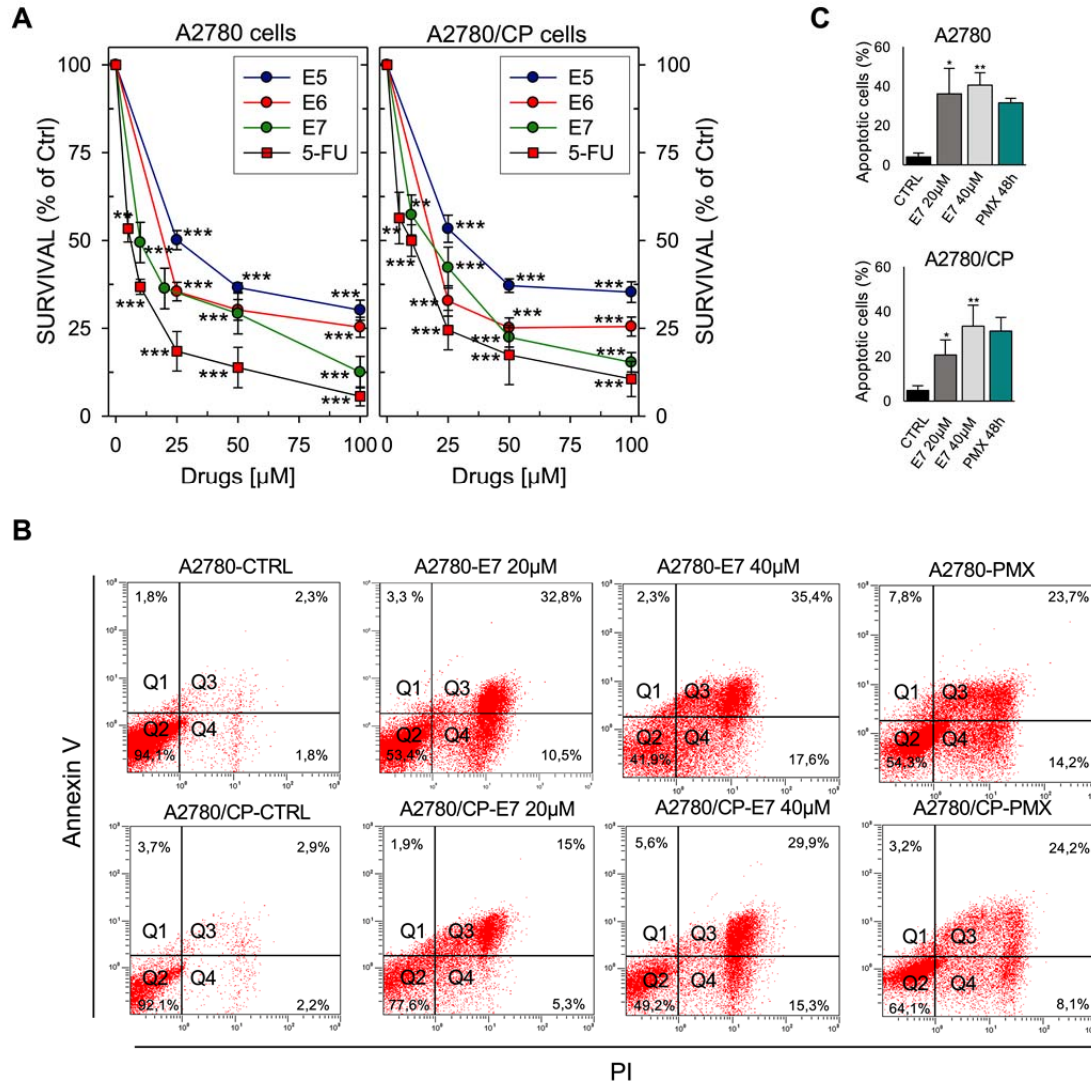


Figure 6. Effects of hTS inhibitors in human cancer cell lines. **A**, Dose-response curves for E5-E7 and 5-FU against A2780 and A2780/CP cell growth. **B**, Flow cytometric analysis of apoptosis of A2780 and A2780/CP cells treated with E7 or PMX (Annexin V⁻/PI⁻: live cells, Annexin V⁺/PI⁻: early apoptotic cells, Annexin V⁺/PI⁺: late apoptotic cells, Annexin V⁻/PI⁺: necrotic cells). (Figure 6-Source data 1). **C**, Quantification of Annexin V-positive cells

(Q2 + Q3) performed using the Annexin V/PI kit. Data indicate mean values and standard deviation of at least two biological repeats performed in duplicate. P values were calculated with two-sided Student's *t*-test and ANOVA followed by the Tukey's multiple comparison. * $p < 0.05$; ** $p < 0.01$; *** $p < 0.001$.

Following treatment of both A2780 and A2780/CP cells with **E5** and **E7**, while we found no change in the levels of the DHFR protein, the level of the hTS protein decreased significantly in a dose-dependent manner (Figure 7A, Figure 7-Source data 1, Figure 7 - Source data 2, Figure 7 - Source data 15, Figure 7 - Source data 16, Figure 7-Source data 3, Figure 7 - Source data 4, Figure 7 - Source data 15, Figure 17 - Source data 18) It was low, nearly undetectable after 12-24 hrs of exposure to **E7** in HT29 cell (*Figure 7-figure supplement 1, Figure 7-figure supplement 1-Source data 2, Figure 7-figure supplement 1-Source data 3, Figure 7-figure supplement 1-Source data 4, Figure 7-figure supplement 1-Source data 5*) and undetectable after 24-36 hrs of treatment in A2780/CP cells (*Figure 7-figure supplement 1, Figure 7-figure supplement 1-Source data 6, Figure 7-figure supplement 1-Source data 7*). In the same cell lines, we observed increased levels of hTS after treatment with both **PMX** and **5-FU** (Figure 7B) (Figure 7-Source data 5. Figure 7-Source data 6, Figure 7 - Source data 15, Figure 7 - Source data 20).

The ubiquitin-independent proteasomal degradation pathway is an important mechanism to destroy destabilized proteins in cells, and hTS is one of the substrates of this pathway (Peña et al., 2009). The observed decrease in hTS protein levels caused by **E5** and **E7** led us to hypothesize that it might be associated with a post-translational regulation mechanism, including proteasomal degradation. To test this hypothesis, we selected **E7**, our best cellular inhibitor, to determine the hTS half-life after blocking the *de novo* protein synthesis with the cycloheximide

(CHX) inhibitor. As shown in Figure 7C (Figure 7-Source data 7, Figure 7 - Source data 8, Figure 7 - Source data 21, Figure 7 - Source data 22), we found that the half-life of hTS was 3 hours in untreated cancer cells and that the degradation rate of the enzyme increased by 20% in **E7**-treated A2780 cell.

To check whether the 26S proteasome was involved in such an accelerated degradation, we added the proteasome inhibitor MG132 (10 μ M, for 5 hrs) to **E7**-treated and untreated A2780 cells. Indeed, as shown in (Figure 7D, Figure 7 - Source data 9, Figure 7-Source data 10, Figure 7 - Source data 23, Figure 7 - Source data 24), MG132 restored the hTS levels in treated cells. These findings are opposite to the known effects on the hTS intracellular life exhibited by the reference inhibitor, **5-FU**. In fact, previous reports on other cell models have shown that **5-FU** causes a remarkable slowdown of the TS degradation rate because most of the protein is engaged in a ternary complex with the folate substrate and the inhibitor, being thus protected from the proteasome (Berger et al., 2004; Peña et al., 2009; Wilson et al., 2014; Kitchens et al., 1999; Kitchens, Forsthoefel, Rafique et al., 1999).

To investigate whether engagement of **E5** and **E7** with hTS in cancer cells could affect the protein catalytic activity, their effect on endogenous TS activity was evaluated on cellular extracts from untreated cells of four cell lines, namely, A2780, A2780/CP, 2008 and C13*. These extracts were incubated with the inhibitors at their IC₅₀ values for 60 min. In these conditions, the catalytic activity of hTS was systematically reduced by 25-30% in the cellular extracts of all cell lines (*Figure 7-figure supplement 1, Figure 7-figure supplement 1-Source data 8*).

Figure 7-figure supplement 1 shows in panel e, the cellular extracts from A2780 and A2780/CP cell lines processed for TS activity after incubation with **E5** and **E7** at concentrations corresponding to IC₅₀ values (28.8 and 34.3 μ M for **E5**; 10.1 and 21.5 μ M for **E7**). In panel f it shows the cellular extracts from 2008 and C13* cell lines processed for TS activity after incubation with **E5** and **E7** at concentrations corresponding to IC₅₀ values (29.8 and 38.3 μ M

for **E5**; 14.6 and 21.1 μ M for **E7**). Data indicate mean values and standard deviation. P values were calculated with two-sided Student's *t*-test and ANOVA followed by the Tukey's multiple comparison. * $p < 0.05$; ** $p < 0.01$; *** $p < 0.001$.

This reduction of the hTS activity supports the hTS target engagement by the dimer destabilizers and links the observed effect with the intracellularly observed dimer to monomer equilibrium shift (Figure 7F in the next section). Based on the above data, we conclude that **E7** reduces the hTS levels in cancer cells by enhancing its proteasomal degradation. Because **E7** behaves as a disrupter of the dimeric recombinant protein, we anticipate that the promotion of its proteasomal degradation in cells is due to an increased fraction of more labile monomers (Figure 7G).

E7 disrupts endogenous hTS dimers yielding monomers that are more rapidly degraded by the proteasome.

We then explored how treatment with **E7** perturbed the intracellular hTS dimer/monomer equilibrium using a cross-linking strategy on endogenous hTS from A2780 cells (Figure 7F, Figure 7 - Source data 11, Figure 7-Source data 25) (Shi et al., 2017). These cells were treated with **E7** or with the vehicle (DMSO) for 3 hrs, after which cross-linking was carried out by adding bis(sulfosuccinimidyl)suberate (BS^3) to the cell lysate. Next, the hTS dimers and monomers were detected via immunoblot after SDS-PAGE in reducing conditions. The treatment caused a significant decrease of the dimer/monomer ratio relative to the control (- 40 \pm 10 %, Figure 7F). We thus confirmed that **E7** disrupts the hTS dimers also in cells.

To confirm that the hTS monomer is less stable than the dimer in cells, we used a model system in which HCT116 cells ectopically express either WT hTS or the hTSF59A dimer interface

mutant tagged with Myc-DDK (Figure 7G, Figure 7-Source data 12, Figure 7- Source data 13, Figure 7-Source data 14, Figure 7 - Source data 26, Figure 7 - Source data 27)). While WT, with its 60-80 nM K_d in buffer, is expected to be essentially dimeric at all physiological concentrations, the F59A variant, with a K_d of 1.3×10^{-4} M in buffer is, instead, expected to be essentially monomeric (Salo-Ahen et al. 2015). We analyzed the protein turnover of WT hTS and of the monomeric F59A variant, in the presence of the *de novo* protein synthesis inhibitor CHX. The expressions of the mRNAs of the two proteins showed no statistically significant differences (Figure 7-figure supplement 3).

Figure 7-figure supplement 3 shows the expression levels of total (exogenous plus endogenous) and exogenous hTS mRNAs 24 hours after transfection of HCT116 cells with wild-type hTS-Myc- DDK tagged or mutant hTS-Myc-DDK-F59A vectors. Quantitative Real Time RT-PCR results showing the expression of total and exogenous hTS mRNAs in HCT116 cells transfected with wild- type hTS-Myc-DDK tagged (WT) or mutant hTS-Myc-DDK-F59A vectors. The mRNA expression was calculated with the $\Delta\Delta C_t$ method (calibrator: average of HCT116 cells transfected with WT hTS- Myc-DDK-tagged vector) with GAPDH as endogenous control. Columns and bars indicate mean values + S.E.M. (n= 6 for two independent experiments)

As for the proteins, the F59A variant was already hardly discernible at time 0 (24 hrs after ectopic expression) while the dimeric WT hTS showed a turnover of about 8.5 hours. Thus, the monomeric hTSF59A variant is unstable and undergoes much faster turnover than the dimeric WT protein.

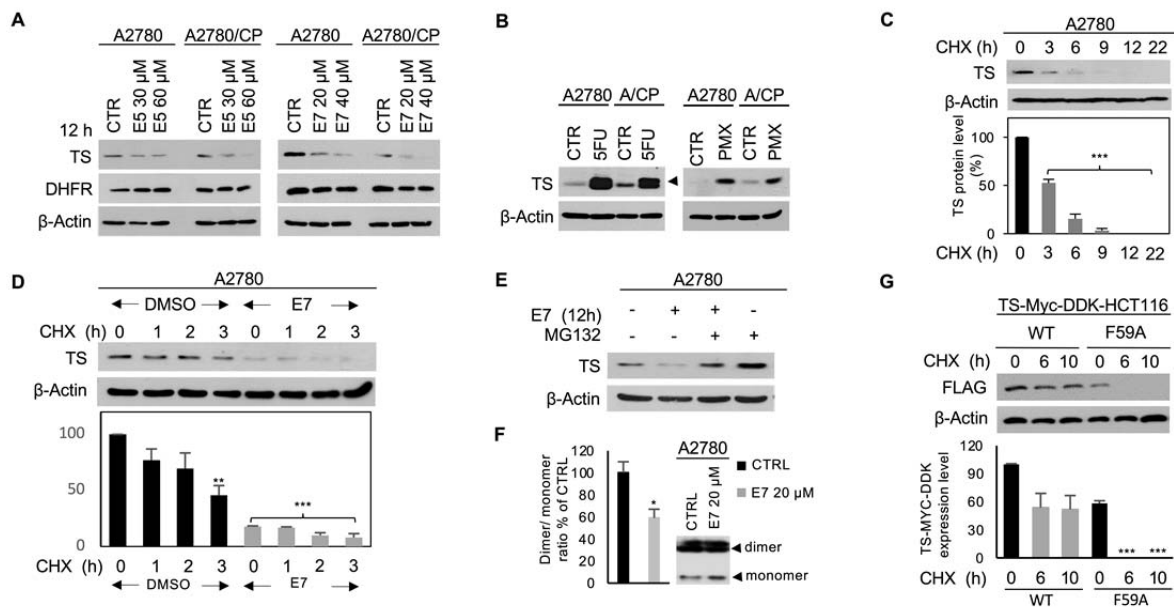


Figure 7. Dimer destabilizers effects on wild type and mutant hTS levels in human cancer cell lines. **A**, Effects of **E5** and **E7** on hTS and DHFR protein levels in A2780 and A2780/CP cells. **B**, Increase of hTS protein level in A2780 and A2780/CP cells following treatment with **5-FU** (5 μ M, 72h) (ternary-complex, arrowhead) or **PMX** (5 μ M, 48h). **C**, hTS half-life determination in A2780 cells after treatment with CHX (90 μ g/ml) for 0-22h. **D**, Stability of hTS in A2780 cells treated with **E7** for 12h, followed by treatment with CHX for the indicated times. **E**, hTS levels in A2780 cells treated with **E7** for 12h, then with 10 μ M MG132 for 5h. **F**, Effects of a 3 hours exposure to **E7** on hTS dimer/monomer equilibrium in A2780 cells. **G**, Half-life determination of exogenous hTS protein (anti-FLAG stain) in HCT116 cells transfected with TS-Myc-DDK (CHX, 0, 6 and 10h) or with the F59A mutant (CHX 0, 6 and 10h) tagged vector. Data indicate mean values and standard deviation of biological repeats performed in duplicate. P values were calculated with two-sided Student's *t*-test and ANOVA followed by the Tukey's multiple comparison. * $p < 0.05$; ** $p < 0.01$; *** $p < 0.001$.

***In vivo* anticancer activity.**

Based on their *in vitro* profile, we tested **E5** and **E7** in appropriate animal models. We first performed pharmacokinetic (PK) studies on healthy mice to determine whether the compounds would show suitable PK. Initial PK data were obtained using intravenous (i.v.) administration of **E5** and **E7** (*Supplementary file 6C*). **E7** showed the best PK profile (Figure 8A). Both after i.v. and oral administration it reached its t_{\max} value after about 5 min with plasma levels in the micromolar range, i.e. concentrations that had caused a cell-growth inhibition *in vitro*. With a half-life of 13.6 hours, a prolonged exposure of the target tissue to the drug is expected. **E7** was then selected to be tested for its antitumor effect *in vivo*. In general, for low molecular weight compounds, intraperitoneal (i.p.) and i.v. administrations result in comparable PK. Furthermore, because of the lipophilicity of the compound, a rapid transfer from the peritoneal cavity to the blood and back is expected. Since we preferred to analyze the antitumor activity of **E7** in a PDAC orthotopic model that recapitulates several human-tumor phenotypic characteristics, we chose an i.p. drug delivery with an intermittent schedule (Figure 8B). Such a relatively frequent schedule would have been too stressful for the mice via the i.v. route because of the damage to veins. The ability of the hTS dimer disrupter **E7** to inhibit tumor growth was evaluated on bioluminescent PDAC models genetically engineered to express Gaussia-luciferase (G-luc), simplifying the monitoring of the tumor volume. Five days after injection, primary pancreatic tumors were detectable in all mice (100% take rate, without surgery-related mortality), and G-luc activity, proportional to the number of cancer cells, increased with time (Figure 8C). This mean signal was significantly lower in mice treated with **E7** compared with control mice (46183 ± 2015 vs. 67905 ± 6159 RLU/sec at day 25; $p = 0.001$, two-sided t test). Moreover, starting from day 30, the group receiving **E7** had significantly lower G-luc intensity compared with mice receiving **5-**

FU (i.e., at day 30, -70% and -48%, relative to control mice, respectively). Mice treated with **E7** had only a slight reduction of body weight (Figure 8D), similar or less evident than that with **5-FU** and showed no other side effects. Tumor growth inhibition was reflected in a significantly longer survival of mice treated with **E7** as compared with control mice ($p = 0.03$, Figure 8E) and **5-FU** (58 days, 43.3 days and 50 days respectively). To demonstrate that the therapeutic effect of **E7** is not cancer-model specific, 2×10^6 human ovarian cancer cells (A2780) were subcutaneously xenotransplanted into the flanks of 7-week-old Athymic Nude-Foxn1nu female mice (Figure 8-figure supplement 1, Figure 8-figure supplement 1-Source data 1).

Figure 8-figure supplement 1. *In vivo* effects of E7 on Athymic Nude-Foxn1nu female mice. **a**, tumor growth kinetics at the indicated time points. Athymic Nude-Foxn1nu female mice were subcutaneously inoculated with 2×10^6 A2780 cells. Implanted xenotransplanted mice, chosen randomly, were subjected to **E7**, 5FU and vehicle treatment, as indicated in the materials and methods section; $n = 4$ mice per group. * **E7**-treatment is statistically different to control (vehicle) for the tumor volume at 6th and 7th day (t-test $p < 0.05$). Error bars indicate SEM. **b**, quantitative analysis of the AUC of tumor growth kinetics in control, **E7** and 5FU-treated mice. Bars are representative of the mean \pm SEM obtained from all mice treated (t-test, * $p < 0.05$). **c**, survival curves (Kaplan Meier) showing the percentage of survival of xenotransplanted mice, placebo control versus **E7** and 5FU-treated mice (Log-rank (Mantel-Cox) test P value=0.0024; $n=4$).

Seven days after injection, as for the orthotopic model, the engrafted mice were randomly divided into three experimental groups and then treated with a similar drug schedule and dose. We found that also in this model, **E7** caused a significant reduction of tumor growth compared with control mice (596.1 ± 167.7 vs. 2319.9 ± 289.7 mm³ at day 6; 776.5 ± 191.6 vs. 3102.0 ± 516.2 mm³ at day 7; $p < 0.05$, two-sided t test), which was confirmed by quantification of the area under curve and resulted in significantly longer survival ($p = 0.0111$; 24 days vs 16 days; Figure 8-figure supplement 1).

To understand whether the antitumor activity of **E7** was associated with an increased anti-TS effect, we measured hTS mRNA (Figure 8F) and protein expression (Figure 8G) in tumor tissues from the PDAC orthotopic model. The mice treated with **5-FU** did not show a decrease in TS mRNA expression and showed a more intense staining for TS, in agreement with earlier studies in which treatment with **5-FU** had induced TS activity both in mice and patients (Van der Wilt et al., 1992; Peters et al., 2002). Conversely, **E7** treatment led to a reduced expression of TS mRNA, down to 40-50% of the reference level (Figure 8 F) in complete agreement with the results obtained with model cancer cells (*Figure 8-figure supplement 2 and Figure 8-figure supplement 2-Source data 1*).

Figure 8-figure supplement 2 shows the real time PCR (qPCR) experiments. Quantitative PCR (qPCR) measurements were performed for hTS transcripts in A2780 and A2780/CP cells treated with **E7** and **E5** for 12h and **5FU** (5 μ M) for 24 and 72h. Data indicate mean values and standard deviation of biological repeats performed in duplicate. P values were calculated with two-sided Student's t-test and ANOVA followed by the Tukey's multiple comparison. * $p < 0.05$; ** $p < 0.01$.

Immunohistochemistry staining showed that **E7** caused a decrease in the levels of hTS protein that was even more pronounced than **5-FU** (Figure 8G). The hTS protein levels measured with the histological score (H-score) was 48 ± 5 a.u. for **E7** vs. 242 ± 26 a.u. for **5-FU** ($p < 0.001$, two-sided t test). Additional analyses showed that **E7** reduced the proliferation of the cancer cells, as detected by the reduced number of Ki67-positive cells, while increasing apoptotic cell death, as assessed by the staining of cleaved caspase-3 (Figure 8-figure supplement 3).

Figure 8-figure supplement 3 shows some representative immunohistochemical images showing extensive caspase-3 activation after treatment with **E7**, which was also able to significantly reduced cell proliferation (Ki67 staining).

Conversely, only a limited caspase-3 staining was found in tumors treated with 5-FU, while most of the untreated tumor tissues showed no caspase-3 activation.

Notably, these effects were markedly stronger in tumors treated with **E7** compared to tumors treated with 5-FU. These results provide clear evidence of the higher anticancer efficacy of **E7** compared to **5-FU** in the cancer animal models employed; moreover, they support our hypotheses of the mechanisms of action of these compounds in cells and in tissues.

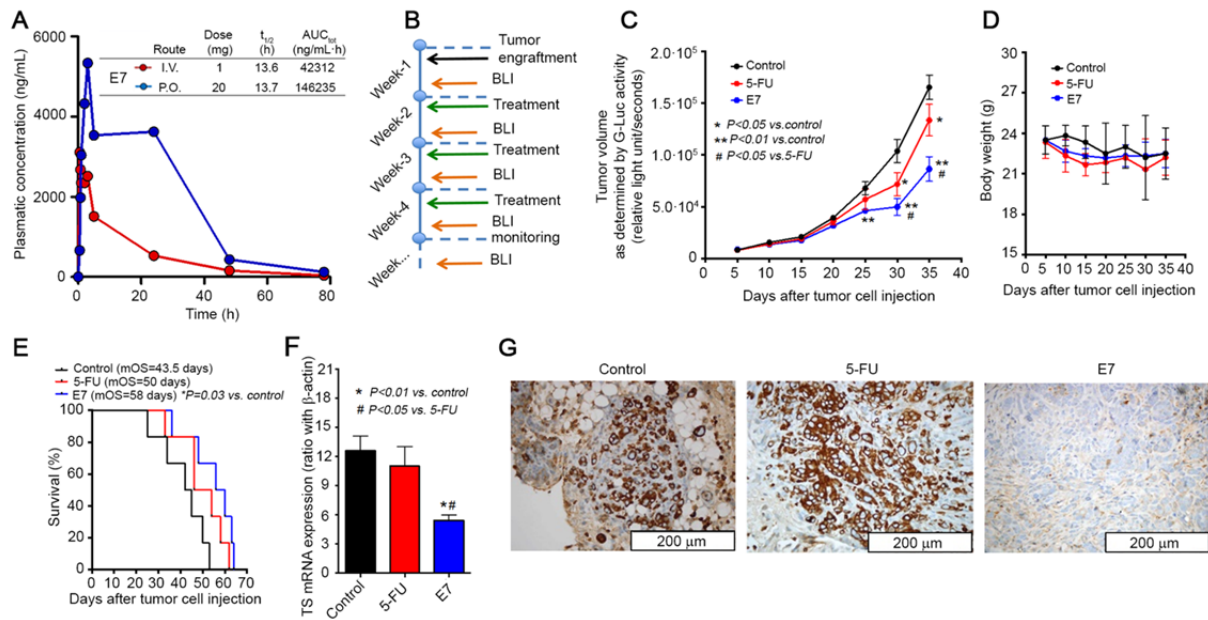


Figure 8. Effects of E7 in vivo pancreatic cancer model. **A**, PK data on healthy mice for **E7**. **B**, Set-up of *in vivo* experiments, using mice injected orthotopically with PDAC-2-primary cells, and monitored every 5 days by bioluminescence imaging (BLI). **C**, Effects of **E7** and **5-FU** on tumor growth, as detected in blood samples with the G-luc (proportional to the number of cancer cells, carrying G-luc). Points indicate mean values obtained from the analysis of the six mice in each group. Bars indicate standard deviation. P values were calculated with two-sided Student's *t*-test and ANOVA followed by the Tukey's multiple comparison. **D**, Effects of **E7** and **5-FU** on

the weight of the mice, demonstrating that tumor shrinkage induced by these treatments was not accompanied by severe toxicity. Points indicate mean values obtained from the analysis of the six mice in each group. **E**, Survival curves in the groups of mice treated with **E7** and **5-FU**. Median overall survival (mos) is reported. Statistically significant differences were determined by two-sided log-rank test. **F**, Quantitative PCR results (calculated with the standard curve method, using the ratio with the housekeeping gene β -actin) showing the reduced expression of hTS mRNA in lysates from frozen tissues from PDAC-2 mice treated with **E7** (24 hours before their sacrifice) compared with untreated control mice. Columns and bars indicate mean values and standard deviation. P values were calculated with two-sided Student t test and ANOVA followed by the Tukey's multiple comparison. **G**, Representative immunohistochemical images showing a weak staining for hTS in the tissues from mice treated with **E7** compared to the strong staining in **5-FU**-treated and control mice. (*Figure 8-Source data 1*)

Discussion

Currently, several first-line chemotherapies commonly comprise cytotoxic agents as 5-FU and its pro-drug derivatives to uproot or control various solid tumors including colorectal cancer.

5-FU induces cytotoxicity either by interfering with essential biosynthetic activity through inhibiting the action of thymidylate synthase (TS) or misincorporating its metabolites into RNA and DNA (Sethy C and Kundu CN, 2021). hTS is an obligate, stable homodimer that plays a crucial role in cell proliferation. As an enzyme, it provides the sole *de-novo* pathway to deoxythymidylate (dTMP) synthesis in human cells. Additionally, by interacting with its own and other mRNAs, this protein regulates its own levels and those of several other proteins involved in apoptotic and proliferation processes. Its inhibition has usually been achieved with compounds that bind at the protein active-site, competing with either the dUMP substrate,

such as 5-fluorodeoxyuridine 5'-monophosphate (FdUMP), or with the folate cofactor, such as raltitrexed (RTX) and pemetrexed (PMX).

Despite several advantages, the clinical application of 5-FU is limited due to the development of drug resistance after chemotherapy. The major mechanism responsible for 5-FU resistance is controlled by key enzymes such as thymidylate synthase (TS), dihydropyrimidine dehydrogenase (DPD) and thymidine phosphorylase (TP). Numerous reports have shown that increased TS expression is a result of the common mechanisms of 5-FU resistance (Longley DB et al, 2003; Iijchi K et al, 2014; Vodenkova S et al, 2020; Ahn JY et al, 2015; Aschele C et al, 2002). Because response to TS-directed chemotherapy critically depends upon the enzyme concentration, such an over-induction has been identified as a barrier to successful therapeutic outcomes. Hence the need to design and develop drugs that, having different mechanisms of action, can prevent or delay the onset of resistance.

In the present work we developed small molecules able to reduce the concentration of hTS dimers by shifting its dimer-monomer equilibrium toward the inactive monomer. As a consequence, they inhibit the activity of the enzyme and produce, as a crucial consequence, its enhanced proteasomal degradation and down-regulation in cells.

Unlike 5-FU, these compounds do not inhibit TS by forming the unproductive enzyme dimer-substrate-inhibitor complex. Formation of this stable complex leads to prolonged engagement of the enzyme by the drug and, eventually, to thymineless cell death. However, it also induces translational derepression of TS-mRNA and results in the enzyme up-regulation, accounting for the occurrence of 5-FU resistance (Chu and Allegra, 1996). Thus, the proposed dimer destabilizers are believed to avoid the onset of drug-resistance based on this mechanism. Additionally, enzyme stabilization has been indicated as an important primary mechanism of TS induction by fluoropyrimidines (Kitchens et al., 1999a). TS turnover is carried out in an ubiquitin-independent manner (Forsthoefel et al., 2004; Pena et al., 2006) and FdUMP binding to the TS protein leads to dramatic conformational changes which account for a stabilization of the enzyme and an increase in its half-life and intracellular levels (Kitchens et al., 1999b; Marverti et al., 2009). Again, use of the dimer destabilizers characterized by a different mechanism of action with respect

to 5-FU, results in a decrease of the TS half-life by accelerating its proteasomal degradation, thus also counteracting this mechanism of TS over-expression and drug resistance.

Indeed, reduction of the intracellular levels of the TS enzyme and a marked decrease of both *in vitro* cancer cell growth and *in vivo* tumor growth, together with a reduced expression of hTS mRNA in lysates from treated frozen tissues and cells, are the most promising results obtained with these dimer destabilizers. Therefore, they represent new, promising tools to fight drug resistance associated with high TS levels in different tumor types such as colorectal, ovarian, and pancreatic cancers.

In conclusion, we have proposed a genuinely new class of inhibitors of a critical anti-cancer drug target, hTS. They act as destabilizers of the active obligate dimer, resulting in the inactive monomers. With their unprecedented mechanism of inhibition, compounds such as **E7** break the long-established link between inhibition and enhanced expression of this essential enzyme, a link that is typical of classical hTS active-site inhibitors, such as 5-FU and PMX. The superior *in vivo* behavior of **E7** relative to **5-FU**, despite its similar capacity to inhibit cancer cell growth, confirms the high potential of this dimer disrupter for further development. Our experiments suggest that it may overcome drug resistance in cancer cells that directly or indirectly increase the hTS levels. By doing so, these compounds, once combined with classical anti-TS drugs in suitably designed anticancer therapeutic schemes, may help avoiding or delaying the onset of anti-hTS drug resistance associated with over-expression of the enzyme, thus maintaining, or restoring cancer-cell drug sensitivity.

Materials and Methods

Computational protein-pocket identification for tethering.

To detect possible pockets for the tethering experiments at the hTS monomer-monomer interface, we examined the crystal structures of both the active (PDB-ID: 1HVV) (Phan et al., 2001) and inactive (PDB-ID: 1YPV) (Lovelace et al., 2005) hTS conformation. SYBYL 7.3 (Tripos Inc., St. Louis, MO) and PyMOL (version 1.8) were used for structure preparation and

visualization of molecular structures. PASS (Brady and Stouten, 2000), SiteIDTM (Tripos Inc., St. Louis, MO) and CASTp (Dundas et al., 2006) were used to identify the pockets at the monomer interface as well as the surface crevices of dimeric hTS that extend into the interface. The GRID software (Goodford, 1985, Wade et al., 1993, Wade and Goodford, 1993, Case et al., 2005) was used to calculate molecular interaction fields of different probes. The KYG server (Kim et al., 2006) was used to predict the interface residues that could bind to RNA to avoid selecting interface pockets that would overlap with the predicted RNA binding site(s). We searched possible transient interface pockets by molecular dynamics (MD) simulations with the AMBER 8 simulation package (Case et al., 2005). We used the ff03 force field (Duan et al., 2003); 7-ns long simulations were performed for the monomeric (active and inactive) hTS both in implicit (NPSA) (Wang and Wade, 2003) and explicit (TIP3P) (Jorgensen et al., 1983) solvent. We performed shorter (4 ns) simulations for dimeric hTS, both active, with and without the dUMP substrate (from 1HVV), and inactive, with or without a phosphate ion in the active site (from 1YPV).

Detailed results description. The MD studies showed that, in general, the hTS structures and the energy of the simulations remained stable throughout the simulation time. The flexible regions (loops) of the inactive hTS were more mobile than in the active hTS structure and especially the modeled small domain was moving relatively much compared with the other loops. The dUMP-bound active dimeric hTS exhibited the smallest residue fluctuations. The identified interface pockets are reported in *Figure 1-figure supplement 1* and *Supplementary file 1*. We examined the interface pockets of the snapshot structures from the MD trajectories at every sharp nanosecond (*Supplementary file 1B*). In all simulations, new pockets were formed while some disappeared,

and others reappeared. Supplementary file 1B shows the pockets along the active monomer simulation in explicit water (without dUMP). Finally, the Y202 pocket was selected as the most promising target for tethering experiments since this pocket does not appear in the hTS dimer, it is not predicted to be part of the mRNA region and it can interact with various functional groups. It is also of reasonable size and there are several smaller crevices around it that can fuse with it, as observed from the simulations.

Details on methods used in MD studies. The proteins and ligand preparation were carried out with the SYBYL 7.3 (*Tripos Inc., St. Louis, MO*) Biopolymer module; modified cysteines were reconstructed as normal cysteine residues, hydrogen atoms and missing side chains were added. The dimeric form of the inactive hTS was built with the Protein Quaternary Structure file server (Henrick and Thornton, 1998) and the missing small domain (residues 107-128) was modeled according to the 1HVY structure. The hydrogen of the sugar hydroxyl group in dUMP was directed toward the neighboring H256. The Antechamber tool (Wang et al., 2006) of AMBER 8 was used to create the ligand parameters for the MD simulations. The ligand partial charges were modified manually: for the phosphate ion, the charge of phosphorus (P) atom was set to 1.216e (NPSA) or 1.4e (TIP3P) and the oxygen (O) atoms to -0.55e (NPSA) or -1.1e (TIP3P). The total charge of the phosphate ion in the NPSA model was -1e, and in the explicit water -3e. For dUMP, the charges were partly taken from the all_nucleic02.lib of AMBER 8: the uracil moiety from the RU unit and the sugar moiety from the DT3 unit. The phosphate group was set to have a total charge of -2e. Firstly, the systems were energy minimized, heated and equilibrated. For the implicit water (NPSA) simulations: 30 ps (10 K --> 100 K), 20 ps (100 K --> 200 K), 20 ps (200 K --> 300 K) and then 400 steps of minimization were carried out. For the explicit water

simulations, an octahedral box extending 10 Å from the protein was filled with TIP3P water (including the crystallographic water sites) and neutralizing Na⁺ ions. Energy minimization was performed in six steps, decreasing the constraints on the protein stepwise from 5 to 0 kcal/molÅ². Each step was carried out for a maximum of 200 iterations. Equilibration: (i) restrained solute (5 kcal/mol restraint force constant, 10 K --> 100 K, 10 ps, constant volume, Langevin dynamics); (ii) free solute (10 K --> 100 K, 10 ps, constant volume, Langevin dynamics); (iii) free solute (100 K --> 200 K, 10 ps, constant volume, Langevin dynamics); (iv) free solute (200 K --> 300 K, 10 ps, constant volume, Langevin dynamics); (v) free solute (300 K, 10 ps, constant volume and temperature, Langevin dynamics); (vi) free solute (300 K, 10 ps, constant pressure and temperature). The production simulations were performed at a constant temperature of 300 K and a pressure of 1 bar with Berendsen coupling constants of 5.0 and 2.0 ps, respectively (Berendsen et al., 1984). Periodic boundary conditions, particle-mesh Ewald electrostatics (Essmann et al., 1995) and a cut-off of 9 Å for non-bonded interactions were used. A time step of 2 fs was applied together with the SHAKE algorithm (Ryckaert et al., 1977) to constrain the bonds to hydrogen atoms.

Site directed mutagenesis, protein purification

The mutants Y202C and C195S were generated by site directed mutagenesis using the plasmid hTS-pQE801 as template, as already reported (Salo-Ahen et al., 2015) (forward primer Y202C: *CATGCGCTGTGTCAATTTGCGTAGTCAACAGTGAAGT*; forward primer C195S: *CTCATGGCTCTTCCGCCAAGCCATGCGCTGTGTCAATTT*). The double mutant C195S-Y202C was generated using the plasmid hTS-Y202C pQE801 as template. Wt-hTS and mutants were produced and purified according to established protocols (Salo-Ahen et al., 2015).

X-ray crystallography.

Crystals of the mutants hTS-Y202C and hTS-C195S-Y202C were obtained under high salt conditions by established protocols (Cardinale et al., 2011, Salo-Ahen et al., 2015), and grew in 4 months and in about one year, respectively. X-ray diffraction data were collected at ESRF (Grenoble, France), processed with MOSFLM 7.0.4 (Leslie et al., 2006) and scaled with SCALA (Evans, 2006) from the CCP4 suite (Winn et al., 2011). Structures were solved by molecular replacement using MOLREP (Vagin and Teplyakov, 1997) (search model either inactive or active wt-hTS, PDB-IDs 3N5G (Cardinale et al., 2011) and 1HVY (Phan et al., 2001), respectively) and refined with REFMAC5 (Winn et al., 2003) and PHENIX (Adams et al., 2011) with TLS parameterization (Murshudov et al., 1997). Water molecules were added using ARP/wARP (Langer et al., 2008) and Coot (Emsley et al., 2010) was used for manual rebuilding and modeling. The model stereochemical quality was assessed using Coot and PROCHECK (Laskowski et al., 1993). Final coordinates and structure factors were deposited in the Protein Data Bank under the accession codes 4O1U (hTS Y202C) and 4O1X (hTS C195S-Y202C). Data collection and refinement statistics are reported in *Supplementary file 2*. Figures were generated using CCP4MG (McNicholas et al., 2011).

X-ray crystal structure determination of hTS-Y202C and hTS C195S-Y202C.

The hTS mutants Y202C and C195S-Y202C were crystallized under the same high salt conditions previously reported for the WT enzyme. The hTS-Y202C crystallized in the space group P3₁ with an enzyme dimer in the inactive conformation in the asymmetric unit (ASU). The structure of hTS-Y202C closely resembles that of the native enzyme in the inactive conformation

944 (r.m.s.d. upon C α -atom matching of 0.4 Å), explaining the similar biochemical profiles of the
945 two proteins. The hTS C195S-Y202C crystallized in the space group P2₁2₁2₁ with four
946 independent subunits in the ASU, all in the active conformation. The hTS-C195S-Y202C
947 structure is the first example of hTS crystallized in the active conformation under high salt
948 conditions. Since both mutants crystallized under the same conditions, the shift of hTS towards
949 the active conformation seems due to the active site C195S mutation. A possible explanation is
950 that the clustering of the four residues C180 and C195 from the two dimer subunits stabilizes the
951 inactive conformation of hTS, thus the C195S mutation prevents this occurrence. In both
952 structures, the Fourier difference map clearly shows the replacement of the native Y202 by
953 cysteine. Moreover, a positive extra electron density is found extending beyond the cysteine
954 sulfur atom strongly indicating its reaction with β -mercaptoethanol (BME) present in the
955 crystallization solution. Thus, C202 is chemically modified to S,S-(2-hydroxyethyl)thiocysteine
956 (CME) (*Figure 2-figure supplement 1a,b,c*). The other cysteines are modified to either CME or S-
957 methyl-thio-cysteine (SCH), apart for C210 which is in the reduced, unmodified form. The two
958 mutants, Y202C and C195S-Y202C, have essentially the same behavior as regards thiol
959 reactivity. In the A subunit of hTS-Y202C, CME202 entails water-mediated interactions with
960 D173, R175, K47', T55', and D254' (*Figure 2-figure supplement 1d*). In subunit B, CME202 is
961 H-bonded to K47' and forms water-mediated interactions with P172, D174, and V203 (*Figure 2-*
962 *figure supplement 1e*). Analogous intra- and inter-subunit interactions of CME202 are also
963 observed in the structure of the double mutant. Thus, the structure of hTS C195S-Y202C
964 validates the choice of Y202 as tethering mutation site, showing that this residue is prone to react
965 with thiol compounds independently of the enzyme conformation. C202 is located in a dimer
966 interface pocket considered important for protein-protein interactions. The CME modification,

observed in both structures, indicates that C202 is exploitable for tethering with reactive molecules aimed at disrupting the hTS dimer interface (*Figure 2-figure supplement 1f,g*). In both variants, the loop K47-T55 of the facing subunit is displaced with respect to the structure of wt-hTS, increasing the intersubunit distances by 1.0-2.5 Å. As already suggested by the structure of wt-hTS in complex with the LR peptide (Cardinale et al., 2011), small-to-medium-sized molecules, such as BME or the LR octapeptide, can access the dimer interface of the enzyme. Thus, the structural evidence indicates that the hTS dimer undergoes either monomer/dimer interconversion or “breathing” movements that allow the binding at the dimer interface of exogenous molecules, such as disulfide fragments.

Several attempts were made to obtain the co-crystal structure of the monomeric hTS in complex with C compounds. All trials failed, always yielding the uncomplexed dimeric hTS structure.

Design of a disulfide-compound library (A1-A55).

Version 8 of the ZINC archive (Irwin and Shoichet, 2005) was screened to recover compounds containing a disulfide function. A preliminary search for S-S bonds was performed using the SMILES notation, finding 1066 molecules. Compounds with the disulfide bond within a cyclic structure (167/1066), and those with a disulfanyl group (SSH, 16/1066) or an oxidized sulphur atom (211/1066) were excluded. The remaining disulfides were subjected to a fragment-likeness analysis: molecular descriptors were calculated with VolSurf+ (Cruciani et al., 2000). LogP and molecular weight (MW) were used to filter out very large and flexible compounds, as well as too hydrophilic or too hydrophobic ones. Finally, multivariate statistical methods such as the Principal Component Analysis (PCA) were used for the final selection of 55 disulfides. The disulfide library is reported in *Supplementary file 3A*.

Design of a library of commercially available compounds (B1-B26) and docking of C3-C5.

A dataset of 331,600 compounds, commercially available from Specs, was downloaded from the ZINC website (www.zinc.org; ZINC version 8) (Irwin and Shoichet, 2005). We retained 242,590 compounds with a MW between 300 and 500 amu. Then we used SMARTS open babel (O'Boyle et al., 2011), (http://openbabel.org/wiki/Main_Page) to search for the presence of specific fragments (Figure 3): 97% of compounds were filtered out. Then, a library of 5,774 compounds was screened against WT hTS (1HVV) focusing on the subunit-subunit interface close to Y202. We used FLAP (Cross et al., 2010) to build two receptor-based pharmacophore models, to screen the library versus these receptor-models, and to dock the most interesting candidates into the binding pockets. Each molecule was subjected to a conformational analysis and the Molecular Interaction Fields (MIF) were generated with the GRID probes DRY, O, N1 and H. Out of compounds with the highest overall scores (> 0.60 for both receptor-based pharmacophore models), we selected a subset of 26 compounds, available for purchase at the time of study, and displaying reasonable structural diversity (Supplementary file 4A). Compounds **C3**, **C4** and **C5** were docked against WT hTS (1HVV) focusing on the subunit-subunit interface close to Y202, using Autodock, version 4.2, software (Morris et al., 1998).

Mass Spectrometry (MS) studies. Matrix-Assisted Laser Desorption/Ionization (MALDI) - Time of Flight (TOF) (Voyager-Pro MALDI-TOF (Applied Biosystems)) was chosen for a medium-throughput screening of the disulphide-compound library (**A1-A55**). The results obtained were validated using an Electron Spray Ionization Quadrupole - Time of Flight (ESI-QTOF) MS (Quadrupole - Time of Flight (ESI-QTOF) mass spectrometer (Agilent Technologies

Inc.)). Analyzing our pools with both platforms allowed us to exclude any ionization-related issue in the ligand selection process. The screening approach was an iterative selection of the best ligands in a competitive environment obtained by arranging the ligands in pools properly chosen to avoid ambiguous assignments. Successive screening steps were performed in which the selected ligands from the previous screening were subjected to further screening using a differently constituted pool. For the disulphide-compound library screening up to 3 ligands were pooled and mixed a hTS-C195S-Y202C solution in a buffer containing 1 mM 2-mercaptoethanol and 20 mM potassium phosphate (pH 7.5). The reaction mixture was incubated at room temperature for 1 hour and then purified on a C4 ZipTip® (Millipore) to remove salts and unbound ligands. Details of the methods used for MS disulphide-compound library screening are reported in *Appendix I*. To identify the binding site of these molecules, the protein-ligand complexes underwent enzymatic digestion in a bottom-up proteomic analysis using both ionization techniques for result evaluation. Details of the methods used are reported in *Appendix I*.

Fluorescence experiments.

To investigate the dimer/monomer equilibrium modulation by the selected compounds, we employed a previously developed FRET assay in which hTS was tagged with fluorescein (F, excitation energy donor) and tetramethylrhodamine (T, acceptor) probes as described in (Genovese et al., 2010). Tagging yielded samples with spectrophotometrically determined F:T:protein-dimer concentration ratios near the expected 1:1:1 values. Absorption spectra were measured on a Varian Cary 100 UV-vis spectrophotometer. Fluorescence spectra were measured on a Spex-JobinYvon Fluoromax2 spectrofluorometer. Usually, samples with

spectrophotometrically determined protein and probe concentrations in the range 50-490 nM in phosphate buffer at pH 7.5 were excited at 450 nm, a wavelength at which the F/T excitation ratio is very high and T emission is almost negligible. All measurements were performed at 20 ± 3 °C. The value of the observed FRET efficiency, Φ_{FRET} , was determined from the emission intensities at 580 nm, I_{580} , the maximum of sensitized T emission, and at 520 nm, the maximum of residual F emission, I_{F} (Genovese et al., 2010) (Figure 5A). In the unperturbed dimer such an efficiency is near 1 because a distance that is roughly half the critical Förster distance for the F/T pair separates the C43 and C43' residues of the two subunits (25 Å). On the other hand, it is zero when the protein is fully dissociated. Developed on a spectrofluorometer, the assay has later been adapted to a medium-throughput format. In short, 1 or 2 μL of a 10 mM DMSO solution of each inhibitor was distributed in a 96 well multiplate to a final concentration of 10 or 20 μM together with 300 nM hTS properly derivatized with the two fluorescent probes (at this concentration, in the absence of inhibitors, the more than 95% of the protein is in the dimer form). Control wells contained only hTS, either alone or with 2 μL of DMSO. Each sample was assayed in duplicate. The Tecan GeniusPRO equipment was employed to read the fluorescence emission from each well at both 535 nm (fluorescein signal) and 590 nm (fluorescein and tetramethylrhodamine signals) following excitation at 470 nm. From the I_{590}/I_{535} ratio, the FRET efficiency in each well and its difference with respect to the control wells were determined.

hTS inhibition assay and IC_{50} determination.

All compounds were tested against the hTS enzyme and IC_{50} was measured spectrophotometrically using Spectramax 190 UV/Vis spectrophotometer, 96 wells multiplate reader. The inhibition reactions were conducted as reported (Salo-Ahen et al., 2015). The

compounds were all tested in two different modes: without incubation and after 60' incubation time selected optimization studies. The reaction was followed at $\lambda=340$ nm for 180 seconds in triplicates. Each inhibitor was firstly dissolved in DMSO in a 10mM stock solution. At least 8 concentrations were evaluated considering the compounds solubility (1-100uM) at 37°C. The reaction mixture included the following reagents solutions (a-e) added in the proper order: a, TES buffer 50% v/v (TES/water) (where TES=2-[[1,3-dihydroxy-2-(hydroxymethyl)propan-2-yl]amino]ethane sulfonic acid), 100mM; MgCl₂ 50mM; Ethylenediaminetetraacetic acid (EDTA) 2mM; β -mercapto ethanol-(BME) 150mM; pH 7.4); b, hTS enzyme (0.37uM); c, the inhibitor at the appropriate concentration; d. MTHF cofactor (55uM). e. dUMP is added as last reagent to start the reaction. For incubation studies, solutions a, b and c were added to each well. After a 1-hour incubation, solution d and e were added, and the reaction monitoring started. For both experimental conditions, the final DMSO concentration into the experimental cuvette (for each assayed concentration) was less than 1% v/v to remove a potential DMSO interfering inhibition effect on the catalytic activity of the target enzyme protein. Results were analyzed according to the standard double reciprocal or Dixon plots. Additionally, IC₅₀ values were obtained from nonlinear regression analysis of the initial rate data. All results showed an experimental standard error within the 20%. All the IC₅₀ values are collected in Supplementary file 4.

Enantioseparation and racemization of E7

The enantiomeric separation and biological characterization of E7 are reported in Appendix 3.

Co-elution of compound C3 with the hTS dimer and monomer with anionic exchange Chromatography

hTS monomer and dimer were separated according to their isoelectric point with preparative Anion Exchange Chromatography (AEX) on a Q HP 16/10 column, Cytiva. 300µL of a 50uM hTS solution were injected onto the column and eluted at 2mL/min with a 70mL gradient of 0-1M NaCl in 30mM Tris-HCl, pH=8.2. Two main peaks emerged from the 280nm UV chromatograms of hTS only, that were attributed to protein's monomer and dimer fraction. Indeed, when hTS was incubated with 250µM dUMP and RTX prior to injection to induce dimer formation, the second UV peak was suppressed as expected. hTS was incubated with different **C3** concentrations (4-80µM) prior to FPLC injection to measure its ability to disrupt hTS dimer. The UV-Vis spectrum of each fraction was collected with a Multiskan GO multiplate reader (Thermo Fisher) to confirm hTS-**C3** co-elution by measuring its absorbance at 350nm. Also, all FPLC collected fractions from 4µM experiment were treated to precipitate proteins, and the amount of **C3** was measured by UHPLC tandem HRMS (Orbitrap Q Exactive, Thermo Fisher) (Supplementary file 5). **C3** was quantified in SIM mode after area interpolation into a calibration curve, revealing an excess of compound co-eluting with hTS monomer with respect to dimer. Also, hTS identity and activity of the two peaks was validated with a spectrophotometric kinetic specific assay.

Analysis of combined equilibria and fitting to FRET data and Analysis of a dissociative inhibition mechanism and fitting to data are described in *Appendix 4*. The availability of kinetic inhibition data and FRET study results on compounds **C2-C4** allowed a detailed mechanistic analysis to test the suitability of the proposed mechanism to fit the experimental inhibition results.

Cellular *in vitro* experiments

Fluorescence microscopy. HT-29 cells were plated at $4 \times 10^4/\text{cm}^2$ in IBIDI 15 μ -Slide 8 Well plates for 24 hours and maintained at 37°C, 5% CO₂. Then they were transfected with 500 ng/well of either TS-TC or WT TS using the Lipofectamine 3000 transfection Kit (Invitrogen) and following the manufacturer's recommendations. 24 hours later the medium was removed and 50 μ M **E5-FITC** was added to the cells for 6 hours. Subsequently, the compound was removed, cells were washed with Opti-MEM reduced Serum Medium (Gibco), stained with the TC-ReAsh II in-cell Tetracysteine Tag Detection Kit (Life Technologies Corporation) according to the manufacturer's recommendations for 60 minutes. Then, the cells were washed three times with Opti-MEM, twice with BAL and placed in Opti-MEM until visualization. The image acquisition was done on a Leica SP8 confocal microscope. Subsequent FRET analysis was performed using PixFRET (Version 1.5.0) within ImageJ (Version 1.52e). Each dot represents the total FRET area of an individual field with at least 10 cells. The statistical analysis was performed using unpaired two tailed t-test (P value >0,0001) using Prism 8 for windows (version 3.1.1).

Experiments on cells.

Cell lines. The human ovarian cancer cell lines IGROV-1, TOV112D, 2008, C13*, A2780 and A2780/CP were grown as monolayers in RPMI 1640 medium. The C13* and A2780-CP human ovarian carcinoma cell lines are 9- to 15-fold resistant to cisplatin (cDDP) and derived from the parent 2008 and A2780 cell lines (Marverti et al., 2013; Beaufort et al., 2014). The HT29, HCT116, and LoVo cell lines were cultured in DMEM medium (Euroclone, Devon, UK). Cell culture media were supplemented with 10% heat-inactivated fetal bovine serum (Euroclone) and 1% Pen/Strep (Euroclone). The PDAC primary cell cultures were established from patients undergoing pancreatic duodenectomy, as described previously (Giovannetti et al., 2014). All

experiments in the present study utilized cells collected during passages 5 to 8. Cultures were equilibrated with humidified 5% CO₂ in air at 37 °C. All studies were performed in Mycoplasma negative cells, as routinely determined with the Myco Alert Mycoplasma detection kit (Lonza, Walkersville, MD, USA).

Cell density. Cell growth was determined using a modified crystal violet assay (Marverti et al., 2009). After 72-h treatment with **E5**, **E7** and **5FU**, the cell monolayer was fixed and stained with 0.2% crystal violet solution in 20% methanol for at least 30 minutes. After washing to remove excess dye, the incorporated dye, proportional to the cell number, was solubilized in acidified isopropanol (1N HCl: 2-propanol, 1:10) and determined spectrophotometrically at 540 nm. The percentage of cytotoxicity was calculated by comparing the absorbance of cultures exposed to the drug with un-exposed (control) cultures. The PDAC cell growth was evaluated using the sulforhodamine B assay after exposure for 72 hr (Giovannetti et al., 2014).

Half-life determination using cycloheximide. A2780 cells were analysed for hTS protein half-life using cycloheximide (90 µg/mL; for 0, 3, 6, 9, 12 and 22 hrs).

Treatment of cancer cells with cycloheximide. Cells were treated with **E5** or **E7** at concentrations corresponding to their IC₅₀ values or 2xIC₅₀ and harvested at different times (0, 1, 2 and 3 hrs) in the presence of medium containing 90 µg/ml of cycloheximide. The A2780 cells were treated with **E7** and then with a proteasome inhibitor (MG132 10 µM) for 5h.

HCT116 cell transfection and cycloheximide treatment. HCT116 cells were transfected by the reverse transfection, using MirusIT-X2 reagent. The reverse transfection increases the % of transfection and makes it homogeneous. The complexes were made with a ratio of 1:3 between DNA and reagent (2.5ug of TS-MYC-DDK-WT or TS-MYC-DDK-F59A and 7.5 ul of the reagent). The complexes were incubated 20 min at RT and in the meantime the cells were

1151 counted to be seeded (500.000 cells/well of a 6-well). After 24 hours from transfection the cells
1152 were treated with cycloheximide (CHX, 60 ug/ml) for 0, 6 and 10 hours to evaluate the hTS
1153 degradation.

1154 *Cellular TS catalytic assay.* Extracts from exponentially growing cells were used for the TS
1155 catalytic assay, by measuring the amounts of ^3H released during the TS-catalyzed conversion of
1156 $[5\text{-}^3\text{H}]\text{dUMP}$ to dTMP, as previously reported (Marverti et al., 2009). Briefly, the enzyme and
1157 650 μM MTHF were contained in a final volume of 50 μl of the assay buffer. The reaction was
1158 started by adding $[5\text{-}^3\text{H}]\text{dUMP}$ (1 μM final concentration, specific activity 5 mCi/mol), followed
1159 by incubation at 37°C for 60 min, and was stopped by adding 50 μl of ice-cold 35%
1160 trichloroacetic acid. Residual $[5\text{-}^3\text{H}]\text{dUMP}$ was removed by adding 250 μl of 10% neutral
1161 activated charcoal. The charcoal was removed by centrifugation at 14,000g for 15 min at 4°C,
1162 and a 150- μl sample of the supernatant was assayed for tritium radioactivity in the liquid
1163 scintillation analyzer Tri-Carb 2100 (Packard).

1164 *Western blotting.* Cells were harvested and washed in ice-cold PBS and suspended in RIPA
1165 buffer supplemented with protease and phosphatase inhibitors (Sigma Aldrich). The insoluble
1166 debris was removed by centrifugation at 14,000g for 30 min. Cellular extracts were resolved
1167 using 12% SDS-PAGE and transferred to PVDF membranes (Hybond-P, Amersham).
1168 Immunoblot analysis was performed using anti-hTS (clone TS106, Millipore, 1:500 dilution),
1169 anti-hDHFR (clone 872442, Millipore, 1:1000) and anti-FLAG M2 (clone M2, F1804, Sigma-
1170 Aldrich, 1:1000 dilution), anti- β -Actin (clone AC-15, Santa Cruz Biotechnology, 1:1500
1171 dilution). Horseradish peroxidase-conjugated secondary antibody (GE Healthcare UK Limited)
1172 was used to detect the bound primary antibody. Immune complexes were visualized by enhanced
1173 chemiluminescence (Amersham™ ECL™ Prime Western blotting reagent) following the

1174 manufacturer's instructions. Band density was calculated using Image J software or an image
1175 analyzer (GS-690 BIORAD).

1176 *Treatment of A2780 with E7 and cross-linking experiments.* The human ovarian cancer cell line
1177 A2780 were exposed to E7 (stock solution 20 mM) at the final concentrations of 20 μ M or
1178 vehicle (DMSO 0.1%) for 3 hours. The E7 dose was decided based on the IC₅₀ of this compound
1179 in these cells. Proteic extracts from human A2780 cells exposed to E7 or vehicle (DMSO) were
1180 cross-liked for 1 h at room temperature with Bis(sulfosuccinimidyl)suberate (BS³) (3mM)
1181 (Sigma) on a rocker and then processed with the standard procedure (see western-blotting
1182 section) (Shi et al., 2017).

1183 *RNA Extraction and qPCR.* Total RNA was isolated from the cells using TRIzol Reagent
1184 (Invitrogen). Reverse transcription was performed with 0.5 μ g or 0.25 μ g of total RNA using
1185 SuperScript first-strand synthesis for RT-PCR (Invitrogen). RT-PCR was performed with 50 ng
1186 of cDNA using SsoAdvanced Universal SYBR Green Supermix (Bio-Rad Laboratories).
1187 Samples were amplified by an initial denaturation at 95°C for 30 s, followed by 40 cycles of
1188 denaturation at 95°C for 10 s, primer annealing at 60°C for 30 s, in CFX Connect Real-Time
1189 PCR machine (Bio-Rad Laboratories). The amplified were analyzed by the CFX maestro
1190 software (Bio-Rad Laboratories). The amount of target expressed was normalized with GAPDH.

1191 24 hours after transfection, total RNA was isolated from HCT116 tranfected with hTS-Myc-
1192 DDK-F59A mutant and hTS-Myc-DDK tagged wild type vectors (N= 6 for each vectors from
1193 two indipendent experiment) and analyzed as previously described. Two primer pairs were
1194 designed for hTS target, one pair to amplify the total hTS mRNA and one pair for the exogenous
1195 hTS mRNA: FW_hTS1, *GCCCAAGTCCCCTTCTTCTC*; REV_hTS,
1196 *AGCGAGAACCCAGACCTTTC*; FW_hTS2, *AGCGAGAACCCAGAC CTT TC*; REV-FLAG,

1197 *TCATTGCTGCCAGATCCTCTT*. For the reference target: GAPDH primer forward (hGAPDH1
1198 fw) (Sigma Genosys 1062, 3174-083): 5'-*CAAGGTCATCCATGACAACCTTTG*-3', reverse: 5'-
1199 *GGGCCATCCACAGTCTTCTG*-3' (hGAPDH1 rw) (Sigma Genosys 1062, 3174-084). The
1200 expressions levels of total (endogenous plus exogenous) and exogenous hTS mRNAs were not
1201 significantly different ($t= 0.248$, $p= 0.809$ and $t= 1.583$, $p= 0.145$ respectively (see
1202 *Supplementary file 3*).

1203 TS mRNA expression in the primary pancreatic cancer cells were measured by standard curves
1204 obtained with dilutions of cDNA from Quantitative-PCR Human-Reference Total-RNA
1205 (Stratagene), as described previously (Zucali PA et al. 2011).

1206
1207 *hTS-F59A mutant generation*. Human thymidylate synthase (TYMS)-Myc-DDK-tagged vector
1208 (Origene RC204814) was used to generate a hTS-F59A mutant. hTS mutations were introduced
1209 by PCR, using the GENEART® Site-Directed Mutagenesis System (Invitrogen). The mutagenic
1210 oligonucleotides used were: FW_hTS-F59A: *GGC ACC CTG TGC GTA GCC GGC ATG CAG*
1211 *GCG CG*; REV_hTS-F59A: *CAC GCC TGC ATG CCG GCT ACC GAC AGG GTG CC*. PCRs
1212 for single amino acid mutations were run for 18 cycles of 20 seconds at 94°C and 30 seconds at
1213 57°C, followed by 3 minutes and 40 seconds at 68°C. Then, the products were analyzed on a
1214 0.8% agarose gel, the recombination reaction was performed and DH5α-T1 competent cells were
1215 transformed. The resulting mutated plasmid were verified by DNA sequencing. After
1216 sequencing, 0.5 ug of hTS-MYC-DDK and hTS-MYC-DDK-F59A vectors were loaded on the
1217 agarose gel to determine the purity of DNA isolation.

1218 *Apoptosis*. After treatment, cells were stained with Annexin V and PI according to the
1219 manufacturer's protocol (Immunological Sciences, IK-11130). Then, apoptotic cells percentage

was evaluated by flow cytometry. 1×10^6 cells were washed with PBS and stained with 2 μ l of Annexin V and 2 μ l of PI in $1 \times$ binding buffer for 15 min at room temperature in the dark. Early apoptotic cells (Annexin V-positive, PI-negative), late apoptotic cells (Annexin V-positive and PI positive) and necrotic cells (Annexin V-negative, PI-positive) were included in cell death measurements (*Figure 7-figure supplement 2*). Staurosporine treatment was used as a positive control (FACS Coulter Epics XL flow cytometer). An example of the gating strategy used for cell analysis is in *Figure 7 - Figure supplement 2*.

Pharmacokinetic studies on BALB/c mice of E5 and E7.

We tested both compounds in a preliminary pharmacokinetic study (Snapshot-PK) (Li et al., 2013).

Female BALB/c mice were purchased from Charles River Laboratories and maintained at IBMC Animal Facilities, in sterile IVC cabinets, with food and water available ad libitum. All animals used in experiments were aged from six to eight weeks. The mice were randomized into four groups of six and then treated with **E7** or **E5** evaluating two independent administration routes, oral or intra-venous (IV). The doses administered were 1 mg/kg for I.V. (administered in 100 μ l in the tail vein) and 20 mg/kg for per os (oral gavage with 100 μ l). Blood samples were taken from the tail vein at specific time points to heparinized tubes (two animals for each time point were used with around 20 μ l of total blood recovered), plasma was recovered by centrifugation and stored at -20°C until quantification by UHPLC-MS/MS ESI+. Plasma samples from 6 BALB/c mice treated with (1m/kg/IV or 20 mg/kg/oral) compound **E5** or **E7** recovered at 0, 5, 15, 30, 45, 60, 120, 300 min and 24, 48 or 72 hours post administration for IV or 0, 30,45,60,120,180, 300 min and 24, 48 and 72 hours post administration. The detection of the compounds in the plasma was done by UHPLC-MS/MS ESI+ (Acquity Quattro Premier

1243 WATERS, column Acquity BEH HILIC 1,7 μ m (2,1 x 100 mm). All data are reported in *Figure*
1244 *8-source data 1*. All animal experiments were carried out in accordance with the IBMC.INEB
1245 Animal Ethics Committees and the Portuguese National Authorities for Animal Health
1246 guidelines, according to the statements on the Directive 2010/63/EU of the European Parliament
1247 and of the Council. NS and ACS have an accreditation for animal research given by the
1248 Portuguese Veterinary Direction (Ministerial Directive 1005/92).

1249

1250 ***In vivo* cancer mouse model studies**

1251 *Orthotopic model*. The orthotopic pancreatic ductal adenocarcinoma (PDAC) cancer mouse
1252 model was generated via direct injection of the primary PDAC-2 cells, transduced with a
1253 lentiviral vector containing Gaussia luciferase (G-luc), in the pancreas of female nude mice (age
1254 6–8 weeks) anesthetized with isoflurane, as described previously (Giovannetti et al., 2014,
1255 Wurdinger et al., 2008). Pre-/post-operative pain was counteracted by administering Temgesic
1256 (0.05-0.1 mg/kg SC). Frozen tumors from PDAC-2 mice treated with E7 or 5FU (24 hours
1257 before their sacrifice) were used for RNA and protein extraction, as described above, to evaluate
1258 the mRNA expression of hTS, compared with untreated control mice using already validated
1259 primers for Real-time PCR (FW: 5'-CAGATTATTCAGGACAGGGAGTT-3'; RW: 5'-
1260 CATCAGAGGAAGATCTCTTGGAT T-3'). Immunohistochemical (IHC) staining were performed
1261 according to standard procedures. Sections of 3 μ m pancreatic slices were cut from paraffin-
1262 embedded specimens. IHC was performed with the anti-hTS antibody described above (dilution
1263 1:100), as well as with the anti-Cleaved Caspase-3 (Asp175) Antibody #9661 (dilution 1:100,
1264 Cell Signaling, Danvers, MA, USA) and the anti-Ki67 monoclonal antibody (dilution 1:100,
1265 clone MIB1; DBA, Milan, Italy), as described previously (Bianco C. et al. 2004, Jun-Jun Su et al.

1266 2018). Visualization was obtained with Bench Mark Special Stain Automation system (Ventana
1267 Medical Systems, inc., USA).

1268 *Antitumor activity.* Orthotropic PDAC models were generated via injection of 10^6 primary cells
1269 into the pancreas of six six/eight weeks old female athymic nude mice (Charles River). Tumor
1270 growth was monitored using bioluminescence imaging (BLI) of Gaussian luciferase (G-luc)
1271 reporter. Five days after surgery, mice were stratified based on BLI intensities into three groups
1272 with comparable G-luc activity. Six mice per group were treated with 10 mg/kg **E7** 3
1273 times/week (every 2 days) every 3 weeks (administered intraperitoneally, i.p.), or 100 mg/kg
1274 **5FU**i.p. once per week for 3 weeks (or q7dx3) (Giovannetti et al., 2014), whereas six control
1275 mice were treated only with sterile saline. Mice were sacrificed upon discomfort or >10% weight
1276 loss, and the log-rank test was used to evaluate significant differences in survival. Pancreas and
1277 internal organs were removed and frozen or fixed in 4% paraformaldehyde. To evaluate the
1278 modulation of hTS *in vivo*, two mice of the control group were exposed to a single dose of **E7** or
1279 **5FU** 24 hours before their sacrifice. qPCR and immunohistochemical studies were performed as
1280 described above. Animal experiments were approved by the Committees on Animal Experiments
1281 of the VU University Amsterdam, The Netherlands and of the University of Pisa, Pisa, Italy, and
1282 were performed in accordance with institutional guidelines and international law and policies.

1283 *Xenograft model.* Athymic Nude-Foxn1nu female mice aged 7 weeks (Envigo RMS Srl, Udine,
1284 Italy) were housed and handled under aseptic conditions, in accordance with the University of
1285 Ferrara Institutional Animal Care and Use Committee guidelines.

1286 *Antitumor activity.* Tumor xenografts in mice were obtained by subcutaneously implanting (s.c.)
1287 with 2×10^6 of A2780 cells suspended in 100 μ L of PBS and 100 μ L of Matrigel (BD

Biosciences). When tumor mass became palpable in successfully engrafted mice (around 7 days after the injection), animals were weighed and randomly divided into three groups to be subjected to various treatments as indicated in *Figure 8-figure supplement 1*. Treatments administrated via intraperitoneal injection were **E7**, 5FU and vehicle solutions. **E7** was administrated 10 mg/Kg three times a week while 5FU (100mg/Kg) one time a week. During the experiment there was no difference in body weight between control and treatment groups. Tumor growth was monitored daily, and tumor diameters were measured with calipers every two days. The tumor volume was calculated using the following equation: $\text{volume} = \pi/6 \times (a \times b^2)$, where **a** is the major diameter and **b** is the minor diameter. All mice that reached the endpoint of the experiment were euthanized and, subsequently, tumors were excised.

1310
1311
1312
1313
1314
1315
1316
1317
1318
1319
1320
1321
1322
1323
1324
1325
1326
1327
1328
1329
1330
1331
1332
1333

References

Adams PD, Afonine PV, Bunkóczi G, Chen VB, Echols N, Headd JJ, Hung L-W, Jain S, Kapral GJ, Kuntsleve RWG, McCoy AJ, Moriarty NW, Oeffner RD, Read RJ, Richardson DC, Richardson JS, Terwilliger TC, Zwart PH. 2011. The Phenix software for automated determination of macromolecular structures. *Methods*. **55**, 94-106.

Avan A, Caretti V, Funel N, Galvani E, Maftouh M, Honeywell RJ, Lagerweij T, Van Tellingen O, Campani D, Fuchs D, Verheul HM, Schuurhuis G-J, Boggi U, Peters GJ, Würdinger T, Giovannetti E. 2013. Crizotinib inhibits metabolic inactivation of gemcitabine in c-Met-driven pancreatic carcinoma. *Cancer Research* **73**: 6745-6756.

Beaufort BM, Helmijr JCA, Piskorz AM, Hoogstraat M, Ruigrok-Ritstier K, Besselink N, Murtaza M, van IJcken WFJ, Heine AAJ, Smid M, Koudijs MJ, Brenton JD, Berns EMJJ, Helleman J. 2014. Ovarian Cancer Cell Line Panel (OCCP): Clinical Importance of In Vitro Morphological Subtypes. *PLoS ONE* **9**, e103988.

Berendsen HJC, Postma JPM, van Gunsteren WF, DiNola A, Haak JR. 1984. Molecular-Dynamics with Coupling to an External Bath. *Journal of Chemical Physics* **81**, 3684–3690.

1334 Berger SH, Berger FG, Lebioda L. 2004. Effects of ligand binding and conformational switching
 1335 on intracellular stability of human thymidylate synthase. *Biochimica et Biophysica Acta*
 1336 **1696**: 15-22.

1337 Bianco C, Giovannetti E, Ciardiello F, Mey V, Nannizzi S, Tortora G, Troiani T, Pasqualetti F,
 1338 Eckhardt G, de Liguoro M, Ricciardi S, Del Tacca M, Raben D, Cionini L, Danesi R. 2006.
 1339 Synergistic antitumor activity of ZD6474, an inhibitor of vascular endothelial growth factor
 1340 receptor and epidermal growth factor receptor signaling, with gemcitabine and ionizing
 1341 radiation against pancreatic cancer. *Clin Cancer Res.* **1**:7099-107.

1342 Bracht K, Nicholls AM, Liu Y, Bodmer WF. 2010. 5-Fluorouracil response in a large panel of
 1343 colorectal cancer cell lines is associated with mismatch repair deficiency. *British Journal of*
 1344 *Cancer* **103**: 340-346.

1345 Brady G, Stouten P. Fast prediction and visualization of protein binding pockets with PASS.
 1346 2000. *Journal of Compututer Aided Molecular Design* **14**, 383-401.

1347 Brunn ND, Dibrov SM, Kao MB, Ghassemian M, Hermann T. 2014. Analysis of mRNA
 1348 recognition by human thymidylate synthase. *Bioscience Reports* **34**: e00168.

1349 Cardinale D, Guaitoli G, Tondi D, Luciani R, Henrich S, Salo-Ahen OMH, Ferrari S, Marverti
 1350 G, Guerrieri D, Ligabue A, Frassineti C, Pozzi C, Mangani S, Fessas D, Guerrini R,
 1351 Ponterini G, Wade RC, Costi MP. 2011. Protein-protein interface-binding peptides inhibit
 1352 the cancer therapy target human thymidylate synthase. *Proceedings of the National Academy*
 1353 *of Sciences USA* **108**, E542-E549.

1354 Cardinale D, Guaitoli G, Tondi D, Luciani R, Henrich S, Salo-Ahen OMH, Ferrari S, Marverti
 1355 G, Guerrieri D, Ligabue A, Frassineti C, Pozzi C, Mangani S, Fessas D, Guerrini R,

1356 Ponterini G, Wade RC, Costi MP.2011. Protein-protein interface-binding peptides inhibit the
 1357 cancer therapy target human thymidylate synthase. *PNAS* **108**: E542-E549.
 1358 Carreras CW, Santi DV. 1995. The catalytic mechanism and structure of thymidylate synthase.
 1359 *Annual Review of Biochemistry* **64**: 721-762.
 1360 Case DA, Cheatham TE III, Darden T, Gohlke H, Luo R, Merz KM Jr, Onufriev A, Simmerling
 1361 C, Wang B, Woods RJ. 2005. The Amber biomolecular simulation programs. *Journal of*
 1362 *Computational Chemistry* **26**, 1668-1688.
 1363 Chu E, Koeller DM, Casey JL, Drake JC, Chabner BA, Elwood PC, Zinn S, Allegra CJ.
 1364 1991. Autoregulation of human thymidylate synthase messenger RNA translation by
 1365 thymidylate synthase. *PNAS* **88**: 8977–8981.
 1366 Costi MP, Ferrari S, Venturelli A, Calò S, Tondi D, Barlocco D.2005. Thymidylate synthase
 1367 structure, function and implication in drug discovery. *Current Medicinal Chemistry* **12**:
 1368 2241-2258.
 1369 Cross S, Baroni M, Carosati E, Benedetti P, Clementi S.2010. FLAP: GRID molecular
 1370 interaction fields in virtual screening. Validation using the DUD data set. *Journal of*
 1371 *Chemical Information and Modeling* **50**: 1442-1450.
 1372 Cruciani G, Crivori P, Carrupt PA, Testa B. 2000. Molecular fields in quantitative structure-
 1373 permeation relationships: the VolSurf approach. *Journal of Molecular Structure*:
 1374 *THEOCHEM* **503**, 17-30.
 1375 Duan Y, Wu C, Chowdhury S, Lee MC, Xiong G, Zhang W, Yang R, Cieplak P, Luo R, Lee
 1376 T, Caldwell J, Wang J, Kollman P. 2003. A point-charge force field for molecular mechanics
 1377 simulations of proteins based on condensed-phase quantum mechanical calculations. *Journal*
 1378 *of Computational Chemistry* **24**, 1999-2012.

1379 Dundas J, Ouyang Z, Tseng J, Binkowski A, Turpaz Y, Liang J. 2006. CASTp: computed atlas
 1380 of surface topography of proteins with structural and topographical mapping of functionally
 1381 annotated residues. *Nucleic Acids Research* **34**, W116-W118.
 1382 Emsley P, Lohkamp B, Scott WG, Cowtan K. 2010. Features and development of Coot. *Acta*
 1383 *Crystallographica Section D***66**, 486-501.
 1384 Erlanson DA, Braisted AC, Raphael DR, Randal M, Stroud RM, Gordon EM, Wells JA.
 1385 2000.Site-directed ligand discovery. *PNAS***97**: 9367-9372.
 1386 Essmann U, Perera L, Berkowitz ML, Darden T, Lee H, Pedersen LG. 1995. A smooth particle
 1387 mesh Ewald method. *Journal of Chemical Physics* **103**, 8577-8593.
 1388 Evans P. 2006. Scaling and assessment of data quality. *Acta Crystallographica Section D***62**, 72
 1389 Genovese F, Ferrari S, Guaitoli G, Caselli M, Costi MP, Ponterini G. 2010.Dimer-monomer
 1390 equilibrium of human thymidylate synthase monitored by fluorescence resonance energy
 1391 transfer. *Protein Science* **19**, 1023-1030.
 1392 Giovannetti E, Wang Q, Avan A, Funel N, Lagerweij T, Lee J-H, Caretti V, van der
 1393 VeldeA, Boggi U, Wang Y. 2014. Role of CYB5A in Pancreatic Cancer Prognosis and
 1394 Autophagy Modulation. *Journal of the National Cancer Institute* **106**,
 1395 djt346, <https://doi.org/10.1093/jnci/djt346>
 1396 Goodford PJ. 1985. A computational procedure for determining energetically favorable binding
 1397 sites on biologically important macromolecules. *Journal of Medicinal Chemistry* **28**, 849-
 1398 857.
 1399 Henrick K, Thornton JM. 1998. PQS: a protein quaternary structure file server. *Trends in*
 1400 *Biochemical Sciences***199823**, 358-361.

1401 IrwinJJ, Shoichet BK.2005. ZINC – A free database of commercially available compounds for
 1402 virtual screening. *Journal of Chemical Information and Modeling***45**: 177-182.

1403 Jennings BA, Willis G.2015. How folate metabolism affects colorectal cancer development and
 1404 treatment; a story of heterogeneity and pleiotropy. *Cancer Letters* **356**: 224-230.

1405 Jorgensen WL, Chandrasekhar J, Madura JD, Impey RW, Klein ML. 1983. Comparison of
 1406 simple potential functions for simulating liquid water. *Journal of Chemical Physics* **79**, 926-
 1407 935.

1408 Su JJ, Xu K, Wang PF, Zhang HY, Chen YL. 2018 Histological analysis of human pancreatic
 1409 carcinoma following irreversible electroporation in a nude mouse model. *World J Gastrointest*
 1410 *Oncol.* 10, 476-486.

1411 Kim OT, Yura K, Go N. 2006. Amino acid residue doublet propensity in the protein-RNA
 1412 interface and its application to RNA interface prediction. *Nucleic Acids Research***34**, 6450–6460.

1413 Kitchens ME, Forsthoefel AM, Barbour KW, Spencer HT, Berger FG. 1999. Mechanisms of
 1414 acquired resistance to thymidylate synthase inhibitors: the role of enzyme stability.
 1415 *Molecular Pharmacology* **56**: 1063-1070.

1416 Kitchens ME, Forsthoefel AM, Rafique Z, Spencer HT, Berger FG.1999. Ligand mediated
 1417 induction of thymidylate occurs by enzyme stabilization. *Journal of Biological Chemistry*
 1418 **274**: 12544-12547.

1419 Langer G, Cohen SX, Lamzin VS, Perrakis A. 2008. Automated macromolecular model building
 1420 for X-ray crystallography using ARP/wARP version 7. *Nature Protocols* **3**, 1171-1179.

1421 Laskowski RA, MacArthur MW, Moss DS, Thornton JM. 1993. PROCHECK - a program to
 1422 check the stereochemical quality of protein structures. *Journal of Applied Crystallography*
 1423 **26**, 283-291.

1424 Leslie AG. 2006. The integration of macromolecular diffraction data. *Acta Crystallographica*
1425 *Section D***62**, 48-57.

1426 Li C, Liu B, Chang J, Groessl T, Zimmerman M, He YQ, Isbell J, Tuntland T. 2013. A modern in
1427 vivo pharmacokinetic paradigm: combining snapshot, rapid and full PK approaches to
1428 optimize and expedite early drug discovery. *Drug Discovery Today* **18**, 71-78.

1429 Lovelace LL, Minor W, Lebioda L. 2005. Structure of human thymidylate synthase under low-
1430 salt conditions. *Acta Crystallographica Section D***61**, 622-627.

1431 Marverti G, Ligabue A, Lombardi P, Ferrari S, Monti MG, Frassinetti C, Costi MP. 2013.
1432 Modulation of the expression of folate cycle enzymes and polyamine metabolism by
1433 berberine in cisplatin-sensitive and -resistant human ovarian cancer cells. *International*
1434 *Journal of Oncology* **43**, 1269-1280.

1435 Marverti G, Ligabue A, Paglietti G, Corona P, Piras S, Vitale G, Guerrieri D, Luciani R, Costi
1436 MP, Frassinetti C, Moruzzi MS. 2009. Collateral sensitivity to novel thymidylate synthase
1437 inhibitors correlates with folate cycle enzymes impairment in cisplatin-resistant human
1438 ovarian cancer cells. *European Journal of Pharmacology* **615**, 17-26.

1439 McNicholas S, Potterton E, Wilson KS, Noble MEM. 2011. Presenting your structures: the
1440 CCP4mg molecular-graphics software. *Acta Crystallographica Section D***67**, 386-394.

1441 Mei G, Di Venere A, Rosato N, Finazzi-Agrò A. 2005. The importance of being dimeric, *FEBS*
1442 *Journal* **272**: 16-27.

1443 Morris GM, Goodsell DS, Halliday RS, Huey R, Hart WE, Belew R, Olson AJ. 1998. Automated
1444 docking using a Lamarckian genetic algorithm and empirical binding free energy function.
1445 *Journal of Computational Chemistry* **19**, 1639–1662.

1446 Murshudov GN, Vagin A, Dodson EJ. 1997. Refinement of macromolecular structures by the
 1447 maximum-likelihood method. *Acta Crystallographica Section D***53**, 240-255.

1448 O'Boyle NM, Banck M, James CA, Morley C, Vandermeersch T, Hutchison GR. 2011. Open
 1449 Babel: An open chemical toolbox. *Journal of Cheminformatics***3**, 33.

1450 Peña MM, Melo SP, Xing YY, White K, Barbour KW, Berger FG. 2009. The intrinsically
 1451 disordered N-terminal domain of thymidylate synthase targets the enzyme to the ubiquitin-
 1452 independent proteasomal degradation pathway. *Journal of Biological Chemistry***284**: 31597-
 1453 31607.

1454 Peters GJ, Backus GJ, Freemantle HHJ, Van Triest S, Codacci-Pisanelli B, Van der Wilt G,
 1455 Smid CL, Lunec K, Calvert J, Marsh AH, McLeod SHL, Bloemena E, Meijer S, Jansen G,
 1456 van Groenigen GC, Pinedo HM. 2002. Induction of thymidylate synthase as a 5-fluorouracil
 1457 resistance mechanism. *Biochimica et Biophysica Acta* **1587**: 194-205.

1458 Peters GJ. 2018. Cancer drug resistance: a new perspective. *Cancer Drug Resistance***1**: 1-5.

1459 Phan J, Koli S, Minor W, Dunlap RB, Berger SH, Lebiada L. 2001. Human thymidylate synthase
 1460 is in the closed conformation when complexed with dUMP and raltitrexed, an antifolate
 1461 drug. *Biochemistry* **40**, 1897-1902.

1462 Ponterini G, Martello A, Pavesi G, Lauriola A, Luciani R, Santucci M, Pelà M, Gozzi G,
 1463 Pacifico S, Guerrini R, Marverti G, Costi MP, D'Arca D. 2016. Intracellular quantitative
 1464 detection of human thymidylate synthase engagement with an unconventional inhibitor using
 1465 tetracysteine-diarsenical-probe technology. *Science Reports* **6**: 27198.

1466 Ryckaert JP, Ciccotti G, Berendsen HJC. 1977. Numerical integration of cartesian equations of
 1467 motion of a system with constraints - molecular dynamics of N-alkanes. *Journal of*
 1468 *Computational Physics* **23**, 327-341.

1469 Salo-Ahen OMH, Tochowicz A, Pozzi C, Cardinale D, Ferrari S, Boum Y, Mangani S, Stroud
 1470 RM, Saxena P, Myllykallio H, Costi MP, Ponterini G, Wade RC. 2015.Hotspots in an
 1471 obligate homodimeric anticancer target. Structural and functional effects of interfacial
 1472 mutations in human thymidylate synthase. *Journal of Medicinal Chemistry* **58**, 3572-3581.
 1473 Shi J-M, Pei J, Liu E-Q, Zhang L. 2017. Bis(sulfosuccinimidyl) suberate (BS3) crosslinking
 1474 analysis of the behavior of amyloid- β peptide in solution and in phospholipid membranes.
 1475 *PLoS ONE***12**(3), e0173871 <https://doi.org/10.1371/journal.pone.0173871>.
 1476 Taddia L, D'Arca D, Ferrari S, Marraccini C, Severi L, Ponterini G, Assaraf YG, Marverti G,
 1477 Costi MP.2015. Inside the biochemical pathways of thymidylate synthase perturbed by
 1478 anticancer drugs: Novel strategies to overcome cancer chemoresistance. *Drug Resistance*
 1479 *Updates* **23**: 20-54.
 1480 Vagin A, Teplyakov A. 1997. MOLREP: an automated program for molecular replacement.
 1481 *Journal of Applied Crystallography***30**, 1022-1025.
 1482 Van der WiltCL, Pinedo HM, Smid K, Peters GJ. 1992. Elevation of Thymidylate Synthase
 1483 following 5-Fluorouracil Treatment Is Prevented by the Addition of Leucovorin in Murine
 1484 Colon Tumors *Cancer Research***52**: 4922-4928.
 1485 Voeller DM, Zajac-Kaye M, Fisher RJ, Allegra CJ. 2002. The identification of thymidylate
 1486 synthase peptide domains located in the interface region that bind thymidylate synthase
 1487 mRNA. *Biochemical and Biophysical Research Communications* **297**: 24-31.
 1488 Wade RC, Goodford PJ. 1993. Further development of hydrogen bond functions for use in
 1489 determining energetically favorable binding sites on molecules of known structure. 2.
 1490 Ligand probe groups with the ability to form more than two hydrogen bonds. *Journal of*
 1491 *Medicinal Chemistry***36**, 148-156.

1492 Wang J, Wang W, Kollman P, Case DA. 2006. Automatic atom type and bond type perception in
 1493 molecular mechanical calculations. *Journal of Molecular Graphics and Modelling* **25**, 247-
 1494 260.

1495 Wang T, Wade RC. 2003. Implicit solvent models for flexible protein-protein docking by
 1496 molecular dynamics simulation. *Proteins* **50**, 158-169.

1497 Wilson PM, Danenberg PV, Johnston PG, Lenz HJ, Ladner RD. 2014. Standing the test of time:
 1498 targeting thymidylate biosynthesis in cancer therapy. *Nature Reviews Clinical Oncology* **11**:
 1499 282-298.

1500 Winn MD, Ballard CC, Cowtan KD, Dodson EJ, Emsley P, Evans PR, Keegan RM, Krissinel
 1501 EB, Leslie AGW, McCoy A, McNicholas SJ, Murshudov GN, Pannu NS, Potterton EA,
 1502 Powell HR, Read RJ, Vagin A, Wilson KS. 2011. Overview of the CCP4 suite and current
 1503 developments. *Acta Crystallographica Section D* **67**, 235-242.

1504 Winn MD, Murshudov GN, Papiz MZ. 2003. Macromolecular TLS refinement in REFMAC at
 1505 moderate resolutions. *Methods in Enzymology* **374**, 300-321.

1506 Wurdinger T, Badr C, Pike L, de Kleine R, Weissleder R, Breakefield XO, Tannous BA. 2008.
 1507 A secreted luciferase for *ex vivo* monitoring of *in vivo* processes. *Nature Methods* **5**, 171-
 1508 173.

1509 Zucali PA, Giovannetti E, Destro A, Mencoboni M, Ceresoli GL, Gianoncelli L, Lorenzi E, De
 1510 Vincenzo F, Simonelli M, Perrino M, Bruzzzone A, Thunnissen E, Tunesi G, Giordano L,
 1511 Roncalli M, Peters GJ, Santoro A. 2011. Thymidylate synthase and excision repair cross-
 1512 complementing group-1 as predictors of responsiveness in mesothelioma patients treated
 1513 with pemetrexed/carboplatin. *Clin Cancer Res.* **17**, 2581-2590.

1514

1515
1516
1517
1518
1519
1520
1521
1522
1523
1524
1525
1526
1527
1528
1529
1530
1531

1532
1533
1534
1535
1536
1537
1538
1539
1540

Acknowledgments: We thank Dr. Hannu Myllykallio for cloning hTS and preparing bacterial cells expressing mutant proteins, and Dr. Amir Avan and Dr. Niccola Funel for their work on PDAC animal models and staining. The authors also acknowledge the ‘Fondazione Cassa di Risparmio di Modena’ for funding the UHPLC-ESI-QTOF system at the Centro Interdipartimentale Grandi Strumenti (CIGS). PP is grateful to Camilla degli Scrovegni for continuous inspirational support.

This work was funded by AIRC2015 IG16977 (MPC), European Union (LIGHTS-A Framework 6 STREP: LSH- 2005-2.2.0-8) Grant agreement n°037852 to M.P.C, R.C.W., G.C., R.M.S; CCA foundation grants-2012/2015 CCA2015-1-19 to E.G. and G.J.P., AIRC 14422 Start-Up grant to E.G., the Klaus Tschira Foundation (R.C.W., S.H., O.M.H.S-A) and the Alexander von Humboldt Foundation, the Finnish Cultural Foundation, the Academy of Finland (137918), and the University of Eastern Finland (O.M.H.S-A). RMS is supported by NIH GM24485. PP is supported by Italian Association for Cancer Research (AIRC, IG23670). AR is supported by the Italian Ministry of Health (GR-2016-02364602) and by the Italian Ministry of Education, University and Research (PRIN, Grant 2017XA5J5N).

1541
1542
1543
1544
1545
1546
1547
1548
1549
1550
1551
1552
1553
1554
1555
1556
1557
1558
1559
1560
1561
1562
1563
1564
1565
1566
1567
1568
1569
1570
1571
1572
1573
1574
1575
1576
1577

LIST OF ADDITIONAL FILES

- 1.**Diffraction data have been deposited in PDB under the accession code PDB-ID 4O1X double humanTS mutant C195SY202C.
- Summary report for the X-ray crystal structures is uploaded as a Related Manuscript File. The maps and coordinates data are uploaded as a Supporting Zip Document and the file is labelled as "maps and coordinates for review".
- 2.** Gels / blots are provided as Source data in (1) the original files of the full raw unedited gels or blots and; (2) figures with the uncropped gels or blots with the relevant bands clearly labelled be provided. Files are: Figure 7-source data 2. Dimer destabilizers and hTS levels in human cancer cell lines, WB; Figure 7 -figure supplement 1-source data 1. Effect of dimer destabilizers on hTS protein levels in cells_WB.
- 3.** Source Data files are available in the files reported below under “Source data” for Figure 3, Figure 3-figure supplement 1, Figure 3-figure supplement 2, Figure 4, Figure 6, Figure 6-figure supplement 1,

Figure 6-figure supplement 2, Figure 6-figure supplement 3, Figure 6-figure supplement 4, Figure 7, Figure 7-figure supplement 1, Figure 8, Figure 8-figure supplement 1. Figure 8-figure supplement 2.

Source data.

Figure 3-figure supplement 1-Source data file 1. Anion-exchange chromatograms of hTS obtained with a 280 nm and 350 nm detection.

Figure 3-figure supplement 2-Source data 1. Profile of the variation in concentration of compound C3 in the AE chromatographic fractions determined by high-resolution MS (UltiMate 3000 UHPLC tandem Orbitrap Q-Ex.

Figure 4-Source data 1. Spectroscopic and mechanistic analysis of hTS dissociative inhibition for compounds C2, C3 and C4.

Figure 4-Source data 2. Inhibition of hTS by compound C3.

Figure 6-figure supplement 1- Source data 1. TS mRNA expression in the primary pancreatic cancer cells. Figure 6-figure supplement 2-Source data1. Pancreatic cancer cells LPc167 growth inhibition for compounds E7, E5 and 5FU.

Figure 6-figure supplement 3-Source data1. Ovarian cancer cell growth inhibition all compounds.

Figure 6-figure supplement 4-Source data1. Colon cancer cell inhibition E7 and E5.

Figure 6-Source data 1. Quantification of Annexin V-positive cells of apoptosis of A2780 and A2780/CP cells treated with E7 or PMX.

Figure 7-Source data for Figures 7A-G are given as individual zip files. Western blot (labelled) data of dimer destabilizers effect on hTS levels in human cancer cell lines (see below the section “Figure 7 contains the following associated files”).

Figure 8-Source data 1. Orthotopic pancreatic cancer in vivo.

Figure 8-figure supplement 1-Source data 1. In vivo effects of E7 on Athymic Nude-Foxn1nu female mice

Figure 8-figure supplement 2-Source data 1. Real time PCR (qPCR). Quantitative PCR (qPCR) measurements of hTS transcripts in A2780 and A2780/CP cells treated with E7, E5 and 5FU.

4. Figure supplements are reported for Figure 1, Figure 2, Figure 3, Figure 4, Figure 6, Figure 7 and Figure 8.

Figure Supplement

Figure 1 - Figure supplement 1. Y202 and K47 pockets at the hTS monomer-monomer interface (PDB ID: 1HVV, A chain)

Figure 2 - Figure supplement 1. X-ray crystallographic structure of hTS-Y202C and hTS C195S-Y202C.

Figure 3-figure supplement 1. Anion-exchange chromatograms of hTS obtained with a 280 nm and 350 nm detection

Figure 3-figure supplement 2. Profile of the variation in concentration of compound C3 in the AE chromatographic fractions determined by high-resolution MS (UltiMate 3000 UHPLC tandem Orbitrap Q-Ex.

Figure 6-supplement 1. TS mRNA expression in the primary pancreatic cancer cells.

Figure 6 – figure supplement 2. Pancreatic cancer cells LPC167 growth inhibition for compounds E7, E5 and 5FU.

Figure 6 - figure supplement 3. Ovarian cancer cell growth inhibition"

Figure 6 - figure supplement 4. Colon cancer cell growth inhibition"

Figure 7 - Figure supplement 1. Effect of cisplatin on cell death, and effect of dimer destabilizers on hTS activity and hTS protein levels in cancer cells.

Figure 7 - Figure supplement 2. Example of gating strategy used for cell analysis

Figure 7 - Figure supplement 3. Expression levels of total (exogenous plus endogenous) and exogenous hTS mRNAs in HCT116 cells with wild-type hTS-Myc-DDK tagged or mutant hTS-Myc-DDK-F59A vectors.

Figure 8 - Figure supplement 1. In vivo effects of E7 on Athymic Nude-Foxn1nu female mice.

Figure 8-figure supplement 2. Representative immunohistochemical images showing extensive caspase-3 activation after treatment with E7.

Figure 8-figure supplement 3. Representative immunohistochemical images showing extensive caspase-3 activation after treatment with E7.

5. Tables are uploaded and cited as Supplementary file 1,2,3,4,5,6 and 7. The separate sections are cited within each file.

Supplementary files (all word files uploaded)

Supplementary file 1. Computational protein-pocket identification for tethering.

Supplementary file 2. X-ray crystallography.

Supplementary file 3. Mass spectrometry data.

Supplementary file 4. Compounds FRET and inhibition data.

Supplementary file 5. Mass Spectrometry analysis of the fractions eluted from AEX.

Supplementary file 6. Cancer cell growth inhibition and pharmacokinetic.

6. Appendix files (uploaded as word) contains the sections with more complex and long analysis content, methods, and synthetic chemistry data:

Appendix 1. Details on Mass Spectrometry methods

Appendix 2. Synthetic chemistry

Appendix 3. Separation of E7 racemic mixture of E7 and characterization.

Appendix 4. Analysis of combined equilibria and fitting to FRET data.

7. All other data generated or analyzed during this study are included in the manuscript and supporting files.

8. All additional files list and description of each Figure with the associated Figure supplement and source data files.

Figure 1 contains the following associated file.

Figure 1 - Figure supplement 1. Y202 and K47 pockets at the hTS monomer-monomer interface (PDB ID: 1HVV, A chain)

Figure 2 contains the following associated file.

Figure 2 - Figure supplement 1. X-ray crystallographic structure of hTS-Y202C and hTS C195S-Y202C

Figure 3 contains the following associated files

Figure 3-figure supplement 1. Anion-exchange chromatograms of hTS obtained with a 280 nm and 350 nm detection

Figure 3-figure supplement 1-Source data file 1. Anion-exchange chromatograms of hTS obtained with a 280 nm and 350 nm detection

Figure 3-figure supplement 2. Concentration profile of compound C3 in the AE chromatographic fractions determined by high-resolution MS (UltiMate 3000 UHPLC tandem Orbitrap Q-Ex).

Figure 3-figure supplement 2-Source data 1. Concentration profile of compound C3 in the AE chromatographic fractions determined by high-resolution MS (UltiMate 3000 UHPLC tandem Orbitrap Q-Ex).

Figure 4 contains the following associated files.

Figure 4-Source data 1. Spectroscopic and mechanistic analysis of hTS dissociative inhibition for compounds C2, C3 and C4.

Figure 4-Source data 2. Inhibition of hTS by compound C3.

Figure 6 contains the following associated files:

Figure 6-Source data 1. Quantification of Annexin V-positive cells of apoptosis of A2780 and A2780/CP cells treated with E7 or PMX.

Figure 6-figure supplement 1. TS mRNA expression in the primary pancreatic cancer cells.

Figure 6-figure supplement 1-Source data 1. TS mRNA expression in the primary pancreatic cancer cells.

Figure 6-figure supplement 2. Pancreatic cancer cells LPc167 growth inhibition for compounds E7, E5 and 5FU.

Figure 6-figure supplement 2-Source data 1. Pancreatic cancer cells LPc167 growth inhibition for compounds E7, E5 and 5FU.

Figure 6-figure supplement 3. Ovarian cancer cell growth inhibition

Figure 6-figure supplement 3-Source data 1. Ovarian cancer cell growth inhibition.

Figure 6-figure supplement 4. Colon cancer cell growth inhibition

Figure 6-figure supplement 4-Source data 1. Colon cancer cell growth inhibition.

Figure 7 contains the following associated files

Figure 7-Source data for Figures 7A-G are given as individual zip files. Western blot (labelled) data of dimer destabilizers effect on hTS levels in human cancer cell lines.

CROPPED

Figure 7 - Source data 1. Effects of E5 on hTS and DHFR protein levels in A2780 and A2780/CP cells.

Figure 7 - Source data 2. Effects of E5 on hTS and DHFR protein levels in A2780 and A2780/CP cells_TS and DHFR_actin.

1717
1718 Figure 7-Source data 3. Effects of E7 on hTS and DHFR protein levels in A2780 and A2780/CP cells.
1719
1720 Figure 7- Source data 4. Effects of E7 on hTS and DHFR protein levels in A2780 and A2780/CP cells_TS
1721 and DHFR_actin.
1722
1723 Figure 7 - Source data 5. hTS protein level in A2780 and A2780/CP cells treated with 5-FU and PMX (
1724 PMX and 5FU Actin).
1725 Figure 7 - Source data 6. hTS protein level in A2780 and A2780/CP cells treated with PMX.
1726
1727 Figure 7 - Source data 7. Stability of hTS in A2780 cells treated with E7 for 12h, followed by treatment
1728 with CHX for the indicated times_actin.
1729 Figure 7 - Source data 8. Stability of hTS in A2780 cells treated with E7 for 12h, followed by treatment
1730 with CHX for the indicated times.
1731
1732 Figure 7 - Source data 9. hTS levels in A2780 cells treated with E7 for 12h, with MG132 for 5h_actin.
1733 Figure 7 - Source data 10. hTS levels in A2780 cells treated with E7 for 12h, with MG132 for 5h.
1734
1735 Figure 7- Source data 11. Effects of a 3 hours exposure to E7 on hTS dimer/monomer equilibrium in
1736 A2780 cells.
1737
1738 Figure 7-Source data 12. Effect of Dimer destabilizers and hTS levels and half-life in human cancer cell
1739 lines (Figure C, D, G).
1740
1741 Figure 7 - Source data 13. Half-life determination of exogenous hTS protein (anti-FLAG stain) in HCT116
1742 cells transfected with TS-Myc-DDK (CHX) or with the F59A mutant (CHX)_actin.
1743 Figure 7 - Source data 14. Half-life determination of exogenous hTS protein (anti-FLAG stain) in HCT116
1744 cells transfected with TS-Myc-DDK (CHX) or with the F59A mutant (CHX).
1745
1746 **UNCROPPED FIGURE 7-SOURCE DATA.**
1747 Figure 7 - Source data 15. Effects of E5 on hTS and DHFR protein levels in A2780 and A2780/CP cells.
1748 uncropped
1749 Figure 7 - Source data 16. Effects of E5 on hTS and DHFR protein levels in A2780 and A2780/CP cells_TS
1750 and DHFR_actin.uncropped
1751
1752 Figure 7-Source data 17. Effects of E7 on hTS and DHFR protein levels in A2780 and A2780/CP cells.
1753
1754 Figure 7- Source data 18. Effects of E7 on hTS and DHFR protein levels in A2780 and A2780/CP cells_TS
1755 and DHFR_actin.
1756
1757
1758 Figure 7 - Source data 19. hTS protein level in A2780 and A2780/CP cells treated with 5-FU and PMX (
1759 PMX and 5FU Actin). uncropped
1760 Figure 7 - Source data 20. hTS protein level in A2780 and A2780/CP cells treated with PMX. Uncropped
1761
1762 Figure 7 - Source data 21. Stability of hTS in A2780 cells treated with E7 for 12h, followed by treatment
1763 with CHX for the indicated times_actin.

Figure 7 - Source data 22. Stability of hTS in A2780 cells treated with E7 for 12h, followed by treatment with CHX for the indicated times.

Figure 7 - Source data 23. hTS levels in A2780 cells treated with E7 for 12h, with MG132 for 5h_actin. uncropped

Figure 7 - Source data 24. hTS levels in A2780 cells treated with E7 for 12h, with MG132 for 5h. uncropped

Figure 7- Source data 25. Effects of a 3 hours exposure to E7 on hTS dimer/monomer equilibrium in A2780 cells. uncropped

Figure 7 - Source data 26. Half-life determination of exogenous hTS protein (anti-FLAG stain) in HCT116 cells transfected with TS-Myc-DDK (CHX) or with the F59A mutant (CHX)_actin. uncropped

Figure 7 - Source data 27. Half-life determination of exogenous hTS protein (anti-FLAG stain) in HCT116 cells transfected with TS-Myc-DDK (CHX) or with the F59A mutant (CHX). uncropped

Figure 7 - figure supplement 1. Effect of cisplatin on cell death, effect of dimer destabilizers on hTS activity and hTS protein levels in cells.

Figure 7-figure supplement 1-Source data 1.Quantification of Annexin V-positive cells by flow cytometric analysis of apoptosis of A2780 and A2780/CP cells treated with cisplatin, E7 and PMX.

Figure 7-figure supplement 1 - Source data 2. Effect of E7 on hTS protein levels in HT29 cells _actin.

Figure 7-figure supplement 1 - Source data 3. Effect of E7 on hTS protein levels in HT29 cells.

Figure 7-figure supplement 1 - Source data 4. Effect of E7 on hTS protein levels in HT29 cells _actin. uncropped

Figure 7-figure supplement 1 - Source data 5. Effect of E7 on hTS protein levels in HT29 cells. uncropped

Figure 7-figure supplement 1 - Source data 6. Effect of dimer destabilizers on hTS protein levels in A2780/CP cells, E7 and actin.

Figure 7-figure supplement 1 - Source data 7. Effect of dimer destabilizers on hTS protein levels in A2780/CP cells, E7 and actin. uncropped

Figure 7-figure supplement 1- Source data 8. TS activity assay for A2780 and A2780/CP cell lines after treatment with E5 and E7.

Figure 7 - figure supplement 2. Example of gating strategy used for cell analysis.

Figure 7 - figure supplement 3. Expression levels of total (exogenous plus endogenous) and exogenous hTS mRNAs in HCT116 cells with wild-type hTS-Myc-DDK tagged or mutant hTS-Myc-DDK-F59A vectors (in Figure 7G).

Figure 8 contains the following associated file.

Figure 8-Source data 1. Orthotopic pancreatic cancer in vivo.

Figure 8 - figure supplement 1. In vivo effects of E7 on Athymic Nude-Foxn1nu female mice

Figure 8-figure supplement 1-Source data 1. *In vivo effects of E7 on Athymic Nude-Foxn1nu female mice*

Figure 8-figure supplement 2. Real time PCR (qPCR). Quantitative PCR (qPCR) measurements of hTS transcripts in A2780 and A2780/CP cells treated with E7, E5 and 5FU.

Figure 8-figure supplement 2-Source data 1. Real time PCR (qPCR). Quantitative PCR (qPCR) measurements of hTS transcripts in A2780 and A2780/CP cells treated with E7, E5 and 5FU.

Figure 8-figure supplement 3. Representative immunohistochemical images showing extensive caspase-3 activation after treatment with E7.

Appendix 2-figures: Appendix 2-figure 1 up to Appendix 2-figure 10.

Appendix 3-figure 1. Structure 2D of the E7 enantiomers.

Appendix 3-figure 2. Chromatograms of single (+/-)-E7 enantiomers.

Appendix 1

Details of Mass Spectrometry (MS) methods.

MS-based disulphide library screening. A solution of each individual library member was prepared in dimethyl sulfoxide (DMSO) to a final concentration of 80 mM per ligand. 1 µL of each ligand solution was then pooled to form groups of a maximum of 3 discrete compounds, having molecular weights that differed by at least 150 Da from one another; each pool was brought to a final volume of 10 µL. 1 µL of the desired ligand pool (8 mM) was added to 20 µL of 19 µM C195S/Y202C hTS double mutant solution in a buffer containing 1 mM 2-mercaptoethanol and 20 mM potassium phosphate (pH 7.5) to a final volume of 40 µL. The protein was present at a concentration of 10 µM while each of the disulphide library members was 0.2 mM. The reaction mixture was incubated at room temperature for 1 hour and then purified on a C4 ZipTip® (Millipore) to remove salts and unbound ligands. A solution of 10 mg/ml of sinapinic acid in acetonitrile/0.1% aqueous TFA in a 1:1 ratio was used to assist the ionization process. 1 µL of the sample was deposited onto a MALDI sample plate and allowed to air-dry at room temperature; 0.5 µL of matrix solution were then deposited on the same spot, resulting in a uniform layer of fine granular protein including matrix crystals. Mass spectra were recorded in positive-ion linear mode at an accelerating voltage of 20 kV and a delayed extraction time of 1200 ns. Each spectrum obtained was the mean of 100 laser shots. The ions were generated using the 337-nm laser beam from a nitrogen laser, having a pulse width of 3 ns. Data were obtained using the following parameters: 95% grid voltage, 0.08% guide wire voltage and a low mass gate of 15000 Da. An external calibration was performed based on the molecular weight of the untreated enzyme mutant previously reduced with DTT, alkylated with

iodoacetamide and diluted 1:10 in TFA 0.1%. The software Data Explorer (Applied Biosystems) was used for mass spectral data processing; raw spectra were smoothed, and the baseline was corrected according to the normally observed peak broadness. Peak m/z values were annotated according to a peak detection algorithm taking into account an average resolution of 3500. The identity of any library member bonded to the protein through a disulphide bond was determined by subtracting the mass of the free protein from the observed higher mass.

For ESI-QTOF measurement 0.5 μ l of ligand (80 mM in DMSO) was added to 12 μ l of 17 μ M C195S/Y202C hTS mutant solution in a buffer containing 1 mM 2-mercaptoethanol and 20 mM potassium phosphate (pH 7.5) to a final volume of 20 μ L. The protein was present at a concentration of 10 μ M and the disulphide at 2mM. After equilibration at room temperature for 1 hour, 1 μ l of the reaction mixture was diluted 1:10 with a solution of 5% formic acid in water/acetonitrile 95:5 and injected onto an HPLC-chip ESI-QTOF. The mobile phase composition was as follows: (A) 0.1%formic acid in a water/acetonitrile 98:2 solution and (B) 0.1%formic acid in a acetonitrile/water 98:2 solution. Chromatographic separations were performed at a flow rate of 400 nL/min with the following gradient: 15% B for 5 min, 15–85% B in 5 min, 85% B for 5 min, 85-15% B in 3 min. Under these conditions the protein-ligand complex was eluted between 6.5 and 8.0 min. The capillary voltage was set to 1600 V and the desolvating temperature was 350°C. Nitrogen was used as a drying gas (flow rate = 6 L/min). The mass spectrometer operated in positive mode in the scan range 200-3200 Da. An external calibration was performed based on the molecular weight of a multi-standard solution (ESI-L Low concentration tuning mixture - SUPELCO). During acquisition, some of these masses were constantly monitored and used for a fine calibration of the instrument. The multiply charged ions

deriving from the free protein and the protein-ligand complex were deconvoluted with available software (MassHunter – Agilent Technologies Inc.).

Analysis of the ligand-protein binding site by MS. To investigate the cysteine residue involved in the binding with the selected ligands, the protein-ligand complexes underwent enzymatic digestion in a classical bottom-up proteomic analysis using both ionization techniques for result evaluation.

In a typical experiment, 1 μ L of the ligand (80 mM in DMSO) was added to 14 μ L of the 29 μ M hTS C195S-Y202C hTS mutant solution in a buffer containing 2 mM 2-mercaptoethanol and 20 mM phosphate buffer (pH 7.5) to a final volume of 20 μ L. The reaction mixture was incubated at room temperature for 1 hour. 6 μ L of iodoacetamide (100 mM) was added and the reaction mixture was incubated in the dark, at room temperature, for 20 min in order to alkylate the unmodified cysteine residues. 3 μ L of 0.1 μ g/ μ L sequencing grade modified trypsin (SIGMA) was added and the sample was incubated at 37 °C. After 1 hour, a second aliquot of 3 μ L of trypsin was added. The digestion was carried out at 37 °C overnight. 1 μ L of trifluoroacetic acid (TFA) 0,1% was added and the reaction mixture was purified by a tip chromatography system (ZipTip C18, Millipore). The bound peptides were eluted from the tip stationary phase with 10 μ L of acetonitrile 75%/TFA 0,1%. and 1 μ L of the mixture was spotted onto a MALDI target for MS analysis. A saturated solution of α -cyano-4-hydroxycinnamic acid in 50% acetonitrile/0.1% trifluoroacetic acid (0.5 μ L) was used to assist the ionization process. Mass spectra were recorded on a 4800plus MALDI TOF/TOF (Applied Biosystems) mass spectrometer, operating in positive ion reflector mode with an accelerating voltage of 20 KV and delayed extraction time of 300 ns. The MALDI ions were generated using a 355-nm Nd:YAG laser pulsed at 200 Hz with an intensity of 4600 (arbitrary units). Each spectrum was obtained by the accumulation of

1200-2500 laser shots. For MS/MS analysis the mass spectrometer was externally calibrated, and the sample mixture was analyzed in the 750 - 3500 Da mass range. Fragmentation experiments were performed with and without a collision gas. Signals from 150 laser shots were averaged to increase the S/N ratio of each mass spectrum. Data Explorer (Applied Biosystems) was used for data processing (baseline correction, deisotoping, calibration and peak detection). Peptide mass lists were searched with the MASCOT server in a swiss-prot-based protein database including the mutant version of hTS.

In parallel, 1 μ L of the reaction mixture was diluted 1:30 with a solution of 0.5% formic acid in water/acetonitrile 98:2 and 3 μ L were injected onto an HPLC-chip ESI-QTOF. The mobile phase composition was as follows: (A) 0.1% formic acid in a water/acetonitrile 98:2 solution and (B) 0.1% formic acid in acetonitrile/water 98:2 solution. A chromatographic separation was performed at a flow rate of 400 nL/min with the following gradient: 3% B for 5 min, 3–30% B in 15 min, 30–40% B in 5 min, 40–85% B in 3 min, 85% B for 2 min, 85-3% B in 5 min. The capillary voltage was set at 1600 V and the desolvating temperature was 350 °C. Nitrogen was used as a drying gas (flow rate = 6 L/min). The mass spectrometer operated in positive mode in the 200-3200 Da scan range. For MS/MS experiment up to three precursors were selected for each acquisition cycle. The precursor ion was automatically excluded for fragmentation if it was present in two consecutive spectra, or if it persisted for more than 0.12 min. An external calibration was performed based on the molecular weight of a multi-standard solution (ESI-L Low concentration tuning mixture - SUPELCO). During the acquisition, some of these masses were constantly monitored and used for a fine calibration of the instrument. The multiply charged ions deriving from the free protein and the protein-ligand complex were deconvoluted with available software (MassHunter – Agilent Technologies Inc.). The results of the trypsin

digestion are reported in Table S8. To investigate which of the three cysteines of the D186-R215 peptide (Fig. 2 in the main text) were involved in the binding with the ligand, MS/MS experiments were performed. Unfortunately, the MS/MS spectra did not allow the identification of the corresponding fragment due to (i) the low abundance of the ligand bound-D186-R215 peptide and (ii) ion suppression effects. However, molecular dynamics and x-ray crystallography highlighted that among the three cysteine residues, cysteine 202 was the one exposed to the solvent and thus available for tethering.

Mass spectrometric identification of tethered ligands.

Matrix-Assisted Laser Desorption/Ionization (MALDI) - Time of Flight (TOF) (Voyager-Pro MALDI-TOF (Applied Biosystems) was chosen for a medium-throughput screening of the disulfide-compound library (**A1-A55**). The results obtained were validated using an Electron Spray Ionization Quadrupole - Time of Flight (ESI-QTOF) mass spectrometer (Agilent Technologies Inc.). Both platforms allowed us to exclude any ionization-related issue in the ligand selection process. The screening approach was an iterative selection of the best ligands in a competitive environment obtained by arranging the ligands in pools properly chosen in order to avoid ambiguous mass peak assignments. Successive screening steps were performed in which the selected ligands from the previous screening were subjected to further screening using differently constituted pool. For the disulfide-compound library screening up to 3 ligands were pooled and mixed into a hTS-C195S-Y202C solution in a buffer containing 1 mM 2-mercaptoethanol and 20 mM K⁺ phosphate (pH 7.5). The reaction mixture was incubated at RT for 1 hour and then purified on a C4 ZipTip® (Millipore) to remove salts and unbound ligands. To identify the binding site of these molecules, the protein-ligand complexes underwent

114 enzymatic digestion in a classical bottom-up proteomic analysis using both ionization techniques
115 for result evaluation.

116

Appendix 2.

Synthetic chemistry for all compounds.

Table of contents

General pg. 1

Synthesis of TPC pg. 3

Synthesis of C1-C5, C10, D5-D8, D11-D14 pg. 5

Synthesis of D9 and D10 pg. 13

Synthesis of C6-C9, C11, E1-E7 pg. 15

Synthesis of F1-F4 pg. 25

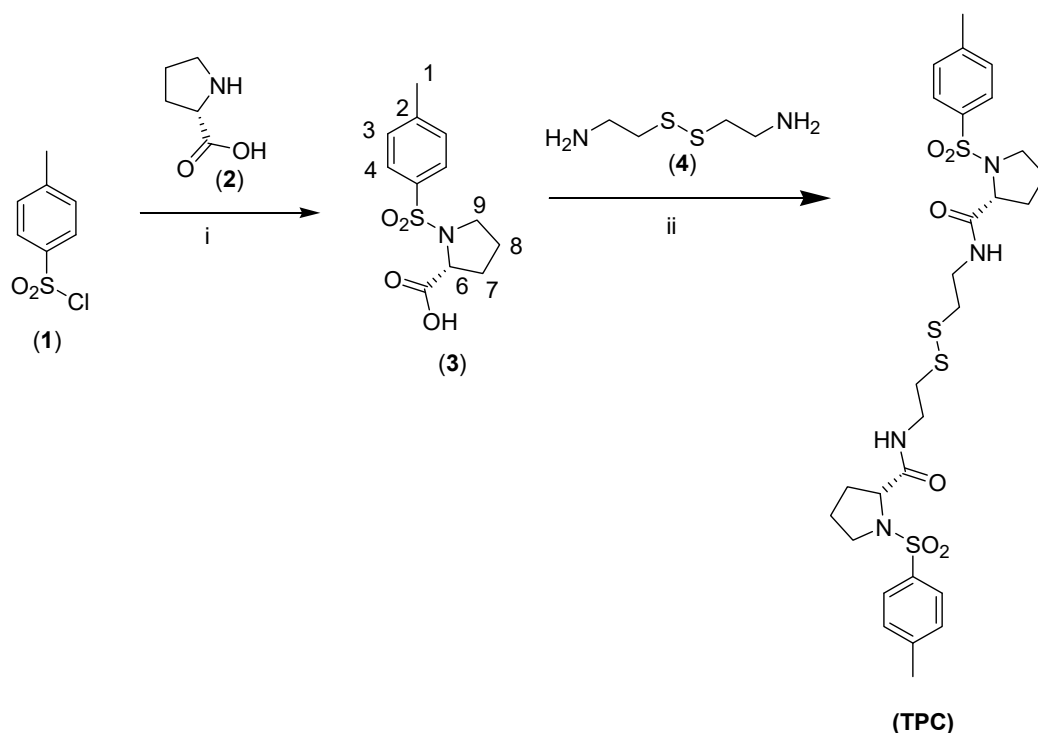
Synthesis of E5-(O2Oc)-CAM and E5-(O2Oc)-CAM-FITC pg. 31

General.

All commercial chemicals and solvents were reagent grade and were used without further purification. The compound purchased from NCI and ChemBridge were used without purification. Reaction progress was monitored by TLC on pre-coated silica gel 60 F254 plates (Merck) and visualization was accomplished with UV light (254 nm). ^1H and ^{13}C NMR spectra were recorded on a Bruker DPX200 or a Bruker FT-NMR AVANCE 400 spectrometers. Chemical shifts are reported as δ values (ppm) referenced to residual solvent (CHCl_3 at δ 7.26 ppm, DMSO at δ 2.50 ppm, MeOD at δ 3.31 ppm, CD_3OCD_3 at δ 2.05 ppm); J values were given in Hz. When peak multiplicities are given the following abbreviations are used: s, singlet; d, doublet; t, triplet; q, quartet; m, multiplet; br, broadened signal. Two-dimensional NMR techniques (heteronuclear single quantum coherence and heteronuclear multiple bond correlation) were used to aid the assignment of signals in ^1H and ^{13}C spectra. Silica gel Merck (60-230 mesh) was used for column

chromatography. Purity of the compounds was assayed by means of TLC (Merck F-254 silica gel). Analysis on compound purity was determined through liquid chromatography UV/Vis using Jasco LC system equipped with a Jasco PU-2080 Plus pump, coupled with a Jasco PU-2075 Plus UV/Vis detector. LC separation was performed on an Agilent Poroshell 120 50 mm × 3.0 mm analytical column, packed with EC-C18 2.7 μM as stationary phase (Agilent Technologies, Milan, Italy). 10 μL of a 100 μg/mL solution of compound in methanol was injected. A gradient was delivered at 0.2 mL/min using (A) 0.1% FA in water and (B) ACN. Samples were eluted with 5% B (0.00–5.00 min); 1–95% B (5.00–20.00 min); 95% B (20.00–300.00 min) and 5% B (30.00–40.00 min). The eluted was detected with UV detection at $\lambda = 220$ nm. All the compounds showed a level of purity above 95%. MS spectra were recorded by means of a Q-TOF Accurate-Mass G6520AA (Agilent Technologies). Microanalyses were carried out in the Microanalysis Laboratory of the Department of Life Sciences, Modena University.

41 **Synthesis of TPC.**



42

43 **Appendix 2-figure 1. Synthesis of TPC.** (i) diethyl ether, NaOH 2M, RT, 4h; HCl conc.; (ii)
 44 HOBT, EDAC, TEA, DCC.

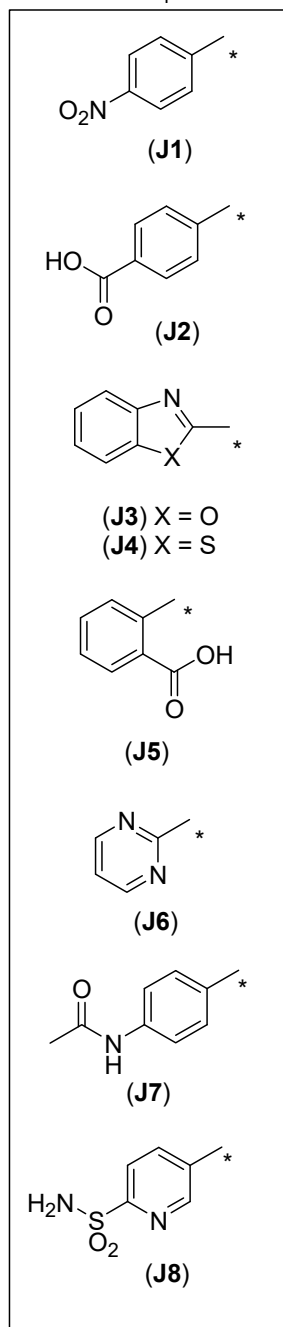
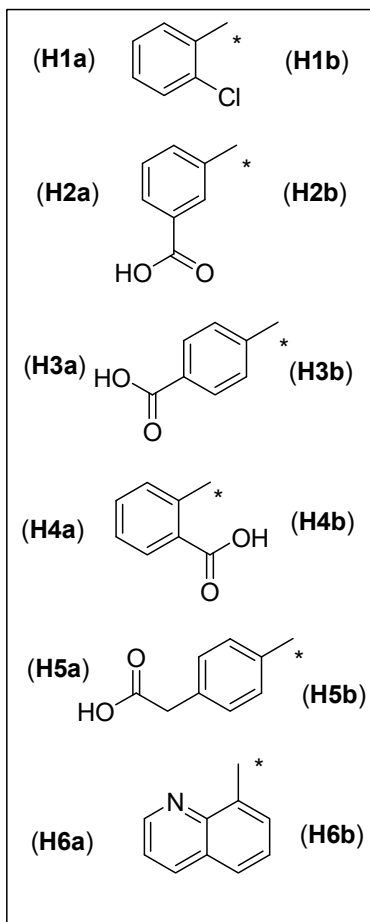
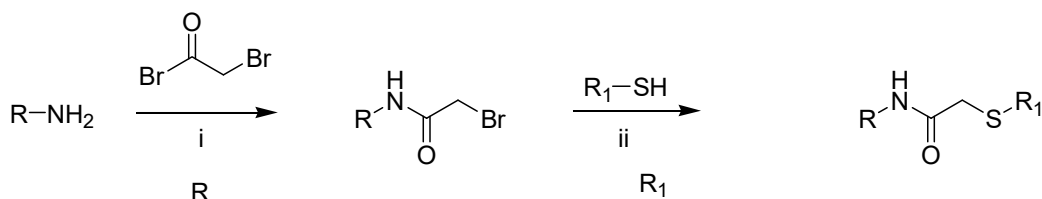
45

46 **N-(4-toluenesulfonyl)-D-proline (3).** A solution of *p*-toluene sulfonyl chloride **1** (1.64 g, 8.6 mmol)
 47 in diethyl ether (16 mL) was added to a cold (0°C) solution of D-proline (**2**) (0.99 g, 8.6 mmol) in
 48 NaOH 2M (8.6 mL, 17.4 mmol). The reaction was stirred 4h at room temperature (RT). The mixture
 49 was treated with concentrated HCl until pH 2. The aqueous solution was then extracted with ethyl
 50 acetate (6 x 10 mL), the organic layer was washed with brine (4 x 10 mL), dried (Na₂SO₄) and the
 51 solvent was removed under reduced pressure to yield a colorless glue. Yield 1.79 g, 77%; ¹H NMR
 52 (CDCl₃, 200 MHz) δ 2.12-1.72 (H-7 and H-8, m, 4H), 2.44 (H-1, s, 3H), 3.29 (H-9B, m, 1H), 3.50
 53 (H-9A, m, 1H), 4.29 (H-6, dd, *J* 3.9, *J* 4.0, 1H), 7.33 (H-3, d, *J* 7.9, 2H), 7.77 (H-4, *J* 8.2, 2H).

54 **N-N'-[D-prolyl-N-(4-toluenesulfonyl)]-cistamine (TPC).** A solution of compound **3** (0.16 g, 0.6
 55 mmol) in dichloromethane (5 mL), N,N'-dicyclohexylcarbodiimide (DCC) (0.16 g, 0.8 mmol) were
 56 added in succession and the solution was stirred at RT for 30 min; after cooling at 0°C, the

suspended cystamine·2HCl (**4**) (0.068 g, 0.3 mmol) in dichloromethane (8 mL) and TEA (0.083 mL, 0.6 mmol) was added dropwise over 5 min. The reaction mixture was stirred at RT overnight, then filtered, and the solution was washed with NaHCO₃ (2 x 5 mL), NH₄Cl (2 x 5 mL) and H₂O (2 x 5 mL). The organic layer was dried over Na₂SO₄, the solvent was evaporated at reduced pressure to produce the product that was purified by column chromatography (EtOAc/CHCl₃ 2:8). Yield g. 0.087, 44% (oil); ¹H NMR (DMSO-d₆, 200 MHz) δ 1.58-1.97 (m, 8H), 2.25 (s, 6H), 2.62 (t, 4H, *j* 5.90), 3.10 (m, 2H), 3.35 (m, 5H), 3.95 (m, 3H), 7.36 (m, 4H), 7.68 (m, 4H), 8.05 (t, 2H, *J* 5.90); ¹³C NMR (DMSO-d₆, 50 MHz) δ 20.9, 23.2, 30.0, 37.9, 39.2, 42.0, 62.9, 129.5, 129.9, 133.5, 144.7, 174.3. ESI-HRMS calcd for C₂₈H₃₉N₄O₆S₄: 655.1752 (M+H⁺), found 655.1723. Anal. Calc. for C₂₈H₃₈N₄O₆S₄: C 51.35, H 5.85, N 8.56, found, C, 51.66, H, 5.90, N, 8.40.

69 Synthesis of compounds C1-C5, C10, D5-D8, D11-D14.



C1 (from H1b and J1)
C2 (from H2b and J1)
C3 (from H3b and J1)
C4 (from H4b and J1)
C5 (from H5b and J1)
C10 (from H6b and J1)
D5 (from H4b and J2)
D6 (from H3b and J2)
D7 (from H3b and J3)
D8 (from H3b and J4)
D11 (from H3b and J5)
D12 (from H3b and J6)
D13 (from H3b and J7)
D14 (from H3b and J8)

Appendix 2-figure 2. Synthesis of compounds C1-C5, C10, D5-D8, D11-D14 . (i): TEA/CH₂Cl₂ (for **H1b, H2b**) or Na₂CO₃/H₂O (for **H2b, H3b, H5b, H6b**); (ii): K₂CO₃/acetone for **C2-C5, D5-D8, D11-D14**) or TEA/THF (for **C1, C10**).

Synthesis of 2-Bromo-N-(substituted-phenyl)acetamide derivatives (H1b, H6b). General procedure. To a solution of o-chloroaniline (**H1a**) or 8-aminoquinoline (**H6a**) (10.0 mmol) and TEA (11.0 mmol) in anhydrous CH₂Cl₂ (30 mL), under stirring at 0°C under N₂ atmosphere, a solution of bromoacetyl bromide (10.0 mmol) in anhydrous CH₂Cl₂ (20 mL) was added dropwise. The suspension thus obtained was stirred at RT for 1 hour, then it was diluted with CH₂Cl₂, washed with a saturated solution of NH₄Cl; afterwards, the organic phase was dried (Na₂SO₄) and the solvent removed under reduced pressure. The residue thus obtained was purified by means of column chromatography as described.

2-Bromo-N-(2-chlorophenyl)acetamide (H1b): Yield 2.49 g (96%), m.p. 83-85°C (column chromatography cyclohexane/EtOAc 17.5:2.5), ¹H-NMR (DMSO-d₆, 200 MHz) (δ) (ppm): 9.90 (1H, broad s), 7.70 (1H, dd, *J* 7.9, *J* 1.7), 7.50 (1H, dd, *J* 7.9, *J* 1.7), 7.35 (1H, dt, *J* 7.6, *J* 1.6), 7.25 (1H, dt, *J* 7.7, *J* 1.7), 4.15 (2H, s); ¹³C-NMR (DMSO-d₆, 50 MHz) (δ) (ppm): 165.77, 135.00, 130.05, 127.99, 127.25, 126.42, 30.13.

2-Bromo-N-(quinolin-8-yl)acetamide (H6b): Yield 2.40 g (91%), m.p. 93-96°C C (column chromatography cyclohexane/EtOAc 8:2), ¹H-NMR (DMSO-d₆, 200 MHz) (δ) (ppm): 10.70 (1H, broad s), 8.90-8.60 (2H, m), 8.15 (1H, dd, *J* 8.3, *J* 1.7), 7.65-7.40 (3H, m), 4.10 (1H, s); ¹³C-NMR (DMSO-d₆, 50 MHz) (δ) (ppm): 148.54, 138.61, 136.31, 127.92, 127.15, 122.43, 121.74, 116.59, 29.68.

Synthesis of Bromo-N-(carboxy- or 4-carboxymethyl- phenyl)-acetamide derivatives (H2b, H3b, H5b). General procedure. These compounds were synthesized according to the published procedure (64-65). To a solution of the appropriate aminobenzoic acid (**H2a** or **H3a** for the

synthesis of **H2b** and **H3b**, respectively) or p-aminophenylacetic acid (**H5a**) for the synthesis of (**H5b**) (19.87 mmol) and Na₂CO₃ (56.60 mmol) in water (60 mL) at 0°C under stirring, a solution of bromoacetyl bromide (27.81 mmol) in anhydrous CH₃CN was added dropwise during 10 min. The suspension thus obtained was stirred at 0°C for another 10 min, then at RT for 10 min. Afterwards, the suspension was acidified (HCl 1 N, pH 1), and the precipitate thus obtained collected and washed with water. The products were then purified by trituration with anhydrous diethyl ether.

Bromo-N-(3-carboxyphenyl)acetamide (H2b). Yield 1.20 g (43%), m.p. 213-216°C (dec.), ¹H-NMR (DMSO-d₆, 200 MHz) (δ) (ppm): 10.51 (1H, broad s), 8.22 (1H, s), 7.79 (1H, m), 7.66 (1H, d, *J* 8.0), 7.45 (1H, t, *J* 7.6), 4.05 (2H, s); ¹³C-NMR (DMSO-d₆, 50 MHz) (δ) (ppm): 167.44, 165.50, 139.27, 131.90, 129.61, 125.06, 123.79, 120.43, 30.71.

Bromo-N-(4-carboxyphenyl)acetamide (H3b). Yield 82%, m.p. 223-226°C (dec.), ¹H-NMR (DMSO-d₆, 200 MHz) (δ) (ppm): 10.65 (1H, broad s), 7.90 (2H, m), 7.70 (2H, m), 4.05 (2H, s); ¹³C-NMR (DMSO-d₆, 50 MHz) (δ) (ppm): 167.26, 165.73, 143.02, 130.91, 126.23, 119.04, 30.72.

Bromo-N-(4-carboxymethylphenyl)acetamide (H5b). Yield 86%, m.p. 130-132°C (dec.), ¹H-NMR (DMSO-d₆, 400 MHz) (δ) (ppm): 12.50 (1H, broad s), 10.50 (1H, s), 7.68 (2H, m), 7.37 (2H, m), 4.19 (2H, s), 3.68 (2H, s); ¹³C-NMR (DMSO-d₆, 100 MHz) (δ) (ppm): 173.18, 165.15, 137.63, 130.93, 130.22, 119.63, 40.60, 30.89.

Bromo-N-(2-carboxyphenyl)acetamide (H4b). The compound was synthesized according to the procedure reported (66). To a solution of anthranilic acid (**H4a**) (1.50 g, 10.9 mmol) in anhydrous DMF (5 mL) and dioxane (5 mL), at -5°C under stirring under N₂ atmosphere, bromoacetyl bromide (2.76 g, 13.67 mmol) was added dropwise. The suspension thus obtained was stirred at RTR for 12 hours, then ice (50 mL) was added to the reaction mixture; the solid thus obtained was collected and washed with water. Yield 2.52 g (89%), m.p. 163-166°C, ¹H-NMR (DMSO-d₆, 200 MHz) (δ) (ppm): 11.55 (1H, broad s), 8.45 (1H, d, *J* 8.6), 8.00 (1H, d, *J* 7.8, *J* 1.2),

121 7.60 (1H, m), 7.20 (1H, m), 4.25 (2H, s); ¹³C-NMR (DMSO-d₆, 50 MHz) (δ) (ppm): 169.65,
122 165.47, 140.42, 134.48, 131.57, 123.89, 120.51, 117.62, 31.10.

123 **2-(Substituted aryl- or heteroarylthio)-N-(substituted phenyl)acetamide derivatives C2-C5,**

124 **D5-D8, D11-D14. General procedure.** To a suspension of K₂CO₃ (3.0 eq.) in anhydrous acetone
125 (20 mL) at RT under stirring in a N₂ atmosphere, the appropriate mercaptoderivative (1.0 eq.) was
126 added, followed by the appropriate (carboxyphenyl)-amidomethyl bromides (1 eq.). The suspension
127 was stirred at RT for 12 hours, then the mixture was cooled, acidified (HCl 1N, pH 1.0) and the solid
128 thus obtained was collected by filtration and washed with water. The crude product was purified by
129 crystallization or column chromatography as reported below.

130 **2-(4-Nitrophenylthio)-N-(3-carboxyphenyl)acetamide (C2):** Yield 0.20 g (26%), m.p. 250-252°C
131 (column chromatography CH₂Cl₂: CH₃OH 9:1), ¹H-NMR (DMSO-d₆, 400 MHz) (δ) (ppm): 13.20
132 (1H, broad s), 10.70 (1H, broad s), 8.37 (1H, s), 8.32 (2H, m), 7.93 (1H, m), 7.80 (1H, d, *J* 7.9),
133 7.75 (2H, m), 7.60 (1H, m), 4.25 (2H, s); ¹³C-NMR (DMSO-d₆, 100 MHz) (δ) (ppm): 166.50,
134 166.71, 147.27, 145.19, 139.40, 131.86, 129.61, 126.91, 124.90, 124.38, 123.75, 120.38, 36.45;
135 ESI-HRMS calcd for C₁₅H₁₃N₂O₅S (M+H⁺) 333.0545, found 333.0544. HPLC-UV/Vis *k* (retention
136 time): 11.76. Anal. Calc. for C₁₅H₁₂N₂O₅S, C, 54.21, H, 3.64, N, 8.43; found, C, 54.43, H, 3.69, N,
137 8.19.

138 **2-(4-Nitrophenylthio)-N-(4-carboxyphenyl)acetamide (C3):** Yield 0.28 g (36%), m.p. 234-236°C
139 (column chromatography CH₂Cl₂: CH₃OH 9:1), ¹H-NMR (DMSO-d₆, 400 MHz) (δ) (ppm): 12.89
140 (1H, broad s), 10.80 (1H, broad s), 8.31 (2H, m), 8.06 (2H, m), 7.83 (2H, m), 7.74 (2H, m), 4.28
141 (2H, s); ¹³C-NMR (DMSO-d₆, 100 MHz) (δ) (ppm): 167.30, 166.97, 147.19, 145.21, 143.16,
142 130.94, 126.92, 126.03, 124.38, 118.99, 36.56; ESI-HRMS calcd for C₁₅H₁₃N₂O₅S (M+H⁺)
143 333.0545, found 333.0526 HPLC-UV/Vis *k*: 11.77. Anal. Calc. for C₁₅H₁₂N₂O₅S, C, 54.21, H, 3.64,
144 N, 8.43; found, C, 54.13, H, 3.66, N, 8.55.

145 **2-(4-Nitrophenylthio)-N-(2-carboxyphenyl)acetamide (C4)**: Yield 0.60 (77%), m.p. 203-206°C
 146 (column chromatography CH₂Cl₂: CH₃OH 9:1), ¹H-NMR (DMSO-d₆, 400 MHz) (δ) (ppm): 13.79
 147 (1H, broad s), 11.83 (1H, broad s), 8.61 (1H, d, *J* 8.2), 8.30 (2H, m), 8.10 (1H, dd, *J* 7.9, *J* 1.2),
 148 7.76-7.70 (3H, m), 7.32 (1H, m), 4.40 (2H, s); ¹³C-NMR (DMSO-d₆, 100 MHz) (δ) (ppm): 169.61,
 149 166.88, 146.47, 145.35, 140.52, 134.50, 131.57, 126.97, 124.47, 123.73, 120.63, 117.49, 36.85;
 150 ESI-HRMS calcd for C₁₅H₁₃N₂O₅S (M+H⁺) 333.0545, found 333.0548. HPLC-UV/Vis *k*: 12.71.
 151 Anal. Calc. for C₁₅H₁₂N₂O₅S, C, 54.21, H, 3.64, N, 8.43; found, C, 54.33, H, 3.45, N, 8.55.

152 **2-(4-Nitrophenylthio)-N-(4-carboxymethylphenyl)acetamide (C5)**. Yield 64%, m.p. 142-144°C
 153 (column chromatography CH₂Cl₂/CH₃OH 9:1), ¹H-NMR (DMSO-d₆, 400 MHz) (δ) (ppm): 12.20
 154 (1H, broad s), 10.30 (1H, s), 8.18 (2H, m), 7.60 (2H, m), 7.55 (2H, m), 7.20 (2H, m), 4.09 (2H, s),
 155 3.50 (2H, s); ¹³C-NMR (DMSO-d₆, 100 MHz) (δ) (ppm): 173.22, 166.29, 147.42, 145.16, 137.70,
 156 130.82, 130.21, 126.88, 124.36, 119.62, 49.06, 36.45. ESI-HRMS calc. for C₁₆H₁₅N₂O₅S (M+H⁺)
 157 347.0702, found 347.0709. . HPLC-UV/Vis *k*: 11.59. Anal. Calc. for C₁₆H₁₄N₂O₅S, C, 55.48, H,
 158 4.07, N, 8.09; found, C, 55.33, H, 3.95, N, 8.44.

159 **2-(4-Carboxyphenylthio)-N-(2-carboxyphenyl)acetamide (D5)**. Yield 53%, m.p. 244-245°C
 160 (trituration with Et₂O), ¹H-NMR (DMSO-d₆, 200 MHz) (δ) (ppm): 13.26 (1 H, broad s), 11.72 (1 H,
 161 s), 8.48 (1 H, d, *J* 8.2), 7.96 (2 H, m), 7.85 (2 H, m), 7.58 (2H, m), 7.43 (2 H, m), 7.15 (1 H, t, *J*
 162 8.2); ¹³C-NMR (DMSO-d₆, 50 MHz) (δ) (ppm): 169.56, 167.31, 167.28, 142.20, 140.60, 134.45,
 163 131.54, 130.32, 128.40, 126.85, 123.58, 120.48, 117.35, 37.23. ESI-HRMS calc. for C₁₆H₁₄NO₅S
 164 (M+H⁺) 332.0593, found 332.0590. HPLC-UV/Vis *k*: 11.01. Anal. Calc. for C₁₆H₁₃NO₅S, C, 58.00,
 165 H, 3.95, N, 4.23; found, C, 58.33, H, 3.85, N, 4.55.

166 **2-(4-Carboxyphenylthio)-N-(4-carboxyphenyl)acetamide (D6)**. Yield 50%, m.p. 294-296°C
 167 (DMF/H₂O), ¹H-NMR (DMSO-d₆, 400 MHz) (δ) (ppm): 12.80 (2H, broad s), 10.60 (1H, s), 7.88
 168 (4H, m), 7.68 (2H, m), 7.48 (2H, m), 4.05 (2H, s); ¹³C-NMR (DMSO-d₆, 100 MHz) (δ) (ppm):
 169 167.37, 167.31, 143.21, 142.96, 130.94, 130.24, 128.08, 127.75, 125.91, 118.93, 36.77. ESI-HRMS

170 calc. for $C_{16}H_{14}NO_5S$ ($M+H^+$) 332.0593, found 332.0578. HPLC-UV/Vis k : 10.06. Anal. Calc. for
171 $C_{16}H_{13}NO_5S$: C 58.00, H 3.95, N 4.23, found, C, 57.96, H, 3.68, N, 4.71.

172 **2-(Benzoxazol-2-ylthio)-N-(4-carboxyphenyl)acetamide (D7).** Yield 77%, m.p. 229-230°C
173 (CH₃OH), ¹H-NMR (DMSO-d₆, 400 MHz) (δ) (ppm): 12.70 (1H, broad s), 10.70 (1H, s), 7.91 (2H,
174 m), 7.75-7.55 (4H, m), 7.32 (2H, m), 4.40 (2H, s); ¹³C-NMR (DMSO-d₆, 100 MHz) (δ) (ppm):
175 167.28, 165.99, 164.22, 151.81, 143.13, 141.67, 130.94, 126.04, 125.12, 124.81, 118.97, 118.71,
176 110.67, 37.28. ESI-HRMS calc. for $C_{16}H_{13}N_2O_4S$ ($M+H^+$) 329.0596, found 329.0592; HPLC-
177 UV/Vis k : 11.83. Anal. Calc. for $C_{16}H_{12}N_2O_4S$: C 58.53, H 3.68, N 8.53, found, C, 58.87, H, 3.44,
178 N, 8.47.

179 **2-(Benzothiazol-2-ylthio)-N-(4-carboxyphenyl)acetamide (D8).** Yield 75%, m.p. 220-222°C
180 (CH₃OH), ¹H-NMR (DMSO-d₆, 400 MHz) (δ) (ppm): 12.78 (1H, broad s), 10.81 (1H, s), 8.03 (1H,
181 d, J 8.0, J 0.6), 7.93 (2H, m), 7.83 (1H, d, J 8.0), 7.73 (2H, m), 7.47 (1H, dt, J 7.4, J 1.2), 7.37 (1H,
182 dt, J 8.2, J 1.1), 4.44 (2H, s); ¹³C-NMR (DMSO-d₆, 100 MHz) (δ) (ppm): 167.31, 166.41, 166.27,
183 152.97, 143.21, 135.26, 130.97, 126.89, 126.00, 125.03, 122.37, 121.56, 118.95, 38.27. ESI-HRMS
184 calc. for $C_{16}H_{13}N_2O_3S_2$ ($M+H^+$) 345.0368, found 345.0366. HPLC-UV/Vis k : 12.31. Anal. Calc. for
185 $C_{16}H_{12}N_2O_3S_2$, C, 55.80, H, 3.51, N, 8.13; found, C, 55.53, H, 3.45, N, 8.38.

186 **2-(2-Carboxyphenylthio)-N-(4-carboxyphenyl)acetamide (D11).** Yield 59%, m.p. 265-266°C
187 (DMF/H₂O), ¹H-NMR (DMSO-d₆, 400 MHz) (δ) (ppm): 11.05 (2H, broad s), 9.10 (1H, s), 6.75
188 (3H, m), 6.56 (2H, m), 6.42 (2H, m), 6.15 (1H, m), 4.01 (2H, s); ¹³C-NMR (DMSO-d₆, 100 MHz) (δ)
189 (ppm): 167.89, 167.87, 167.30, 143.31, 140.83, 132.90, 131.42, 130.89, 128.41, 126.21, 125.90,
190 124.78, 118.93, 37.18. ESI-HRMS calc. for $C_{16}H_{14}NO_5S$ ($M+H^+$) 332.0593, found 332.0581.
191 HPLC-UV/Vis k : 10.09. Anal. Calc. for $C_{16}H_{13}NO_5S$: C 58.00, H 3.95, N 4.23, found, C, 58.19, H,
192 3.85, N, 4.58.

193 **2-(Pyrimidin-2-ylthio)-N-(4-carboxyphenyl)acetamide (D12).** Yield 72%, m.p. 208-210 °C
194 (CH₃OH/Et₂O), ¹H-NMR (DMSO-d₆, 200 MHz) (δ) (ppm): 12.60 (1H, broad s), 10.51 (1H, s), 8.64
195 (2H, d, J 9.2), 7.88 (2H, m), 7.68 (2H, m), 7.23 (1H, t, J 9.2), 4.10 (2H, s); ¹³C-NMR (DMSO-d₆,

50 MHz) (δ) (ppm): 167.31, 167.15, 158.25, 143.43, 130.87, 125.75, 118.86, 117.91, 36.00. ESI-
 HRMS calc. for $C_{13}H_{12}N_3O_3S$ ($M+H^+$) 290.0599, found 290.0594. HPLC-UV/Vis k : 9.04. Anal.
 Calc. for $C_{13}H_{11}N_3O_3S$, C, 53.97, H, 3.83, N, 14.52; found, C, 54.13, H, 3.85, N, 14.55.

2-(4-Acetylaminothiophenylthio)-N-(4-carboxyphenyl)acetamide (D13). Yield 81%, m.p. 262-
 264°C (CH₃OH), ¹H-NMR (DMSO-d₆, 400 MHz) (δ) (ppm): 12.71 (1H, broad s), 10.40 (1H, s),
 9.90 (1H, s), 7.88 (2H, m), 7.66 (2H, m), 7.53 (2H, m), 7.35 (2H, m), 3.80 (2H, s), 2.00 (3H, s);
¹³C-NMR (DMSO-d₆, 100 MHz) (δ) (ppm): 168.75, 167.97, 167.29, 143.31, 138.75, 130.94,
 130.86, 129.00, 125.85, 120.02, 118.92, 39.38, 36.00. ESI-HRMS calc. for $C_{17}H_{17}N_2O_4S$ ($M+H^+$)
 345.0909, found 345.0907. HPLC-UV/Vis k : 9.68. Anal. Calc. for $C_{17}H_{16}N_2O_4S$, C, 59.29, H, 4.68,
 N, 8.13; found, C, 59.55, H, 4.45, N, 8.35.

2-(5-Sulfamoylpyridin-2-ylthio)-N-(2-carboxyphenyl)acetamide (D14). Yield 72%, m.p. 268-
 270°C (CH₃OH/Et₂O), ¹H-NMR (DMSO-d₆, 200 MHz) (δ) (ppm): 12.65 (1H, s), 10.60 (1H, s),
 8.78 (1 H, d, J 1.4), 7.95 (1 H, dd, J 1.4, J 8.6), 7.88 (2 H, m), 7.69 (2 H, m), 7.60 (1 H, d, J 8.6),
 7.49 (2 H, s), 4.23 (2 H, s); ¹³C-NMR (DMSO-d₆, 50 MHz) (δ) (ppm): 167.30, 167.08, 162.49,
 146.57, 143.37, 136.89, 134.29, 130.89, 125.83, 121.92, 118.89, 40.05. ESI-HRMS calc. for
 $C_{14}H_{14}N_3O_5S_2$ ($M+H^+$) 368.0375, found 368.0368. HPLC-UV/Vis k : 9.29. Anal. Calc. for
 $C_{14}H_{13}N_3O_5S_2$, C, 45.77, H, 3.57, N, 11.44; found, C, 45.50, H, 3.45, N, 11.57.

**2-(4-Nitrophenylthio)-N-(substituted)acetamide derivatives (C1) and (C10). General
 procedure.** To a solution of (H1b) or (H6b) respectively (2.0 mmol) and TEA (3.0 mmol) in
 anhydrous THF (30 mL), 4-nitrothiophenol (J1) (2.0 mmol) in anhydrous THF (20 mL) was added
 under stirring at RT under a N₂ atmosphere, and the solution thus obtained was stirred for 2 hours;
 at the end of the reaction, the solution was diluted with CH₂Cl₂, washed with 1N HCl (20 mL); the
 organic phase was dried (Na₂SO₄) and the solvent removed under reduced pressure. The residue
 thus obtained was purified by means of column chromatography (cyclohexane:EtOAc 8:2 then
 100% EtOAc).

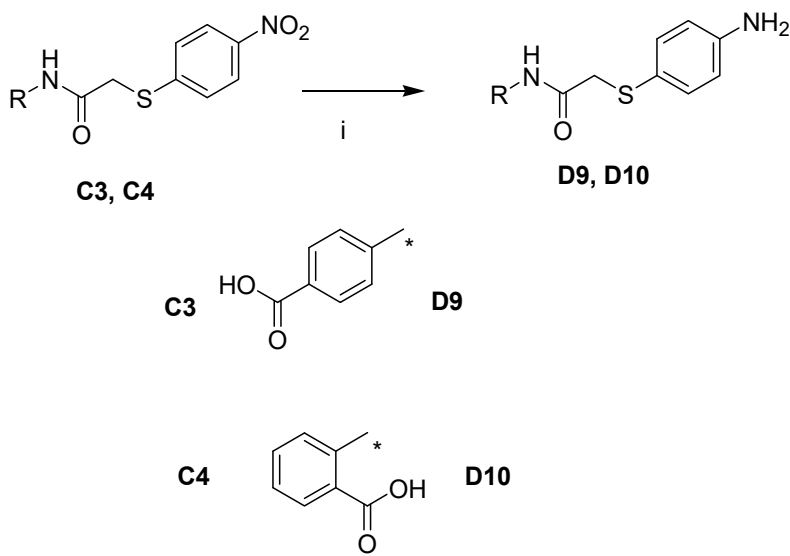
221 **2-(4-Nitrophenylthio)-N-(2-chlorophenyl)acetamide (C1):** Yield 0.44g (67%), m.p. 144-146°C,
222 ¹H-NMR (DMSO-d₆, 400 MHz) (δ) (ppm): 10.10 (1H, broad s), 8.32 (2H, m), 7.87 (1H, d, *J* 7.7),
223 7.76 (2H, m), 7.65 (1H, d, *J* 8.1), 7.47 (1H, m), 7.35 (1H, m), 4.40 (2H, s); ¹³C-NMR (DMSO-d₆,
224 100 MHz) (δ) (ppm): 166.9, 147.15, 145.25, 134.89, 130.02, 128.00, 127.08, 126.99, 126.77,
225 126.29, 124.37, 35.86; ESI-HRMS calcd for C₁₄H₁₂ClN₂O₃S (M+H⁺) 323.0257, found 323.0261;
226 HPLC-UV/Vis *k*: 13.87. Anal. Calc. for C₁₄H₁₁ClN₂O₃S, C, 52.10, H, 3.44, N, 8.68; found C,
227 52.33, H, 3.22, N, 8.80 .

228 **2-(4-Nitrophenylthio)-N-(quinolin-8-yl)acetamide (C10):** Yield 0.30 g (39%), m.p. 160-161°C,
229 ¹H-NMR (DMSO-d₆, 400 MHz) (δ) (ppm): 10.90 (1H, broad s), 9.08 (1H, dd, *J* 4.1, *J* 1.6) 8.75
230 (1H, dd, *J* 7.7, *J* 0.9), 8.56 (1H, dd, *J* 8.4, *J* 1.6), 8.30 (2H, m), 7.87-7.77 (4H, m), 7.73 (1H, m),
231 4.55 (2H, s); ¹³C-NMR (DMSO-d₆, 100 MHz) (δ) (ppm): 166.99, 149.50, 146.85, 145.33, 138.59,
232 137.11, 134.56, 128.33, 127.40, 127.13, 124.43, 122.87, 122.73, 117.18, 35.59; ESI-HRMS calcd
233 for C₁₇H₁₄N₃O₃S (M+H⁺) 340.0756, found 340.0754. HPLC-UV/Vis *k*: 14.37. Anal. Calc. for
234 C₁₇H₁₃N₃O₃S, C, 60.17, H, 3.86, N, 12.38; found, C 60.57, H, 3.60, N, 12.20.

235

236

237 **Synthesis of compounds D9 and D10.**



238

239

240 **Appendix 2-figure 3. Synthesis of D9 and D10.** (i): H₂/Pd:C, CH₃OH.

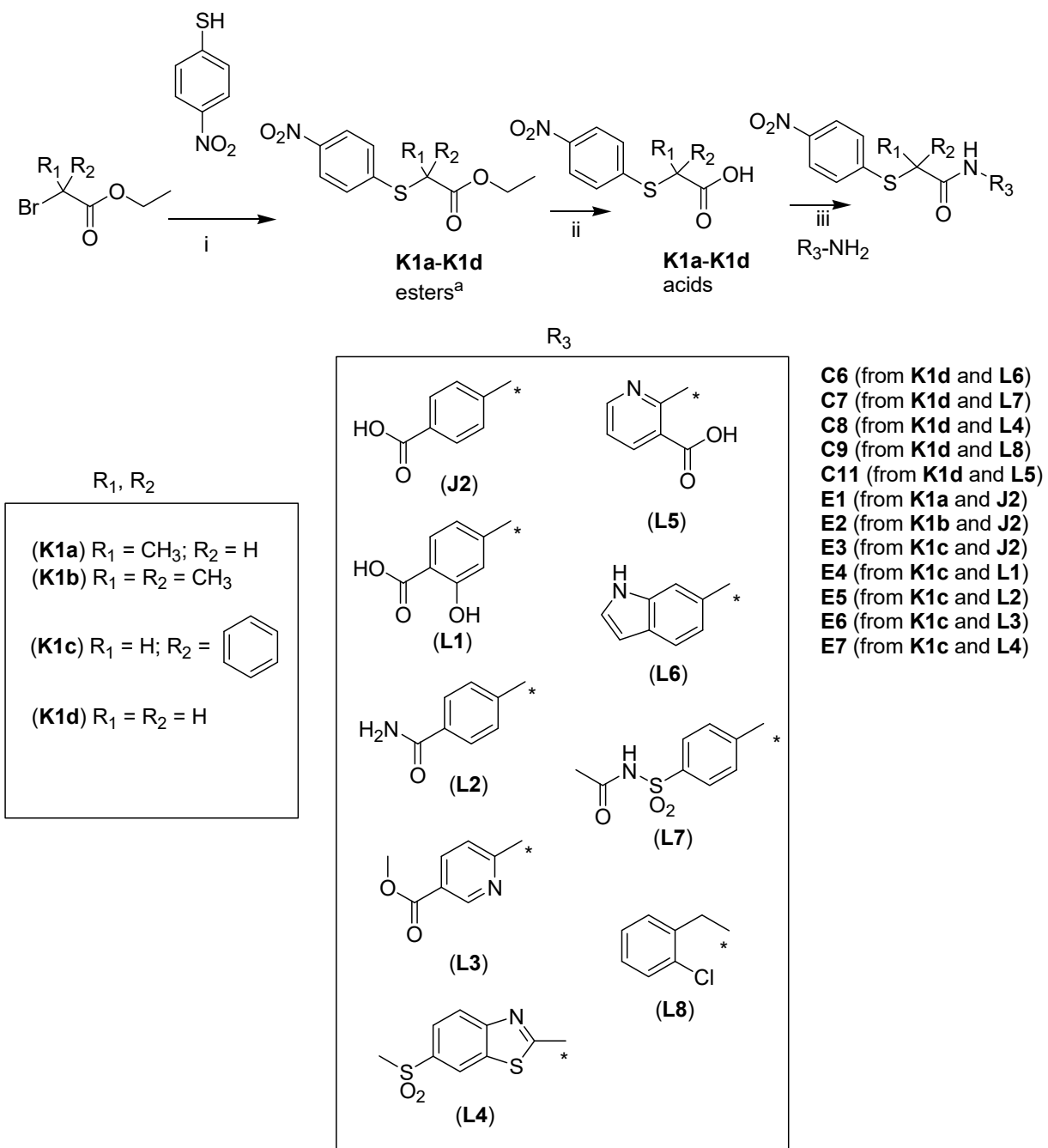
241 **General procedure.** The compounds were obtained by means of catalytic reduction of the
 242 corresponding nitroderivatives (**C3**) and (**C4**), respectively. A solution of **C3** and **C4** (1.77 mmol)
 243 in CH₃OH (100 mL) was hydrogenated on Pd/C 5% (0.26 g) at 2 atm for 6 hours. At the end of the
 244 reaction, the catalyst was filtered and the solvent removed under reduced pressure.

245 **2-(4-Aminophenylthio)-N-(4-carboxyphenyl)acetamide (D9).** Yield 68%, m.p. 238-240°C (dec.)
 246 (CH₃OH/EtOAc), ¹H-NMR (DMSO-d₆, 400 MHz) (δ) (ppm): 10.93 (1H, s), 7.88 (2H, m), 7.68
 247 (2H, m), 7.46 (2H, m), 7.23 (2H, m), 3.90 (2H, s); ¹³C-NMR (DMSO-d₆, 100 MHz) (δ) (ppm):
 248 167.78, 167.32, 143.40, 134.38, 133.01, 132.39, 130.84, 130.16, 125.82, 123.29, 118.93, 112.81,
 249 38.17. ESI-HRMS calc. for C₁₅H₁₅N₂O₃S (M+H⁺) 303.0803, found 303.0808. HPLC-UV/Vis *k*:
 250 8.36. Anal. Calc. for C₁₅H₁₄N₂O₃S, C, 59.59, H, 4.67, N, 9.27; found, C, 59.77, H, 4.60, N, 9.08.

251 **2-(4-Aminophenylthio)-N-(2-carboxyphenyl)acetamide (D10).** Yield 0587 g (90%), m.p. 154-
 252 155°C, ¹H-NMR (DMSO-d₆, 200 MHz) (δ) (ppm): 11.88 (1H, s), 8.50 (1H, d, J 8.4), 7.93 (1H, d, J
 253 7.7), 7.55 (1H, t, J 7.9), 7.15 (3H, m), 6.50 (2H, m), 3.80 (2H, s); ¹³C-NMR (DMSO-d₆, 50 MHz)
 254 (δ) (ppm): 169.66, 168.39, 148.73, 140.95, 134.46, 133.83, 131.57, 123.25, 120.11, 118.68, 116.94,

255 115.26, 42.25. ESI-HRMS calc. for $C_{15}H_{15}N_2O_3S$ ($M+H^+$) 303.0803, found 303.0801. HPLC-
256 UV/Vis k : 9.46. Anal. Calc. for $C_{15}H_{14}N_2O_3S$, C, 59.59, H, 4.67, N, 9.27; found, C, 59.80, H, 4.66,
257 N, 9.55.
258
259

260 **Synthesis of compounds C6-C9, C11, E1-E7.**



261

262 **Appendix 2-figure 4. Synthesis of compounds C6-C9 and C11, E1-E7.** (i): K₂CO₃/acetone. In
 263 the case of **K1d**, methylbromoacetate was used instead of ethylbromoacetate ; (ii): NaOH/EtOH;
 264 (iii): (COCl)₂/THF then TEA (for **E1-E6**, **C6**, **C7**, **C9**, **C11**) or WSC/DMF (for **C8**, **E7**).

265

Synthesis of methyl- or ethyl-2-[(4-nitrophenylthio)]acetate derivatives (K1a-K1d esters).

General procedure. To a suspension of 4-nitrothiophenol (3.87 mmol) and K_2CO_3 (5.79 mmol) in anhydrous acetone (20 mL) under N_2 atmosphere under stirring at RT, the appropriate bromoacetate (**K1a-K1d**) (4.25 mmol) was added dropwise, and the suspension was stirred for 1 hour; in the case of (**K1b**), the reaction time was 12 hours. At the end of the reaction, water was added (40 mL) and the mixture was extracted with EtOAc (3x10 mL); the organic phase was dried (Na_2SO_4) and the solvent removed under reduced pressure.

Ethyl-[2-(4-nitrophenylthio)]propionate (K1a ester). Yield 90%, oil (column chromatography cyclohexane/EtOAc 8:2), 1H -NMR ($CDCl_3$, 400 MHz) (δ) (ppm): 8.16 (2H, m), 7.52 (2H, m), 4.20 (2H, q, J 7.2), 4.05 (1H, q, J 7.2), 1.60 (3H, d, J 7.2), 1.25 (3H, t, J 7.2); ^{13}C -NMR ($CDCl_3$, 100 MHz) (δ) (ppm): 171.82, 146.08, 144.61, 128.94, 126.43, 124.45, 123.93, 61.99, 43.73, 17.26, 14.21.

Ethyl-[2-methyl(4-nitrophenylthio)]propionate (K1b ester). Yield 92%, oil (column chromatography cyclohexane/EtOAc 7.5:2.5), 1H -NMR ($CDCl_3$, 400 MHz) (δ) (ppm): 8.15 (2H, m), 7.60 (2H, m), 4.15 (2H, q, J 7.2), 1.60 (6H, s), 1.28 (3H, t, J 7.2); ^{13}C -NMR ($CDCl_3$, 100 MHz) (δ) (ppm): 173.46, 147.71, 141.41, 135.16, 123.53, 61.63, 51.54, 26.08, 14.08.

Ethyl-[2-phenyl(4-nitrophenylthio)]acetate (K1c ester). Yield 77%, oil, 1H -NMR ($CDCl_3$, 400 MHz) (δ) (ppm): 8.11 (2H, m), 7.54 (2H, dd, J 8.0, J 2.0), 7.40 (5H, m), 4.20 (3H, m), 1.33 (3H, t, J 7.2); ^{13}C -NMR ($CDCl_3$, 100 MHz) (δ) (ppm): 169.50, 146.18, 144.57, 134.33, 129.07, 128.95, 128.91, 128.44, 123.98, 62.37, 54.61, 14.04.

Methyl-2-[(4-nitrophenylthio)]acetate (K1d ester). Yield 82%, m.p. 47-49°C, 1H -NMR ($DMSO-d_6$, 200 MHz) (δ) (ppm): 8.15 (2H, m), 7.50 (2H, m), 4.15 (2H, s), 3.65 (3H, s); ^{13}C -NMR ($DMSO-d_6$, 50 MHz) (δ) (ppm): 169.53, 146.46, 145.30, 135.23, 126.90, 124.39, 124.34, 52.97, 33.58.

2-[(4-Nitrophenylthio)] acetic acid derivatives (K1a-K1d acids). General procedure. To a solution of the appropriate ester (**K1a-K1d esters**) (6.87 mmol) in ethanol (43 ml) aqueous NaOH 2 M (10.31 mmol) was added and the solution thus obtained was stirred elm at RT under N_2 for 1h,

then the solvent was removed under reduced pressure. The residue thus obtained was dissolved in EtOAc, and the organic phase was washed with HCl 0.5N; then the organic phase was dried (Na₂SO₄) and the solvent removed under reduced pressure; the product was then purified as reported below.

[2-(4-Nitrophenylthio)]propionic acid (K1a acid). Yield 70%, m.p. 110-111°C (trituration with isopropyl ether), ¹H-NMR (DMSO-d₆, 400 MHz) (δ) (ppm): 8.16 (2H, m), 7.52 (2H, m), 4.05 (1H, q, J 7.2), 1.60 (3H, d, J 7.2); ¹³C-NMR (DMSO-d₆, 100 MHz) (δ) (ppm): 171.82, 146.08, 144.61, 128.94, 126.43, 124.45, 123.93, 43.73, 17.26.

[2-Methyl-(4-nitrophenylthio)]propionic acid (K1b acid). Yield 59%, m.p. 105-107°C (trituration with diethyl ether), ¹H-NMR (CDCl₃, 400 MHz) (δ) (ppm): 8.15 (2H, m), 7.60 (2H, m), 1.60 (6H, s); ¹³C-NMR (CDCl₃, 100 MHz) (δ) (ppm): 173.46, 147.71, 141.41, 135.16, 123.53, 26.08.

[2-Phenyl(4-nitrophenylthio)]acetic acid (K1c acid). Yield 66%, m.p. 126-128°C (trituration with isopropyl ether), ¹H-NMR (DMSO-d₆, 400 MHz) (δ) (ppm): 8.27 (2H, m), 7.74-7.66 (4H, m), 7.55-7.45 (3H, m), 5.79 (1H, s); ¹³C-NMR (DMSO-d₆, 100 MHz) (δ) (ppm): 171.08, 145.73, 145.59, 135.91, 129.28, 128.87, 128.24, 124.35, 53.22.

[(4-Nitrophenyl)thio]acetic acid (K1d acid). Yield 68%, m.p. 140-142°C (acetone/petrol ether b.p. 40-60°C), ¹H-NMR (DMSO-d₆, 200 MHz) (δ) (ppm): 12.90 (1H, broad s), 8.15 (2H, m), 7.95 (2H, m), 4.0 (2H, s); ¹³C-NMR (DMSO-d₆, 50 MHz) (δ) (ppm): 170.29, 147.07, 145.12, 126.71, 124.30, 34.10.

2-(4-Nitrophenylthio)-N-(aryl- or heteroaryl)-acetamide derivatives C6, C7, C9, C11, E1-E6:

General procedure. To a solution of the appropriate carboxylic acid (**K1a-K1d acids**) (4.69 mmol) in anhydrous THF (17 mL) and anhydrous DMF (0.033 mL) at 0°C under elm stirring in a N₂ atmosphere, oxalylchloride (7.18 mmol) was added dropwise, then the mixture was stirred for 1 hour at RT. At the end of the reaction, the solvent was removed under reduced pressure and coevaporated with anhydrous CH₂Cl₂ three times. The oily material was used in the next step

without purification. The solution of the acyl chloride thus obtained in CH₂Cl₂ (10 mL) was added dropwise to the solution of the appropriate amine derivative (1.2 eq) in anhydrous CH₂Cl₂ (20 mL), TEA (1.2 eq. in the case of (**E5**) and (**E6**), in the other cases 2.2 eq.) and anhydrous DMF (2-4 mL) at 0°C under stirring in a N₂ atmosphere. After 12 hours, solvents were evaporated under reduced pressure, water was added to the residue, pH was adjusted to 1.00 (HCl 1N) and the precipitate thus obtained was collected and washed with water. The crude product thus obtained was purified as reported below.

2-(4-Nitrophenylthio)-N-(indol-6-yl)acetamide (C6): Yield 0.167 g (40%), m.p. 192-194°C (column chromatography (cyclohexane:EtOAc 4:6), ¹H-NMR (DMSO-d₆, 400 MHz) (δ) (ppm): 11.00 (1H, broad s), 10.25 (1H, broad s), 8.18 (2H, m), 7.94 (1H, s), 7.63 (2H, m), 7.46 (1H, d, J 8.3), 7.27 (1H, m), 7.03 (1H, dd, J 8.6, J 1.7), 6.36 (1H, s), 4.10 (2H, s); ¹³C-NMR (DMSO-d₆, 100 MHz) (δ) (ppm): 165.82, 147.63, 145.13, 136.28, 133.27, 126.90, 125.64, 124.65, 124.35, 120.38, 112.64, 102.76, 101.42, 36.60; ESI-HRMS calcd for C₁₆H₁₄N₃O₃S (M+H⁺) 328.0756, found 328.0740. HPLC-UV/Vis *k*: 12.82. Anal. Calc. for C₁₆H₁₃N₃O₃S, C, 58.70, H, 4.00, N, 12.84; found, C, 58.77, H, 4.11, N, 12.89.

2-(4-Nitrophenylthio)-N-(acetylaminosulfonylphen-4-yl)acetamide (C7): The reaction was carried out as described in the general procedure, using a suspension of sodium sulfacetamide (0.54 g, 2.30 mmol) in anhydrous DMF (6 mL) and TEA (0.26 g, 2.53 mmol). Yield 0.37 g (39%), m.p. 227-228°C (methanol), ¹H-NMR (DMSO-d₆, 400 MHz) (δ) (ppm): 12.10 (1H, broad s), 10.90 (1H, broad s), 8.31 (2H, m), 8.15 (2H, m), 7.93 (2H, m), 7.74 (2H, m), 4.30 (2H, s), 2.05 (3H, s); ¹³C-NMR (DMSO-d₆, 100 MHz) (δ) (ppm): 169.13, 167.24, 147.06, 145.25, 143.64, 133.91, 129.45, 126.96, 124.39, 119.24, 36.53, 23.65; ESI-HRMS calcd for C₁₆H₁₆N₃O₆S₂ (M+H⁺) 410.0480, found 410.0479. HPLC-UV/Vis *k*: 11.74. Anal. Calc. for C₁₆H₁₅N₃O₆S₂, C, 46.94, H, 3.69, N, 10.26; found, C, 46.66, H, 3.80, N, 10.33.

342 **2-(4-Nitrophenylthio)-N-(2-chlorobenzyl)acetamide (C9)**: Yield 0.40 g (85%), m.p. 122-123°C
343 (column chromatography cyclohexane:EtOAc 8:2)., ¹H-NMR (DMSO-d₆, 400 MHz) (δ) (ppm):
344 8.90 (1H, t, J 5.5), 8.28 (2H, m), 7.72-7.70 (2H, m), 7.57 (1H, m), 7.43-7.41 (3H, m), 4.50 (2H, d, J
345 5.5), 4.11 (2H, s); ¹³C-NMR (DMSO-d₆, 100 MHz) (δ) (ppm): 167.80, 147.41, 145.15, 136.30,
346 132.62, 129.62, 129.46, 129.26, 127.56, 126.99, 124.28, 40.97, 35.27; ESI-HRMS calcd for
347 C₁₅H₁₄ClN₂O₃S (M+H⁺) 337.0413, found 337.0403. HPLC-UV/Vis *k*: 13.33. Anal. Calc. for
348 C₁₅H₁₃ClN₂O₃S, C, 53.49, H, 3.89, N, 8.32; found, C, 53.66, H, 3.96, N, 8.20.

349 **2-(4-Nitrophenylthio)-N-(3-carboxypyridin-2-yl)acetamide (C11)**. Yield 21%, m.p. 194-196°C
350 (H₂O), ¹H-NMR (DMSO-d₆, 400 MHz) (δ) (ppm): 11.11 (1H, s), 8.53 (1H, dd, J 7.1, J 1.9), 8.22
351 (1H, dd, J 8.2, J 2.3), 8.15 (2H, m), 7.56 (2H, m), 7.28 (1H, dd, J 8.2, J 7.1), 4.30 (2H, s); ¹³C-NMR
352 (DMSO-d₆, 100 MHz) (δ) (ppm): 167.92, 167.31, 151.56, 150.12, 147.26, 147.00, 140.26, 126.97,
353 126.73, 124.31, 120.29, 36.86. ESI-HRMS calc. for C₁₄H₁₂N₃O₅S (M+H⁺) 334.0498, found
354 334.0490. HPLC-UV/Vis *k*: 9.05. Anal. Calc. for C₁₄H₁₁N₃O₅S, C, 50.45, H, 3.33, N, 12.61; found,
355 C, 50.33, H, 3.45, N, 12.85.

356 **2-(4-Nitrophenylthio)-N-(4-carboxyphenyl)propionamide (E1)**. Yield 74%, m.p. 232-234°C
357 (trituration with diethyl ether), ¹H-NMR (DMSO-d₆, 400 MHz) (δ) (ppm): 12.80 (1H, broad s),
358 10.66 (1H, s), 8.18 (2H, m), 7.92 (2H, m), 7.70 (2H, m), 7.61 (2H, m), 4.43 1H, q, J 6.9), 1.58 (3H,
359 d, J 6.9); ¹³C-NMR (DMSO-d₆, 100 MHz) (δ) (ppm): 170.07, 167.29, 145.78, 145.32, 143.06,
360 130.90, 128.82, 126.15, 124.52, 119.22, 45.58, 18.33. ESI-HRMS calc. for C₁₆H₁₅N₂O₅S (M+H⁺)
361 347.0702, found 347.0701. HPLC-UV/Vis *k*: 12.31. Anal. Calc. for C₁₆H₁₄N₂O₅S, C, 55.48, H,
362 4.07, N, 8.09; found, C, 55.23, H, 3.95, N, 8.55.

363 **2-Methyl-2-(4-nitrophenylthio)-N-(4-carboxyphenyl)propionamide (E2)**. Yield 20%, m.p. 215-
364 217°C (column chromatography CH₂Cl₂/CH₃OH 9.5:0.5), ¹H-NMR (DMSO-d₆, 400 MHz) (δ)
365 (ppm): 12.80 (1H, broad s), 10.11 (1H, s), 18.18 (2H, m), 7.90 (2H, m), 7.75 (2H, m), 7.5r8 (2H,
366 m), 1.70 (6H, s); ¹³C-NMR (DMSO-d₆, 100 MHz) (δ) (ppm): 170.28, 167.00, 148.20, 144.10,
367 143.21, 130.42, 130.15, 126.52, 120.44, 120.00, 50.42, 26.51. ESI-HRMS calc. for C₁₇H₁₇N₂O₅S

(M+H⁺) 361.0858, found 361.0844. HPLC-UV/Vis *k*: 13.02. Anal. Calc. for C₁₇H₁₆N₂O₅S, C, 56.66, H, 4.47, N, 7.77; found, C, 56.39, H, 4.45, N, 8.00.

2-Phenyl-2-(4-nitrophenylthio)-N-(4-carboxyphenyl)carboxylic acid (E3). Yield 40%, m.p. 219-221°C (column chromatography CH₂Cl₂/CH₃OH 9.5:0.5), ¹H-NMR (DMSO-d₆, 400 MHz) (δ) (ppm): 12.80 (1H, broad s), 8.18 (2H, m), 7.90 (2H, m), 7.69 (2H, m), 7.64 (2H, m), 7.55 (2H, m), 7.40 (2H, m), 7.35 (1H, m), 5.75 (1H, s); ¹³C-NMR (DMSO-d₆, 100 MHz) (δ) (ppm): 167.63, 167.23, 145.72, 145.66, 142.80, 136.15, 130.93, 129.34, 128.99, 128.74, 128.13, 126.41, 124.60, 119.30, 54.98. ESI-HRMS calc. for C₂₁H₁₇N₂O₅S (M+H⁺) 409.0858, found 409.0867. HPLC-UV/Vis *k*: 13.63. Anal. Calc. for C₂₁H₁₆N₂O₅S, C, 61.76, H, 3.95, N, 6.86; found, C, 61.70, H, 3.70, N, 6.95.

2-Phenyl-2-(4-nitrophenylthio)-N-(3-hydroxy-4-carboxyphenyl)acetamide (E4). Yield 23%, m.p. 218-220°C (column chromatography CH₂Cl₂/CH₃OH 8.5:1.5), ¹H-NMR (DMSO-d₆, 400 MHz) (δ) (ppm): 15.80 (1H, broad s), 10.58 (1H, s), 8.18 (2H, s), 7.63 (3H, m), 7.52 (2H, m), 7.44-7.30 (3H, m), 6.99 (1H, d, *J* 1.9), 6.82 (1H, dd, *J* 8.4, *J* 1.9), 5.71 (1H, s); ¹³C-NMR (DMSO-d₆, 100 MHz) (δ) (ppm): 167.07, 163.59, 145.2, 145.62, 141.97, 136.47, 131.02, 129.28, 128.88, 128.69, 127.99, 124.57, 116.23, 108.31, 106.70, 54.96. ESI-HRMS calc. for C₂₁H₁₇N₂O₆S (M+H⁺) 425.0807, found 425.0793. HPLC-UV/Vis *k*: 13.89. Anal. Calc. for C₂₁H₁₆N₂O₆S, C, 59.43, H, 3.80, N, 6.60; found, C, 59.59, H, 3.95, N, 6.55.

2-Phenyl-2-(4-nitrophenylthio)-N-(4-carboxamidophenyl)acetamide (E5). Yield 59%, m.p. 228-230°C, ¹H-NMR (DMSO-d₆, 400 MHz) (δ) (ppm): 10.90 (1H, s), 8.31 (2H, m), 8.00 (3H, m), 7.80 (4H, m), 7.70 (2H, m), 7.60-7.45 (2H, m), 7.40 (2H, s), 5.81 (1H, s); ¹³C-NMR (DMSO-d₆, 100 MHz) (δ) (ppm): 167.64, 167.43, 145.70, 141.34, 136.20, 130.08, 129.34, 128.95, 128.73, 128.11, 124.61, 119.10, 55.04. ESI-HRMS calc. for C₂₁H₁₈N₃O₄S (M+H⁺) 408.1018, found 408.1038. HPLC-UV/Vis *k*: 12.73. Anal. Calc. for C₂₁H₁₇N₃O₄S, C, 61.90, H, 4.21, N, 10.31; found, C, 61.56, H, 3.99, N, 10.50.

2-(4-Nitrophenylthio)-N-(3-carbomethoxypyridin-6-yl)acetamide (E6). Methyl (6-amino)nicotinate (**L3**), starting material for the synthesis of (**E6**), was obtained via esterification of 6-amino-nicotinic acid in MeOH saturated with HCl_g, prepared in situ adding HCl_g to a suspension of the nicotinic acid (0.730 g, 5.29 mmol) in MeOH (50 ml) at 0°C. Then the reaction mixture was refluxed at 100°C under stirring in a N₂ atmosphere for 3 hours. The solvent was removed under reduced pressure and Na₂CO₃ was added up to pH=9. A white powder was collected. Yield 87%. Compound **E6** was thus obtained following the general procedure described above. Yield 65%, m.p. 138-140°C (EtOH), ¹H-NMR (DMSO-d₆, 400 MHz) (δ) (ppm): 11.64 (1H, s), 8.90 (1H, s), 8.29 (1H, dd, J 8.7, J 2.3), 8.15 (3H, m), 7.63 (2H, m), 7.55 (2H, m), 7.45-7.35 (3H, m), 5.90 (1H, s), 3.94 (3H, s); ¹³C-NMR (DMSO-d₆, 100 MHz) (δ) (ppm): 168.60, 165.16, 154.97, 150.07, 145.78, 145.38, 140.10, 135.87, 129.42, 129.11, 128.77, 128.12, 124.65, 122.07, 113.26, 54.32, 52.65. ESI-HRMS calc. for C₂₁H₁₈N₃O₅S (M+H⁺) 424.0967, found 424.0964. HPLC-UV/Vis *k*: 15.00. Anal. Calc. for C₂₁H₁₇N₃O₅S, C, 59.57, H, 4.05, N, 9.92; found, C, 59.66, H, 3.98, N, 9.75.

2-(4-Nitrophenylthio)- and phenyl-2-(4-nitrophenylthio)-N-(6-methanesulfonylbenzothiazol-2-yl)acetamide (C8) and (E7). General procedure. To a solution of (**K1d acid**) and (**K1c acid**) respectively (0.50 g, 2.35 mmol) in anhydrous DMF (10 mL) under stirring at RT in a N₂ atmosphere, 1-ethyl-3-(3-dimethylaminopropyl)carbodiimide (WSC) (0.45 g, 2.35 mmol), 2-amino-6-methanesulphonylbenzothiazole (**L4**) (0.54 g, 2.35 mmol) and HOBt (0.32 g, 2.35 mmol) were added in sequence. After 12 hours at RT the mixture was treated with water (2 x 10 mL) and the residue thus obtained was purified by trituration with EtOAc.

2-(4-Nitrophenylthio)-N-(6-methanesulfonylbenzothiazol-2-yl)acetamide (C8): Yield 35%, m.p. 217-218°C (ethyl acetate). ¹H-NMR (DMSO-d₆, 400 MHz) (δ) (ppm): 13.00 (1H, broad s), 8.64 (1H, s), 8.18 (2H, m), 7.97 (2H, s), 7.61 (2H, m), 4.30 (2H, s), 3.22 (3H, s); ¹³C-NMR (DMSO-d₆, 100 MHz) (δ) (ppm): 168.48, 162.22, 152.43, 146.42, 145.41, 136.09, 132.48, 127.12, 125.39, 124.45, 122.65, 121.49, 44.48, 35.33. ESI-HRMS calc. for C₁₆H₁₄N₃O₅S₃ (M+H⁺) 424.0096, found

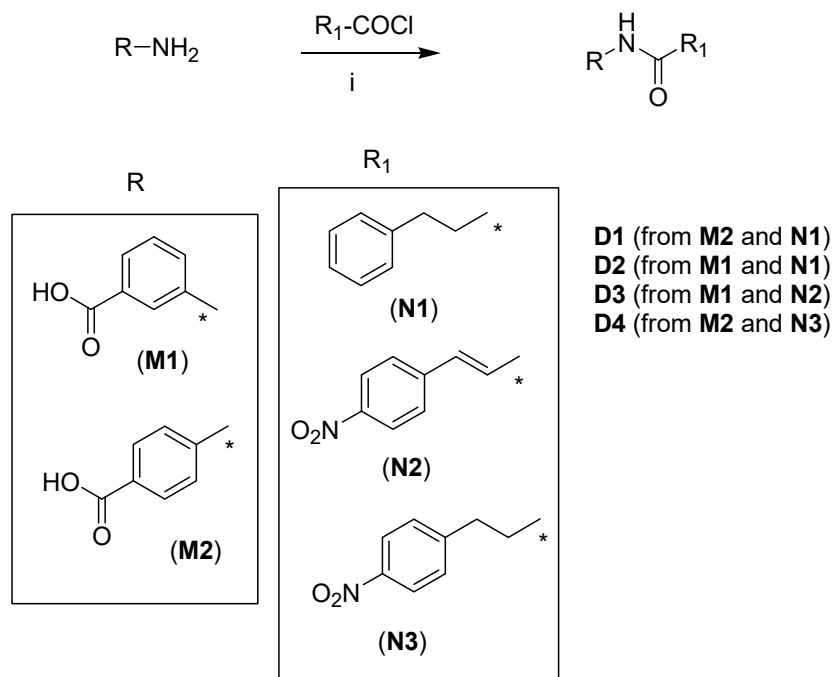
419 424.0096. HPLC-UV/Vis *k*: 12.44. Anal. Calc. for C₁₆H₁₃N₃O₅S₃, C, 45.38, H, 3.09, N, 9.92;
420 found, C, 45.65, H, 3.25, N, 9.75.

421 **Phenyl[2-(4-nitrophenylthio)-N-(6-methanesulfonylbenzothiazol-2-yl)]acetamide (E7):** Yield
422 18%, m.p. 95°C (dec.) (column chromatography CH₂Cl₂:CH₃OH 9.5:0.5, then trituration with
423 diisopropyl ether). ¹H-NMR (DMSO-d₆, 200 MHz) (δ) (ppm): 13.30 (1H, broad s), 8.66 (1H, s),
424 8.12 (2H, m), 7.95 (2H, s), 7.70-7.30 (7H, m), 5.83 (1H, s), 3.20 (3H, s); ¹³C-NMR (DMSO-d₆, 50
425 MHz) (δ) (ppm): 174.01, 168.10, 152.09, 146.03, 136.30, 134.99, 129.52, 129.35, 128.93, 128.67,
426 125.44, 124.67, 122.72, 121.62, 53.98, 44.46. ESI-HRMS calc. for C₂₂H₁₈N₃O₅S₃ (M+H⁺)
427 500.0409, found 500.0404. HPLC-UV/Vis *k*: 14.16. Anal. Calc. for C₂₂H₁₇N₃O₅S₃, C, 52.89, H,
428 3.43, N, 8.41; found, C, 52.65, H, 3.35, N, 8.65.

429

430

431 **Synthesis of compounds D1-D4.**



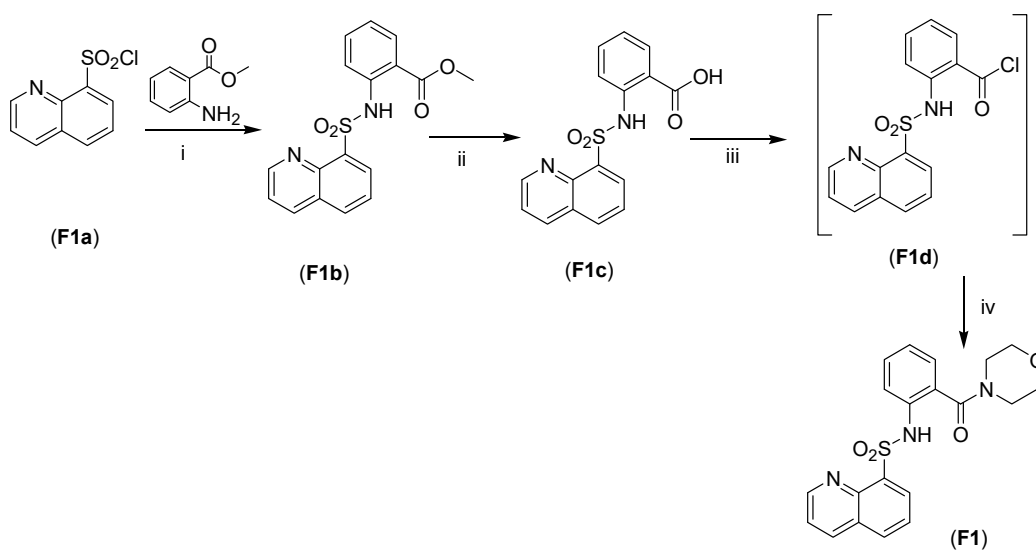
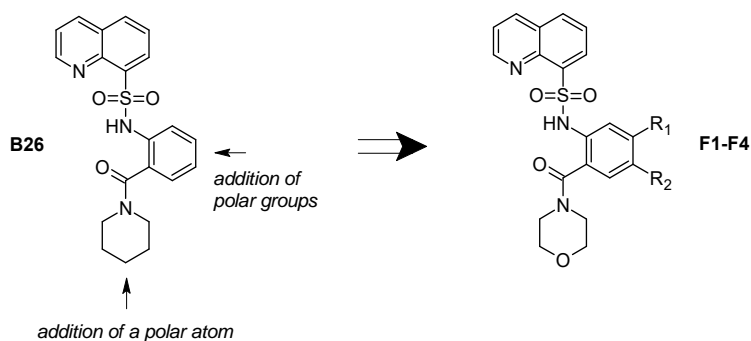
432
433
434 **Appendix 2-figure 5. Synthesis of compounds D1-D4.** (i): TEA/CH₂Cl₂

435
436 **General procedure.** To a solution of aminobenzoic acid (**M1**) or (**M2**) (3.56 mmol) and TEA (6.52
437 mmol) in anhydrous CH₂Cl₂ (20 mL) was added, during 10 min, a solution of the opportune acyl
438 chloride (**N1**)-(N3) (2.96 mmol) in anhydrous CH₂Cl₂ (6 mL) under stirring elm at 0°C in a N₂
439 atmosphere. The solution was stirred for 12 hours at RT, then the solvent was removed under
440 reduced pressure, the residue was diluted with water/ice, acidified (HCl 0.5N) and the precipitate
441 was collected and washed with water.

442 **3-phenyl-N-(4-carboxyphenyl)propionamide (D1).**Yield 0.156 g (20%) (CH₃OH), m.p. 240-
443 242°C, ¹H-NMR (DMSO-d₆, 400 MHz) (δ) (ppm): 12.80 (1H, broad s), 10.21 (1H, s), 7.89 (2H, m),
444 7.70 (2H, m), 7.30-7.15 (5H, m), 2.93 (2H, t, J 8.0), 2.68 (2H, t, J 8.0); ¹³C-NMR (DMSO-d₆, 100
445 MHz) (δ) (ppm): 171.40, 167.39, 143.70, 141.52, 130.85, 128.80, 128.71, 126.44, 125.40, 118.73,

446 38.50, 31.00. ESI-HRMS calc. for $C_{16}H_{16}NO_3$ ($M+H^+$) 270.1130, found 270.1127. HPLC-UV/Vis
 447 k : 11.87. Anal. Calc. for $C_{16}H_{15}NO_3$, C, 71.36, H, 5.61, N, 5.20; found, C, 71.45, H, 5.65, N, 5.35.
 448 **3-phenyl-N-(3-carboxyphenyl)propionamide (D2)**. Yield 63%, m.p. 214-216°C (CH_3OH), 1H -
 449 NMR (DMSO- d_6 , 200 MHz) (δ) (ppm): 12.90 (1H, broad s), 10.05 (1H, s), 8.22 (1H, s), 7.82 (1H, d,
 450 J 8.2), 7.60 (1H, d, J 8.2), 7.40 (1H, t, J 8.2), 7.30-7.10 (5H, m), 2.90 (2H, t, 8.0), 2.50 (2H, t, J 8.0);
 451 ^{13}C -NMR (DMSO- d_6 , 50 MHz) (δ) (ppm): 171.09, 167.62, 141.57, 139.88, 131.73, 129.37, 128.78,
 452 128.69, 126.40, 124.30, 123.60, 120.28, 38.39, 31.20. ESI-HRMS calc. for $C_{16}H_{16}NO_3$ ($M+H^+$)
 453 270.1130, found 270.1124. HPLC-UV/Vis k : 11.55. Anal. Calc. for $C_{16}H_{15}NO_3$: C 71.36, H 5.61, N
 454 5.20, found, C, 71.28, H, 5.58, N, 5.24.
 455 **3-(4-Nitrophenyl)-N-(3-carboxyphenyl)prop-2-enamide (D3)**. Yield 43%, m.p. 295-297°C
 456 (CH_3OH), 1H -NMR (DMSO- d_6 , 200 MHz) (δ) (ppm): 12.90 (1H, broad s), 10.65 (1H, s), 8.28 (3H,
 457 m), 7.90 (3H, m), 7.68 (1H, d, J 8.0), 7.65 (1H, d, J 15.5), 7.45 (1H, t, J 8.0), 6.98 (1H, d, J 15.5);
 458 ^{13}C -NMR (DMSO- d_6 , 50 MHz) (δ) (ppm): 165.53, 163.48, 148.18, 141.65, 139.70, 138.48, 131.89,
 459 129.58, 129.26, 126.79, 124.87, 124.61, 123.85, 120.52. ESI-HRMS calc. for $C_{16}H_{13}N_2O_5$ ($M+H^+$)
 460 313.0824, found 313.0812. HPLC-UV/Vis k : 12.04. Anal. Calc. for $C_{16}H_{12}N_2O_5$: C 61.54, H 3.87,
 461 N 8.97, found, C, 61.34, H, 4.00, N, 8.77.
 462 **3-(4-Nitrophenyl)-N-(4-carboxyphenyl)propionamide (D4)**. Yield 0.072 (10%), m.p. 292-294°C
 463 (trituration with CH_2Cl_2), 1H -NMR (DMSO- d_6 , 400 MHz) (δ) (ppm): 12.80 (1H, broad s), 10.40
 464 (1H, broad s), 8.31 (2H, m), 8.02 (2H, m), 7.83 (2H, m), 7.70 (2H, m), 3.21 (2H, m), 2.90 (2H, m);
 465 ^{13}C -NMR (DMSO- d_6 , 100 MHz) (δ) (ppm): 170.91, 167.36, 150.05, 146.46, 143.58, 130.85,
 466 130.10, 125.48, 123.93, 118.76, 37.56, 30.78; ESI-HRMS calcd for $C_{16}H_{15}N_2O_5$ ($M+H^+$) 315.0981,
 467 found 315.0980. HPLC-UV/Vis k : 11.60. Anal. Calc. for $C_{16}H_{14}N_2O_5$, C, 61.14, H, 4.49, N, 8.91;
 468 found, C, 61.50, H, 4.33, N, 8.89.
 469

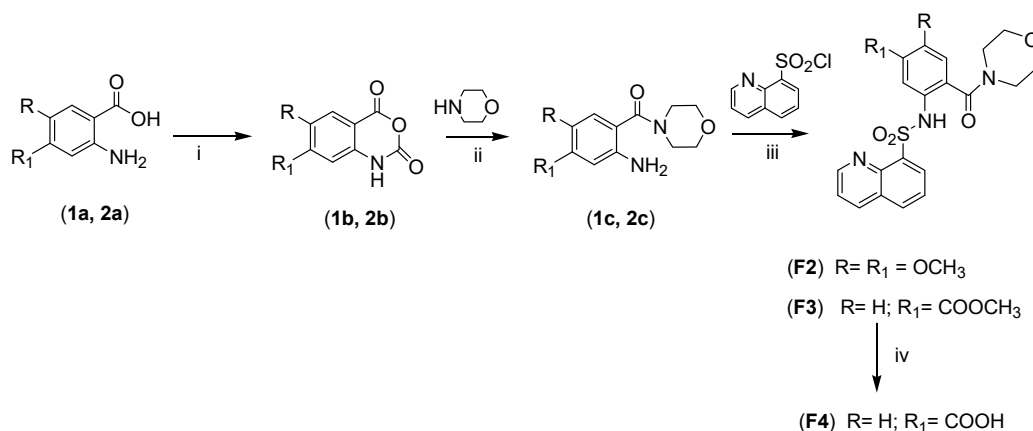
470 **Synthesis of compounds F1-F4.**



475 **Appendix 2-figure 6. Design of compounds F (upper panel). Synthesis of compound F1**
 476 **(bottom panel).** (i): CH₂Cl₂/pyridine/DMAP, RT; (ii): THF/LiOH 2M; (iii): THF/DMF, (COCl)₂;
 477 (iv): morpholine, CH₂Cl₂/TEA 0°C.

478

479



Appendix 2-figure 7. Synthesis of compounds F2-F4. (i): THF/triphosgene, r.t.; (ii): DMF/DMAP; (iii): CH₂Cl₂/pyridine/DMAP; (iv): THF/LiOH 2M.

Methyl 2-[(quinolin-8-ylsulphonyl)amino]benzoate (F1b): To a solution of methyl anthranilate (0.63 g, 4.18 mmol) in anhydrous CH₂Cl₂ (10 mL) at RT were added 8-quinolinesulfonyl chloride (F1a) (1.00 g, 4.39 mmol), pyridine (0.99 g, 12.5 mmol), and DMAP (0.03 g, 0.21 mmol) under elm stirring at RT in N₂ atmosphere. The mixture was stirred at RT for 12 hours, then the solvent was removed under reduced pressure. Water was added to the residue thus obtained and the mixture was extracted with EtOAc (2 x 20 mL); the organic phase was dried (Na₂SO₄) and the solvent removed under reduced pressure. This material was used in the next step without further purification. Yield 1.40 g (98%), m.p. 206-209°C, ¹H-NMR (DMSO-d₆, 200 MHz) (δ) (ppm): 11.05 (1H, broad s), 8.98 (1H, m), 8.60-8.20 (3H, m), 7.80-7.55 (4H, m), 7.42 (1H, m), 6.95 (1H, m), 3.90 (1H, s); ¹³C-NMR (DMSO-d₆, 50 MHz) (δ) (ppm): 167.57, 151.99, 139.75, 137.54, 135.33, 134.88, 133.08, 131.41, 128.81, 126.10, 123.28, 123.24, 117.73, 116.57, 53.09.

2-[(Quinolin-8-ylsulphonyl)amino]benzoic acid (F1c): A suspension of (F1b) (1.26 g, 3.67 mmol) and aqueous LiOH 2M (7.1 mL) in THF (8.5 mL) was stirred at RT for 12 hours. The solution thus obtained was cooled with ice and HCl 0.5 N (20 mL) was added until pH 2. The residue thus obtained was filtered and washed with water. Yield 1.10g (92%), m.p. 253-259°C

(dec.), ¹H-NMR (DMSO-d₆, 200 MHz) (δ) (ppm): 11.50 (1H, broad s), 8.95 (1H, m), 8.60-8.40 (2H, m), 8.25 (1H, d, *J* 8.2), 7.85-7.50 (4H, m), 7.50-7.30 (1H, m), 7.0-6.80 (1H, m); ¹³C-NMR (DMSO-d₆, 50 MHz) (δ) (ppm): 169.36, 151.87, 142.84, 140.19, 137.43, 135.20, 134.74, 134.51, 133.04, 131.82, 128.81, 126.06, 123.18, 122.91, 117.19, 117.09.

1-[[Quinoline-8-yl-sulfonyl]amino]benzoyl]morpholine (F1): To a solution of (F1c) (0.3 g, 0.91 mmol) in anhydrous THF (5 mL) and DMF (0.01 mL) at 0°C, oxalylchloride (0.13 g, 1.35 mmol) was added dropwise, then the mixture was stirred for 1 hour at RT. At the end of the reaction, the solvent was removed under reduced pressure. The solid thus obtained was coevaporated with anhydrous CH₂Cl₂ three times, and the compound (F1d) thus obtained was used in the next step without purification. To a solution of (F1d) (0.32 g, 0.91 mmol) and TEA (0.23 g, 2.28 mmol) in anhydrous CH₂Cl₂ (20 mL) morpholine (0.07 g, 0.82 mmol) was added and the solution thus obtained was stirred at RT for 6 hours. Then the solvent was removed under pressure and the residue thus obtained was purified by column chromatography (EtOAc 100%). Yield 0.099 g (31%), m.p. 191-194°C, ¹H-NMR (DMSO-d₆, 400 MHz) (δ) (ppm): 9.50 (1H, broad s), 9.25 (1H, d, *J* 2.9), 8.75 (1H, d, *J* 7.9), 8.45 (2H, m), 7.91 (2H, m), 7.63 (1H, m), 7.48 (1H, m), 7.27 (2H, m), 3.8-3.0 (8H, m); ¹³C-NMR (DMSO-d₆, 100 MHz) (δ) (ppm): 167.39, 152.16, 142.85, 137.76, 135.59, 134.78, 131.34, 130.89, 128.96, 128.49, 127.47, 126.27, 124.99, 123.94, 123.34, 66.04, 65.38, 47.60, 42.30, 15.63; ESI-HRMS calcd for C₂₀H₂₀N₃O₄S (M+H⁺) 398.1174, found 398.1189. HPLC-UV/Vis *k*: 10.97.

Substituted (isatoic anhydrides) (1b) and (2b). General procedure. To a solution of the appropriate (substituted)-2-aminobenzoic acid (1a, 2a) (5.10 mmol) in anhydrous THF (25 mL), triphosgene (2.20 mmol) was added at RT under stirring elm. The suspension thus obtained was stirred for 24 hours; then, water was added and the solution was extracted with EtOAc (2 x 50 mL); the organic phase was dried (Na₂SO₄) and the solvent removed under reduced pressure.

524 **5,6-Dimethoxy isatoic anhydride (1b)**: Yield 1.03 g (91%), m.p. 260-261°C (dec.), ¹H-NMR
525 (DMSO-d₆, 200 MHz) (δ) (ppm): 11.5 (1H, broad s), 7.20 (1H, s), 6.60 (1H, s), 3.80 (6H, s); ¹³C-
526 NMR (DMSO-d₆, 50 MHz) (δ) (ppm): 159.78, 157.01, 147.83, 146.13, 138.06, 109.06, 101.62,
527 98.14, 56.53, 56.34.

528 **5-Methoxycarbonyl isatoic anhydride (2b)**: Yield 1.00 g (88%), m.p. 192-194°C, ¹H-NMR
529 (DMSO-d₆, 200 MHz) (δ) (ppm): 11.85 (1H, broad s), 8.0 (1H, d, *J* 8.1), 7.70 (2H, m), 3.9 (3H, s);
530 ¹³C-NMR (DMSO-d₆, 50 MHz) (δ) (ppm): 165.31, 147.28, 141.94, 136.86, 130.03, 123.64, 116.39,
531 114.37, 53.31.

532 **Substituted quinolines (1c) and (2c). General procedure.** To a suspension of the appropriate
533 (substituted)isatoic anhydride (**1b**) or (**2b**) (4.6 mmol) in anhydrous DMF (30 mL) morpholine (4.6
534 mmol) and DMAP (0.46 mmol) were added under stirring at RT in a N₂ atmosphere. The solution
535 was stirred for 8 hours at RT, then, water was added to the reaction mixture and the product was
536 extracted with EtOAc, the organic phase was dried (Na₂SO₄) and the solvent removed under
537 reduced pressure.

538 **1-(2-Amino-4,5-dimethoxybenzoyl)morpholine (1c)**: Yield 0.36g (30%), m.p. 100-102°C, ¹H-
539 NMR (DMSO-d₆, 200 MHz) (δ) (ppm): 6.60 (1H, s), 6.35 (1H, s), 4.95 (2H, s), 3.70 (3H, s), 3.65
540 (3H, s), 3.58 (4H, m), 3.45 (4H, m); ¹³C-NMR (DMSO-d₆, 50 MHz) (δ) (ppm): 168.00, 151.62,
541 142.04, 113.53, 100.76, 66.63, 56.93, 55.66.

542 **1-[(2-Amino-4-methoxycarbonyl)benzoyl]morpholine (2c)**: Yield 0.65 g (54%), m.p. 112-113°C,
543 ¹H-NMR (DMSO-d₆, 200 MHz) (δ) (ppm): 7.35(1H, s), 7.10 (2H, s), 5.45 (2H, s), 3.80 (3H, s), 3.7-
544 3.3 (8H, m); ¹³C-NMR (DMSO-d₆, 50 MHz) (δ) (ppm): 168.04, 166.66, 146.07, 131.36, 128.47,
545 123.83, 116.46, 116.42, 66.53, 52.48.

546 **1-[[Quinoline-8-yl-sulfonyl]amino]-3,4-dimethoxybenzoyl]morpholine (F2)**: To a solution of
547 (**1c**) (0.33 g, 1.25 mmol) in anhydrous CH₂Cl₂ (10 mL) under stirring at RT, 8-
548 quinolinesulfonylchloride (0.28 g, 1.26 mmol), pyridine (0.30 g, 3.75 mmol) and DMAP (8 mg,

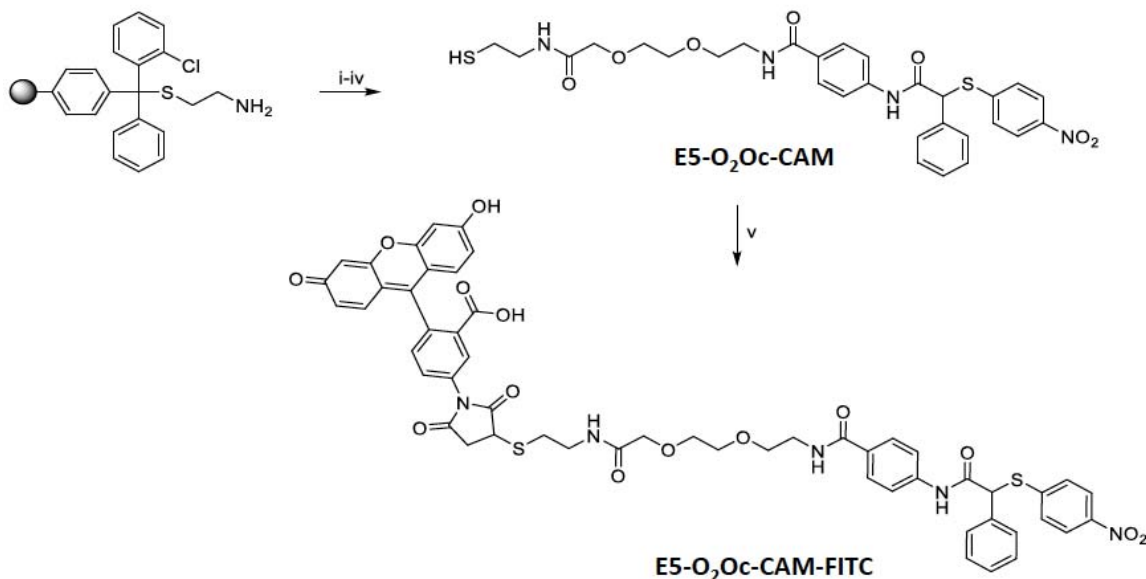
0.06 mmol) were added. The mixture was stirred at RT for 12 hours, then the solvent was removed under pressure; water and ice were added to the oily residue, and the solid thus formed was filtered, washed with water, dried and purified by trituration with anh. diethyl ether (4 mL). Yield 0.57 g 100%, m.p. 166-168°C, ¹H-NMR (DMSO-d₆, 400 MHz) (δ) (ppm): 9.42 (1H, broad s), 9.25 (1H, m), 8.82-8.68 (1H, m), 8.55-8.33 (2H, m), 8.02-7.78 (2H, m), 7.15 (1H, m), 6.80 (1H, m), 3.80 (6H, m), 3.70-2.70 (8H, m); ¹³C-NMR (DMSO-d₆, 100 MHz) (δ) (ppm): 167.26, 152.14, 150.60, 145.99, 142.88, 137.64, 135.46, 134.74, 131.60, 129.10, 128.89, 126.26, 123.34, 119.89, 111.37, 108.68, 81.154, 65.92, 56.194, 55.93; ESI-HRMS calcd for C₂₂H₂₄N₃O₆S (M+H⁺) 458.1386, found 458.1386. HPLC-UV/Vis *k*: 10.54.

Methyl 3-[(quinoline-8-yl-sulfonyl)amino]-4-[(morpholin-1-yl)oxo] benzoate (F3): To a solution of (2c) (0.59 g, 2.22 mmol) in anhydrous CH₂Cl₂ (15 mL) at RT under stirring elm, were added 8-quinolinesulfonylchloride (0.56 g, 2.44 mmol), pyridine (0.53 g, 6.66 mmol) and DMAP (0.014 g, 0.11 mmol). The solution was stirred at RT for 12 hours, then the solvent was removed under reduced pressure. A mixture of water and ice (10 mL), then EtOAc (4 mL) was added to the oily residue; the precipitate thus obtained was filtered, washed with water, dried and purified by trituration with diethyl ether. Yield 1.00 g (99%), m.p. 174-176°C, ¹H-NMR (DMSO-d₆, 400 MHz) (δ) (ppm): 9.65 (1H, broad s), 9.26 (1H, dd, *J* 4.3, *J* 1.8), 8.77 (1H, dd, *J* 8.4, *J* 1.4), 8.50 (1H, m), 8.43 (1H, dd, *J* 7.3, *J* 1.2), 8.19 (1H, d, *J* 1.4), 7.95 (1H, m), 7.88 (1H, m), 7.82 (1H, dd, *J* 7.9, *J* 1.6), 7.59 (1H, d, *J* 8.1), 4.00 (3H, s), 3.70-3.2 (8H, m); ¹³C-NMR (DMSO-d₆, 100 MHz) (δ) (ppm): 166.24, 165.55, 152.21, 142.79, 137.80, 135.65, 135.58, 134.97, 132.24, 131.59, 131.25, 128.99, 126.31, 125.71, 124.87, 123.44; ESI-HRMS calcd for C₂₂H₂₂N₃O₆S (M+H⁺) 456.1229, found 456.1227. HPLC-UV/Vis *k*: 11.37.

1-[[[(Quinoline-8-yl-sulfonyl)amino]-4-carboxybenzoyl]morpholine (F4): A suspension of (2c) (0.25 g, 0.59 mmol) in THF (3 mL) and aqueous LiOH 2M (1.15 mL) was stirred at RT for 12 hours. The solution thus obtained was cooled with ice and HCl 0.5 N (20 mL) was added until pH

574 2.0. The solid thus obtained was filtered and washed with water. Yield 0.22 g (91%), m.p. 255-
575 258°C, ¹H-NMR (DMSO-d₆, 400 MHz) (δ) (ppm): 13.40 (1H, broad, s), 9.60 (1H, broad, s), 9.25
576 (1H, dd, *J* 4.3, *J* 1.8), 8.76 (1H, dd, *J* 8.4, *J* 1.6), 8.49 (1H, dd, 8.4, *J* 1.2), 8.43 (1H, dd, *J* 7.3, *J*
577 1.4), 8.18 (1H, d, *J* 1.4), 7.95 (1H, m), 7.92-7.85 (1H, m), 7.83-7.77 (1H, dd, *J* 7.9, *J* 1.6), 7.46 (1H,
578 d, *J* 7.9), 3.70-3.10 (8H, m); ¹³C-NMR (DMSO-d₆, 100 MHz) (δ) (ppm): 166.56, 166.43, 152.20,
579 142.79, 137.78, 135.60, 135.57, 134.93, 132.88, 131.74, 131.23, 128.70, 128.83, 126.03, 125.79,
580 124.90, 123.42, 66.00; ESI-HRMS calcd for C₂₁H₂₀N₃O₆S (M+H⁺) 442.1073, found 442.1068.
581 HPLC-UV/Vis *k*: 9.85.
582

583 **Synthesis of E5-(O₂Oc)-CAM and E5-(O₂Oc)-CAM-FITC.**



584

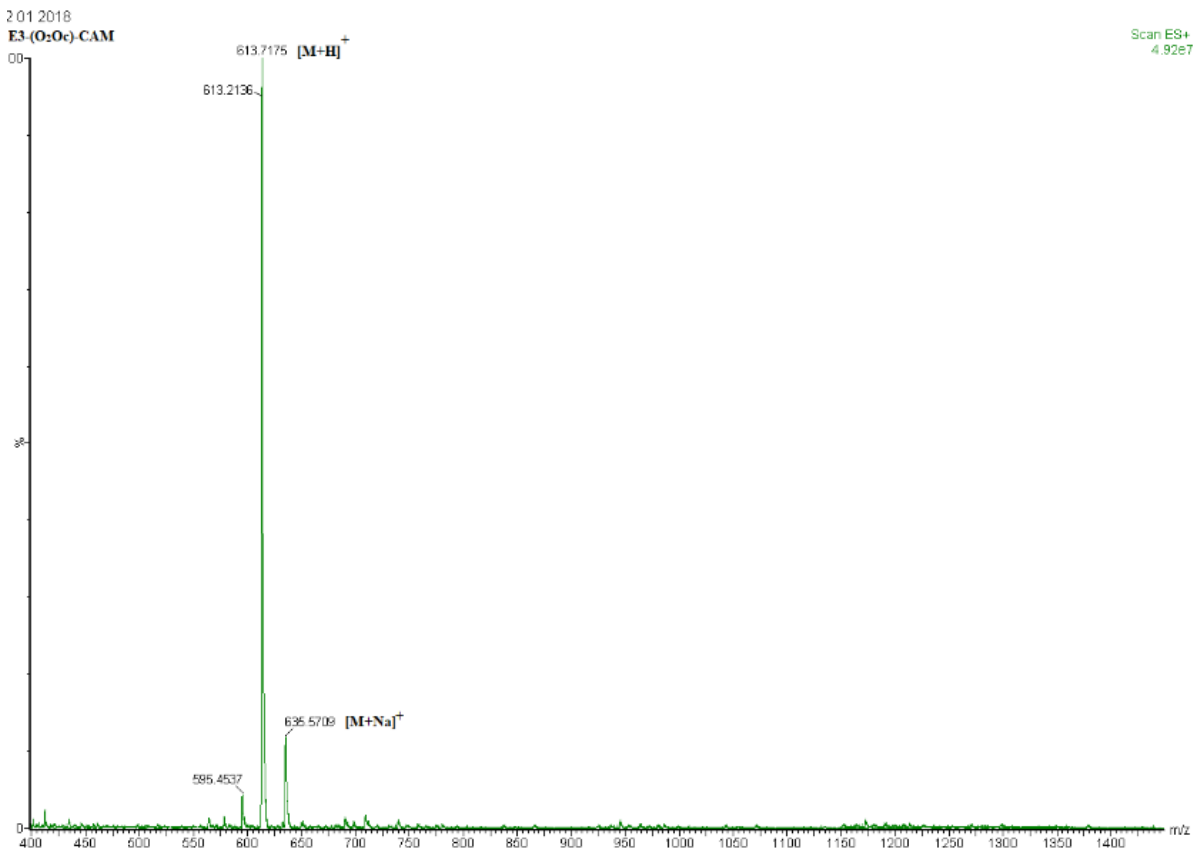
585 **Appendix 2-figure 8. Synthesis of compounds E5-O₂Oc-CAM and E5-O₂Oc-CAM-FITC.** (i)
 586 cysteamine 2-chlorotrityl resin (1 eq.), Fmoc-O₂Oc-OH (4 eq.), DIC (4 eq.), HOBT (4 eq.), DMF,
 587 r.t., 30 min; (ii) 40% piperidine in DMF, r.t., 5 min; (iii) **E3** (2 eq.), HATU (3 eq.) DIPEA (2 eq.),
 588 DMF, r.t., 3 h; (iv) trifluoroacetic acid (TFA)/H₂O/phenol/triisopropylsilane 88:5:5:2 v/v (10 mL /
 589 0.2 g of resin); r.t., 30 min; (v) E5-(O₂Oc)-CAM (1 eq.), Fluorescein-5-Maleimide (0.06 eq.),
 590 CH₃CN/H₂O, r.t., 5 min.

591

592 **Synthesis of E5-(O₂Oc)-CAM**

593 The Cysteamine (CAM) 2-chlorotrityl resin (0.079 mmol) was swelled in DMF and suspended in a
 594 solution of Fmoc-amino-3,6 dioxaoctanoic acid (Fmoc-O₂Oc-OH) (0.316 mmol), N,N'-
 595 Diisopropylcarbodiimide (DIC) (0.316 mmol) and hydroxybenzotriazole (HOBT) (0.316 mmol) in
 596 DMF (2 mL). This suspension was shaken for 30 minutes. After this time the solid phase was
 597 filtered and washed with DMF (3x2mL). The polymer was successively suspended in a 40%
 598 solution of piperidine in DMF (3x2 mL) and shaken for 5 minutes. The resin was filtered and
 599 washed with DMF (3x2 mL). In the final step the solid support was suspended in a solution of **E3**,

600 (0.158 mmol), (1-[Bis(dimethylamino)methylene]-1H-1,2,3-triazolo[4,5-b]pyridinium 3-oxid
 601 hexafluorophosphate (HATU) (0.237 mmol) and diisopropylethylamine (DIPEA) (0.237 mmol) in
 602 DMF and shaken for 3 hours. The functionalized resin was washed with DMF (3x2mL) and the
 603 desired molecule was released after a treatment with a mixture of trifluoroacetic acid
 604 (TFA)/H₂O/phenol/triisopropylsilane 88:5:5:2 v/v (10 mL per 0.2 g of resin) for 30 minutes at room
 605 temperature. After filtration of the resin, the solvent was concentrated in vacuo and the residue
 606 triturated with ethyl ether. The crude of reaction was purified by preparative HPLC giving, after
 607 lyophilization, the E3-(O₂Oc)-CAM as a pale yellow amorphous solid (49% yield). ESI-HRMS
 608 calcd for C₂₉H₃₃N₄O₇S₂⁺ (M+H⁺): 613.1785 (Figure 9); found: 613.7175.

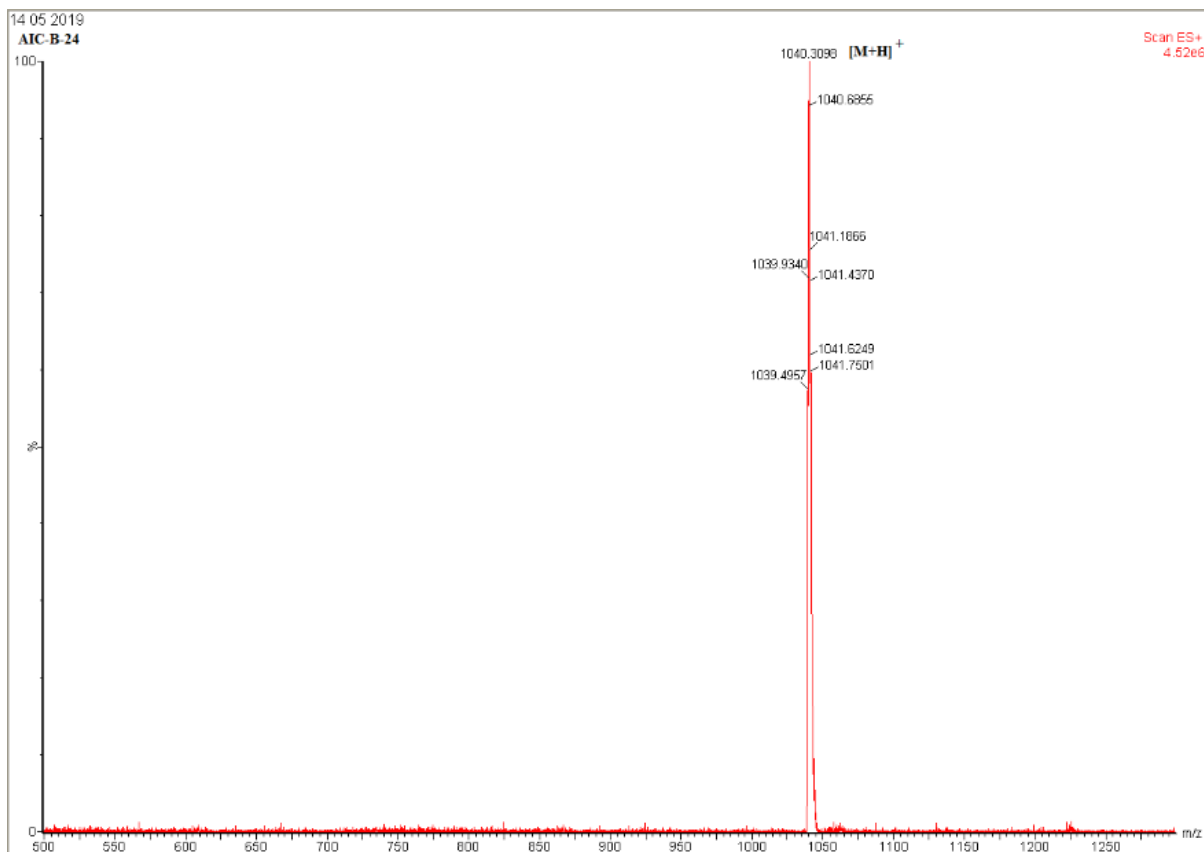


Appendix 2-figure 9. Mass spectrum of E5-(O₂Oc)-CAM ESI-HRMS calcd for C₂₉H₃₃N₄O₇S₂⁺
 (M+H⁺): 613.1785.

609

610 **Synthesis of E5-(O₂Oc)-CAM-FITC.**

611 To a stirred solution of **E5-(O₂Oc)-CAM** (0.0277 mmol) in CH₃CN (0,5 mL), Fluorescein-5-
612 Maleimide (FITC) (0.00156 mmol) solubilized in CH₃CN/H₂O (250μL/250μL) was added followed
613 by 20 μL of 5% solution of NaHCO₃. The reaction was stirred in the dark and the MS monitoring
614 showed a complete consumption of the fluorescent probe in about 5 minutes. After this time the
615 reaction solution the product was purified directly by preparative HPLC using the same
616 experimental conditions as for the purification of E3-(O₂Oc)-CAM. After lyophilization in the dark,
617 a yellow amorphous solid was obtained in quantitative yield and with a purity grade > 95%. ESI-
618 HRMS calcd for C₅₃H₄₆N₅O₁₄S₂⁺ (M+H⁺): 1040.2477 (Figure 10); found: 1040.3098.



619 **Appendix 2-figure 10.** Mass spectrum of E5-(O₂Oc)-CAM-FITC. ESI-HRMS calcd for
620 C₅₃H₄₆N₅O₁₄S₂⁺ (M+H⁺):1040.2477.

Appendix 3

Enantioseparation and racemization of E7

Materials. The columns used were Chiralcel OD-RH [cellulose tris (3,5-dimethylphenylcarbamate); 250 × 4.6 mm I.D.; 5 µm], Chiralcel OD [cellulose tris (3,5-dimethylphenylcarbamate); 250 × 10 mm I.D., 10 µm] purchased from Chiral Technologies Europe, Illkirch, France. HPLC analyses were performed on an Agilent Technologies (Waldbronn, Germany) modular model 1200 system, consisting of a vacuum degasser, a binary pump, an autosampler, a thermostatted column compartment and a variable ultraviolet detector (UV). Chromatograms were acquired at 254 nm. HPLC-grade acetonitrile and water were obtained from Baker.

Analytical and semipreparative enantioseparation. The analytical enantioseparation of chiral E7 was performed in reversed phase using a Chiralcel OD-RH column with mobile phases of water:acetonitrile mixtures at different percentages. The separation was carried out isocratically at 25 °C. The racemic compound mixture was dissolved in acetonitrile and subsequently diluted 1:10 (v/v) with the mobile phase at a final concentration of 100 µg/mL. The injection volume was 6 µL. The detector was set at 254 nm. The retention factors (k_1 and k_2) were calculated as $k_1 = (t_1 - t_0)/t_0$ where t_1 and t_2 are the retention times of the first and second eluted enantiomers and the separation factor (α) as k_2/k_1 . The resolution factor (R_s) was calculated as $R_s = 2(t_2 - t_1)/(w_1 + w_2)$, where w_1 and w_2 are the peak widths at the base for the two eluted enantiomers. The dead time of the columns (t_0) was determined by injection of 1,3,5-tri-*tert*-butylbenzene. Among the mobile phases used, water:acetonitrile 2:98 (v/v) was chosen for the subsequent semipreparative separation because it gave a good baseline

enantiomeric resolution, with $k_1 = 0.36$, $k_2 = 0.62$ and $R_s = 4.76$. Semipreparative enantioseparation of (\pm)-**E7** was carried out on Chiralcel® OD employing water:acetonitrile 2:98 (v/v) as the mobile phase at 5 mL/min. By injecting 15 mg of the racemic mixture, the single enantiomers were collected with acceptable enantiomeric excess (99.0% and 80.1% e.e. for the first and second eluted enantiomer, respectively, (Supplementary 5, Figure 1 and 2). 8.8 mg of the first enantiomer and 4.4 mg of the second one was obtained and were sufficient for further stability studies. The specific rotation in acetonitrile of first and second eluted enantiomers were acquired on a Perkin-Elmer 241 Polarimeter resulting in $[\alpha]_D^{20} = +7.95^\circ$ (c 0.00088 g/mL; acetonitrile) and $[\alpha]_D^{20} = -9.10^\circ$ (0.00044 g/mL, acetonitrile), respectively.

Racemization. Racemization is the conversion of an enantiomer into a racemic mixture and is associated with a loss in optical activity of the chiral compound over time. The rate constant of racemization k_{rac} refers to this first-order kinetic process and can be calculated from the linear plot of the logarithmic values of the enantiomeric excess ($\ln(e.e.)$) versus time, according to Eq. (S1):

$$(S1) \quad \ln(e.e.) = -k_{rac} \cdot t$$

The half-life of racemization ($t_{1/2rac}$) is the time during which the enantiomeric purity of a chiral compound reduces to 50% of its original e.e. For a first-order racemization, the half-life can be calculated by Eq. (S2):

$$(S2) \quad t_{1/2rac} = \ln 2 / k_{rac}$$

Single enantiomers of (\pm)-**E7** were dissolved in acetonitrile [1 mg/mL] and then diluted 1:100 with buffer solution at final concentration of [0.1 μ g/mL]. The solution was thermostated at 37.5 °C and racemization was monitored by injecting the solution at fixed times on a Chiralcel

OD-RH column using water and acetonitrile 2:98 (v/v) as mobile phase. Four repeats of each experiment were carried out.

Racemization kinetics. The previously obtained single enantiomers of (±)-**E7** were solubilized in buffer solutions to simulate *in vitro* test conditions and then incubated for a set of times at 37.5 °C. After the selected times, they were injected in a Chiralcel OD-RH column (water:acetonitrile 2:98 (v/v)) to evaluate racemization rates. The data were analyzed. The kinetic parameters were calculated from the corresponding peak areas according to Eqs. S1 and S2.

Enantiomer and racemate inhibition of hTS.

The capability of (±) **E7** compound to inhibit the kinetic activity of hTS protein enzyme was spectrophotometrically evaluated using the JASCO V730 UV/Vis spectrophotometer. The reaction was monitored by following the absorption change of MTHF substrate at 340 nm for 180 seconds.

*Inhibition Potency Evaluation of (+)-**E7** compound*

The (+)-**E7** compound does not show activity at time zero (% of enzyme inhibition below 10%) at the two 10 and 20 uM; after one hour of incubation with hTS, (+)-**E7** is able to inhibit the enzyme activity at the 34% and 39% at 10 and 20uM respectively with respect to the non-inhibited enzyme. (-)-**E7** enantiomer shows the same potency of (+)-**E7** compound at time zero (30%-48% at 10-20uM) and, after 1 hour, it doubles the efficacy to 51 and 67% at the same assayed concentrations. Regarding racemic **E7**, the compound results to be active just at time zero (26% and 40%, 10-20uM) and it also maintains unaltered the efficacy after 1 hour of incubation (25%-52%, 10-20uM). We did not analyze the data further at this stage.

66

67 **Racemization rate constants of (+)-E7 and (-)-E7 determined in buffer solutions.**

68 Time intervals for enantiomerization kinetics analysis: 0', 10', 20', 30', 40' and 50'. T = 37.5 °C.

| | (+)-E7 | (-)-E7 |
|-----------------------------|--------------------------------|--------------------------------|
| $k \text{ (s}^{-1}\text{)}$ | $2.03 \pm 0.18 \times 10^{-4}$ | $2.10 \pm 0.16 \times 10^{-4}$ |
| $t_{1/2} \text{ (min)}$ | 56.80 | 54.98 |

69

70

71

72

73

74

75

76

77

78

79

80

81

82

83

84

85

86

87

88

89

90

91

92

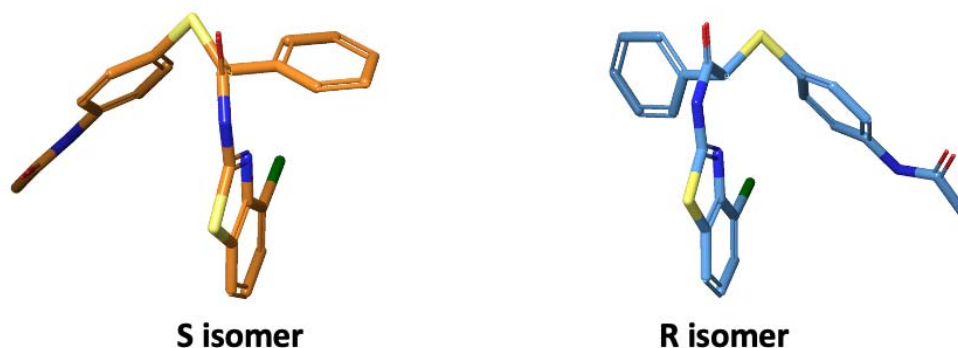
93

94

95

96

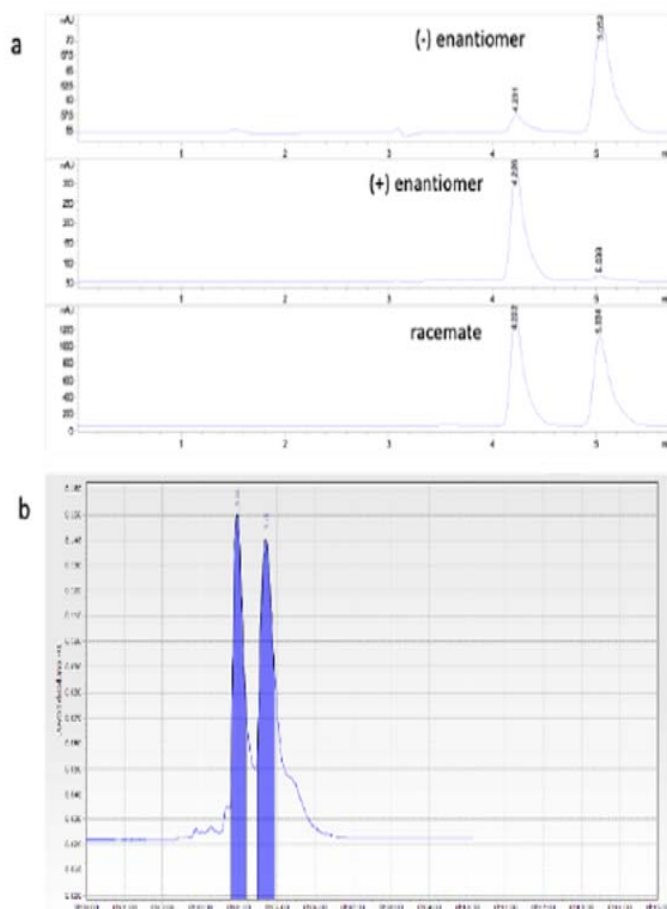
Enantioseparation of E7



Appendix 3-figure 1. Structure 2D of the E7 enantiomers.

A. Representation of S and R isomers of compound **E7** obtained with B, Structural modification of compound **B12**. The changes in chemical structure and the associated IC₅₀s for recombinant-enzyme inhibition, DFFRET, abilities to dissociate the hTS dimers in cells, cellular growth inhibition and in vivo data of the key compounds **C3**, **E5** and **E7** of the sub-series are reported.

Chromatograms of single (+/-)-E7 enantiomers.



Appendix 3-figure 2. Chromatograms of single (+/-)-E7 enantiomers. Column: Chiracel OD(250x4.6mm I.D., 5mm), mobile phase: water:acetonitrile 2:98 (v/v), flow rate:1mL/min; λ =254 nm. B Semipreparative enantioseparation of (+/-)-E7. Column: Chirasphere OD, mobile phase water:acetonitrile 2:98 (v/v), flow rate:5mL/min, λ :254nm, room temperature.

140
141
142
143
144
145
146

Appendix 4

Analysis of combined equilibria and fitting to FRET data. With the aim of extracting quantitative mechanistic data from the dose dependencies of the Φ_{FRET} data, we have written and solved the equilibrium scheme in Fig. 4C of the main text. E_T is the total concentration of enzyme dimers:

$$E_T = \frac{K'_D K''_I}{2K''_D [I]} [MI] + \frac{K''_I}{K''_D [I]} [MI]^2 + \frac{[MI]}{2} + \frac{K'_D{}^2 K''_I{}^2 [MI]^2}{K_D K''_D{}^2 [I]^2} + \frac{[MI]^2}{K''_D}$$

where M represents an enzyme monomer and I an inhibitor molecule. Φ , the FRET efficiency, is near one for M_2 ; if we assume the same for M_2I and M_2I_2 , i.e., that binding of the inhibitor does not cause a structural change able to significantly reduce the efficiency of FRET, then the observed efficiency, Φ_{FRET} , will coincide with the total fraction of dimeric protein:

$$\Phi_{\text{FRET}} = \frac{[M_2] + [M_2I] + [M_2I_2]}{E_T} = \frac{[E_T] - \frac{1}{2}([M] + [MI])}{E_T} = 1 - \frac{([M] + [MI])}{2[E_T]}$$

Our goal is to express $[M]$ and $[MI]$ in terms of E_T , I_T (the total inhibitor concentration) and the pertinent equilibrium constants.

$$[I_T] = [I] + [MI] + [M_2I] + 2[M_2I_2]$$

$$K_D = \frac{[M]^2}{[M_2]} \quad K'_D = \frac{[M][MI]}{[M_2I]} \quad K''_D = \frac{[MI]^2}{[M_2I_2]} \quad K_I = \frac{[I][M]}{[MI]} \quad K'_I = \frac{[I][M_2]}{[M_2I]} \quad K''_I = \frac{[I][M_2I]}{[M_2I_2]}$$

Because $I_T \gg E_T$, we simplify $[I] \approx I_T$, and rewrite:

$$\Phi_{\text{FRET}} = 1 - \frac{([M] + [MI])}{2E_T} = 1 - \frac{1}{2E_T} \left(\frac{K_i}{[I]} + 1 \right) [MI] = 1 - \frac{1}{2E_T} \left(\frac{K_i}{I_T} + 1 \right) [MI]$$

[MI] is calculated from the positive root of the quadratic equation obtained by expressing each term contributing to E_T in terms of [MI], [I] and the K s, and replacing $[I] \approx I_T$:

$$E_T = \frac{K'_D K''_I}{2K''_D [I]} [MI] + \frac{K''_I}{K''_D [I]} [MI]^2 + \frac{[MI]}{2} + \frac{K'_D{}^2 K''_I{}^2 [MI]^2}{K_D K''_D{}^2 [I]^2} + \frac{[MI]^2}{K''_D}$$

$$\left(\frac{1}{K''_D} + \frac{K''_I}{K''_D I_T} + \frac{K'_D{}^2 K''_I{}^2}{K_D K''_D{}^2} \frac{1}{I_T^2} \right) [MI]^2 + \left(\frac{1}{2} + \frac{K'_D K''_I}{2 K''_D I_T} \right) [MI] - E_T = a[MI]^2 + 2b[MI] - E_T = 0$$

$$(S3) \quad \phi_{FRET} = 1 - \frac{1}{2E_T} \left(\frac{K_i}{I_T} + 1 \right) \left(\frac{-b \pm \sqrt{b^2 + aE_T}}{a} \right)$$

The dependence of the observed ϕ_{FRET} on I_T for the three inhibitors was fitted to eq. S3 (Fig. 4B in the main text). To narrow the amount of fitting parameters, K_D was kept fixed at the value obtained from FRET measurements without inhibitors (6×10^{-8} M) and K'_D was estimated by assuming that the effect of each inhibitor molecule on the standard free energy for the enzyme dimer dissociation was constant: $\Delta G^{\circ\circ}_D = (\Delta G^{\circ}_D + \Delta G^{\circ\circ}_D)/2$. From the above value of K_D and the K''_D obtained from the limit values of ϕ_{obs} at high [C3], $K''_D = 3.3 \times 10^{-7}$ M (paragraph Mechanistic analysis of dissociative inhibition, main text), we estimated $K'_D = 1.5 \times 10^{-7}$ M and used this value in the fitting procedure. K''_D values were obtained from the high I_T behavior of ϕ_{obs} , while K_I and K''_I were adjusted to fit the low and intermediate I_T data.

Analysis of a dissociative inhibition mechanism and fitting to data. Here, to test the suitability of the proposed mechanism to fit the experimental inhibition results, rather than searching for linear plots, we aim at expressing the dependence of the observed reaction rate on the total substrate concentration, S_T , at different total inhibitor, I_T , and total enzyme, E_T , concentrations.

$$v = k[M_2][S] + k' [M_2I][S] + k'' [M_2I_2][S] = k \frac{[M_2][S]}{K_1} + k' \frac{[M_2I][S]}{K_2} + k'' \frac{[M_2I_2][S]}{K_3} =$$

$$= k \frac{[M_2][S]}{K_1} + k' \frac{[M_2][I][S]}{K_2K'_I} + k'' \frac{[M_2][I]^2[S]}{K_3K'_IK''_I}$$

So, $v = [M_2][S]D$ with

$$D = \left(\frac{k}{K_1} + \frac{k'[I]}{K_2K'_I} + \frac{k''[I]^2}{K_3K'_IK''_I} \right)$$

We now express E_T in terms of v , $[I]$ and $[S]$:

$$E_T = \frac{[M]}{2} + \frac{[MI]}{2} + [M_2] + [M_2I] + [M_2I_2] + [M_2S] + [M_2IS] + [M_2I_2S] =$$

$$= \frac{1}{2} (K_D[M_2])^{1/2} \left(1 + \frac{[I]}{K_I} \right) + [M_2] \left(1 + \frac{[I]}{K'_I} + \frac{[I]^2}{K'_IK''_I} \right) + [M_2][S] \left(\frac{1}{K_1} + \frac{[I]}{K_2K'_I} + \frac{[I]^2}{K_3K'_IK''_I} \right)$$

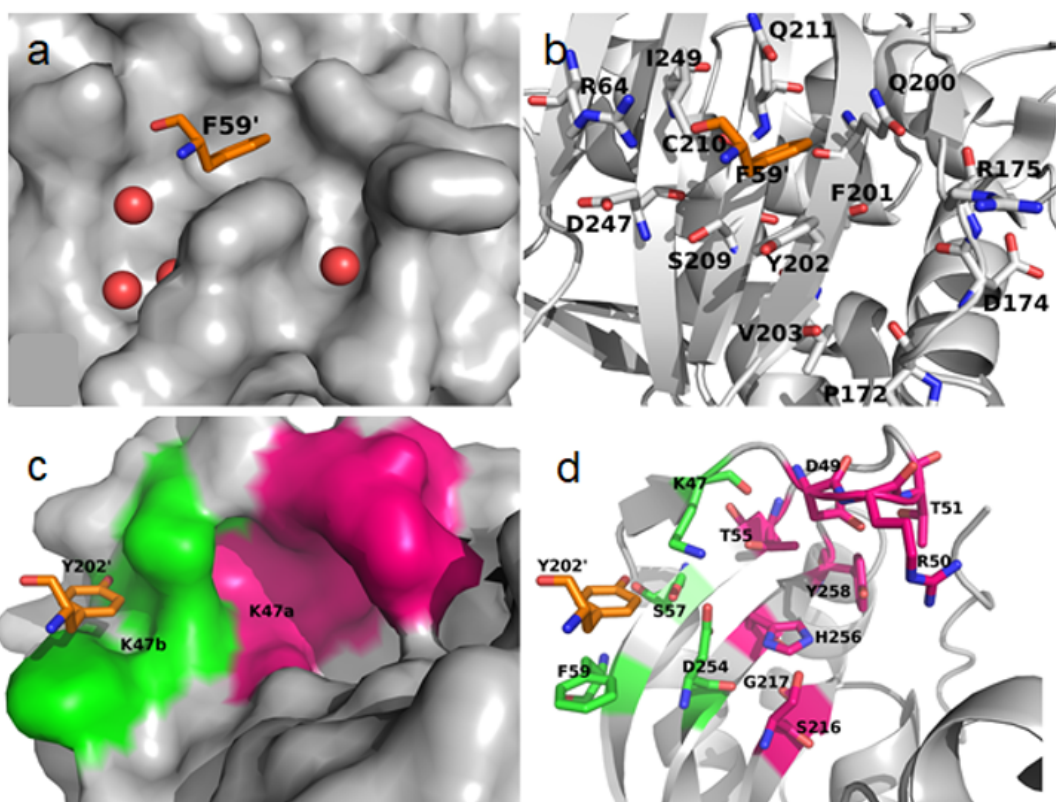
Because $S_T, I_T \gg E_T$, we approximate $[S] = S_T$ and $[I] = I_T$. Calling 2a, b and c the coefficients that multiply $[M_2]^{1/2}$, $[M_2]$ and $[M_2][S]$ in the three terms and writing $x = [M_2]^{1/2}$, we obtain the second-degree equation:

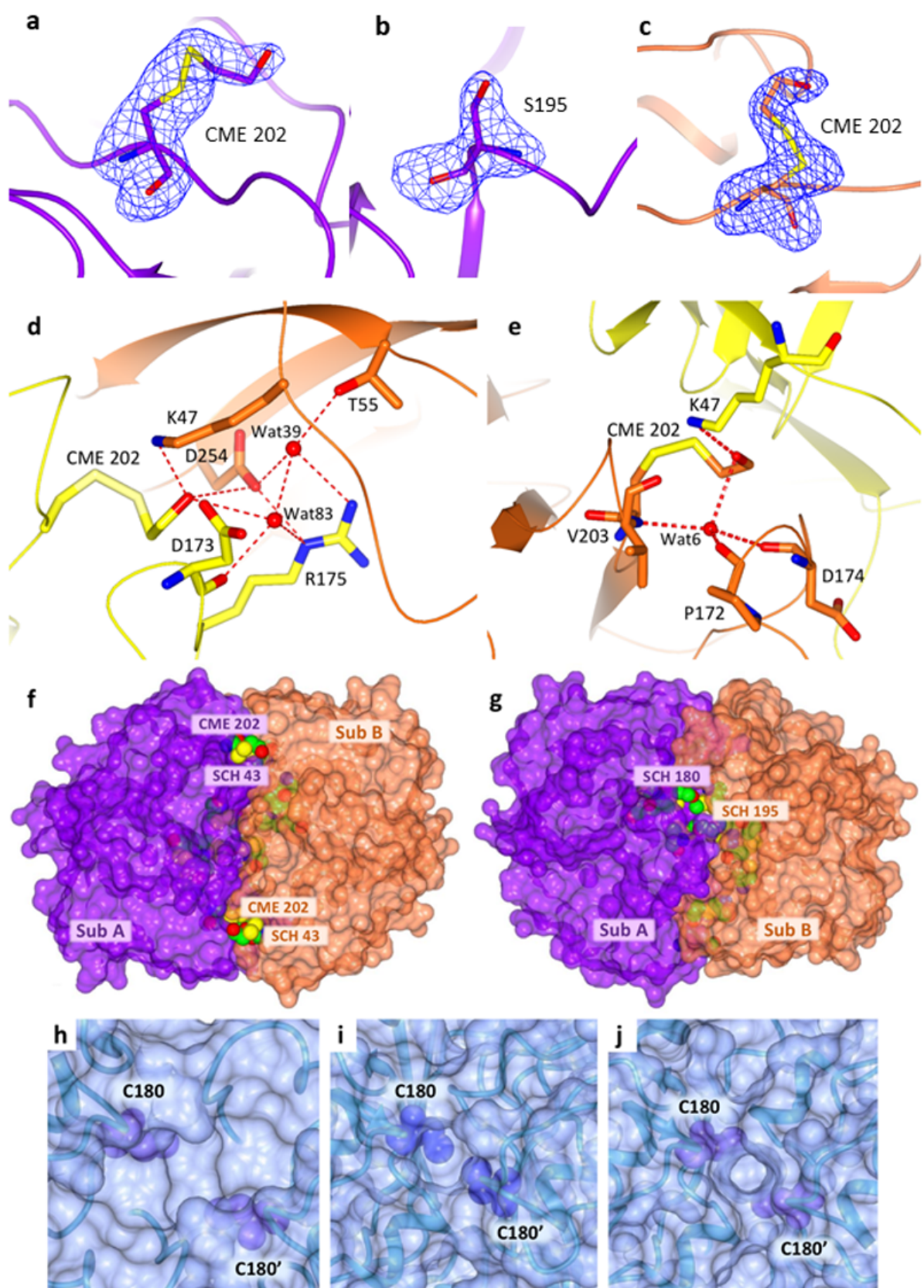
$$(b + cS_T)x^2 + 2ax - E_T = 0$$

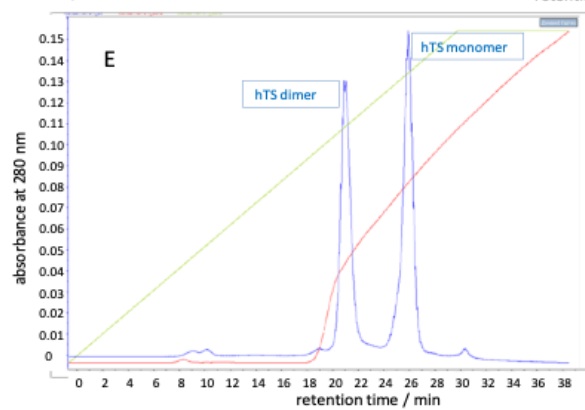
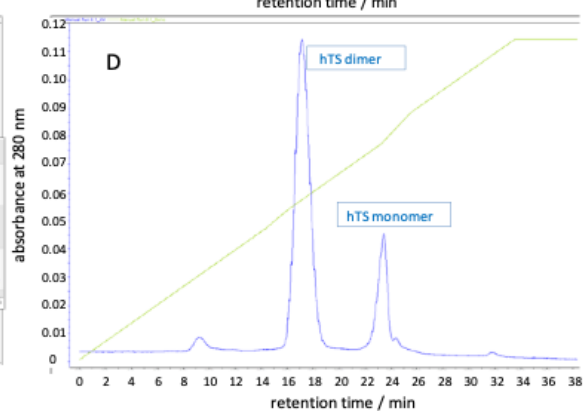
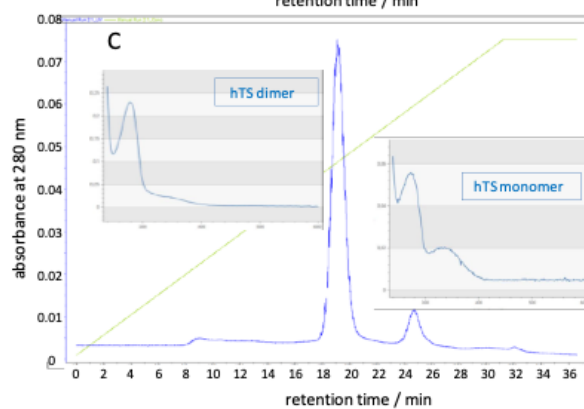
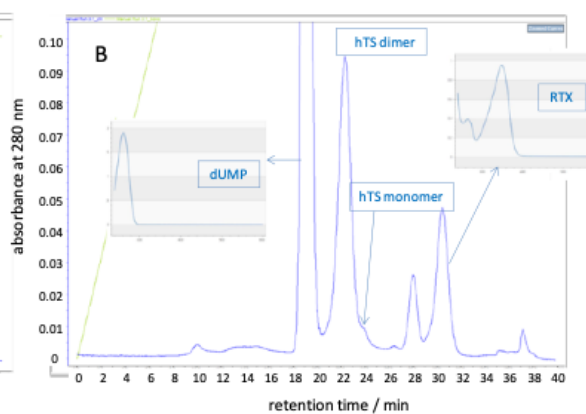
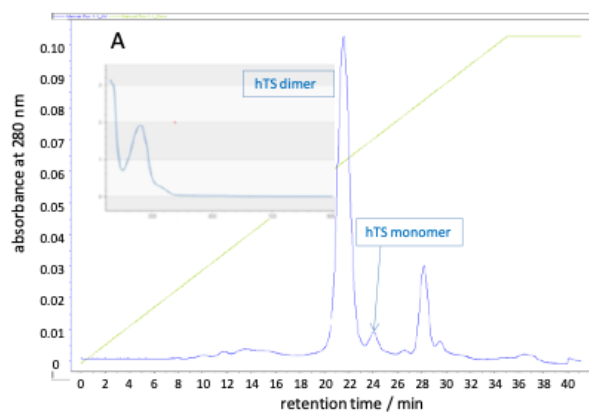
whose positive root, x_r , yields the desired value of v : $v = x_r^2 S_T D$.

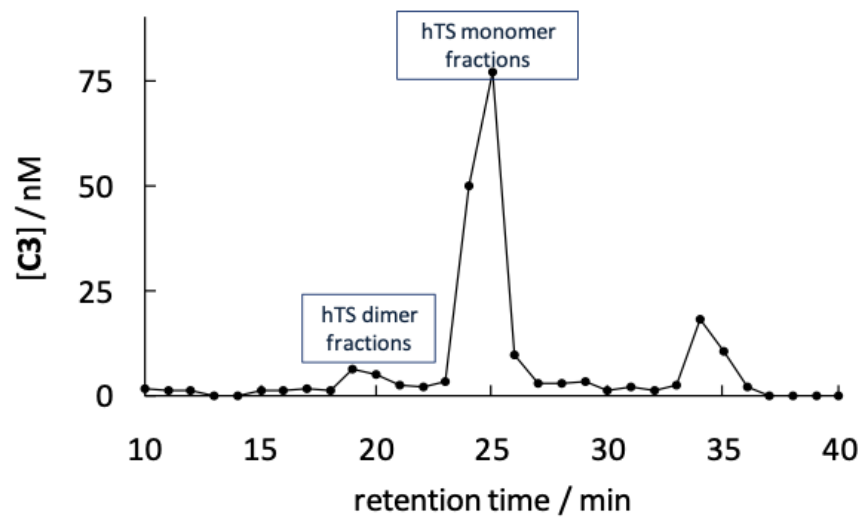
So, given the experimental values of E_T , S_T and I_T , we can calculate v using the equilibrium and rate constants in the scheme in Fig. 4C of the main text. In the fitting analysis, we kept K_D fixed at 6×10^{-8} M, as obtained from dilution experiments in the absence of inhibitors. We also kept the equilibrium constant for the binding of mTHF to hTS saturated with dUMP, K_I , fixed to the value obtained in the absence of inhibitors, 10^{-5} M. Also, K_I was taken equal to 10^{-6} M for the

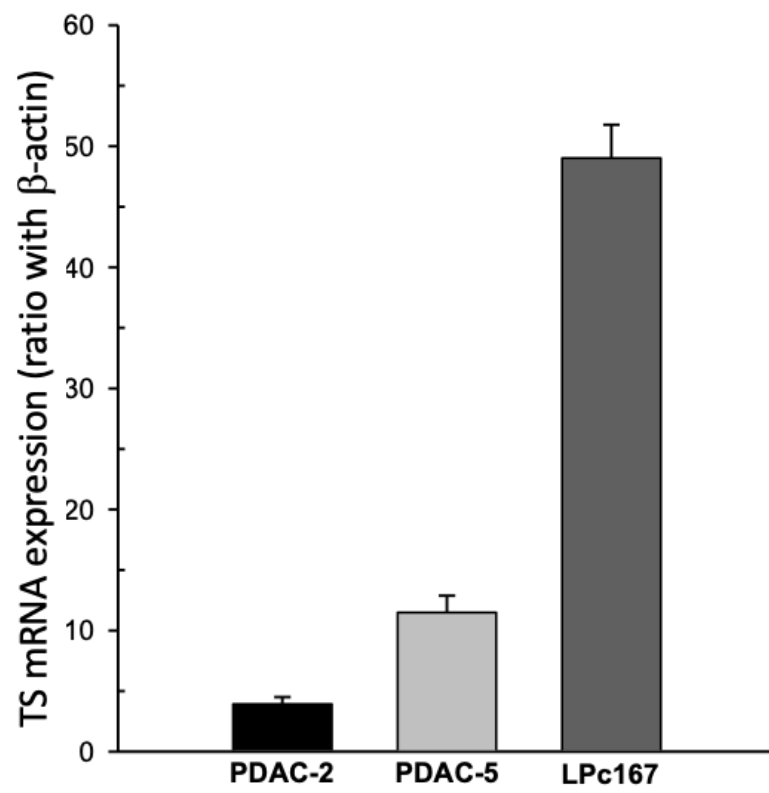
three inhibitors from the results of the fitting of FRET data. The other equilibrium constants were explored subject to the conditions imposed by the combined equilibria in Fig. 4C of the main text, i.e.: $K_D/K_I = K'_D/K'_I$ and $K'_D/K_I = K''_D/K''_I$. So, K'_I and K''_I were kept one order of magnitude larger than K_I , i.e., 10^{-5} M. Finally, the catalytic rate constant, k , was fixed at its value with no inhibitor, 0.9 s^{-1} ; k' and k'' were variable fitting parameters.

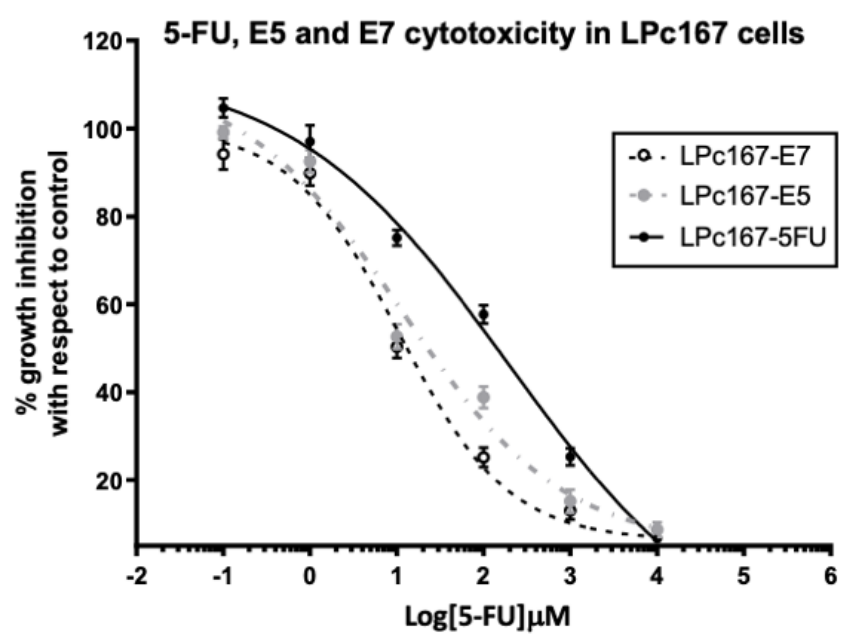


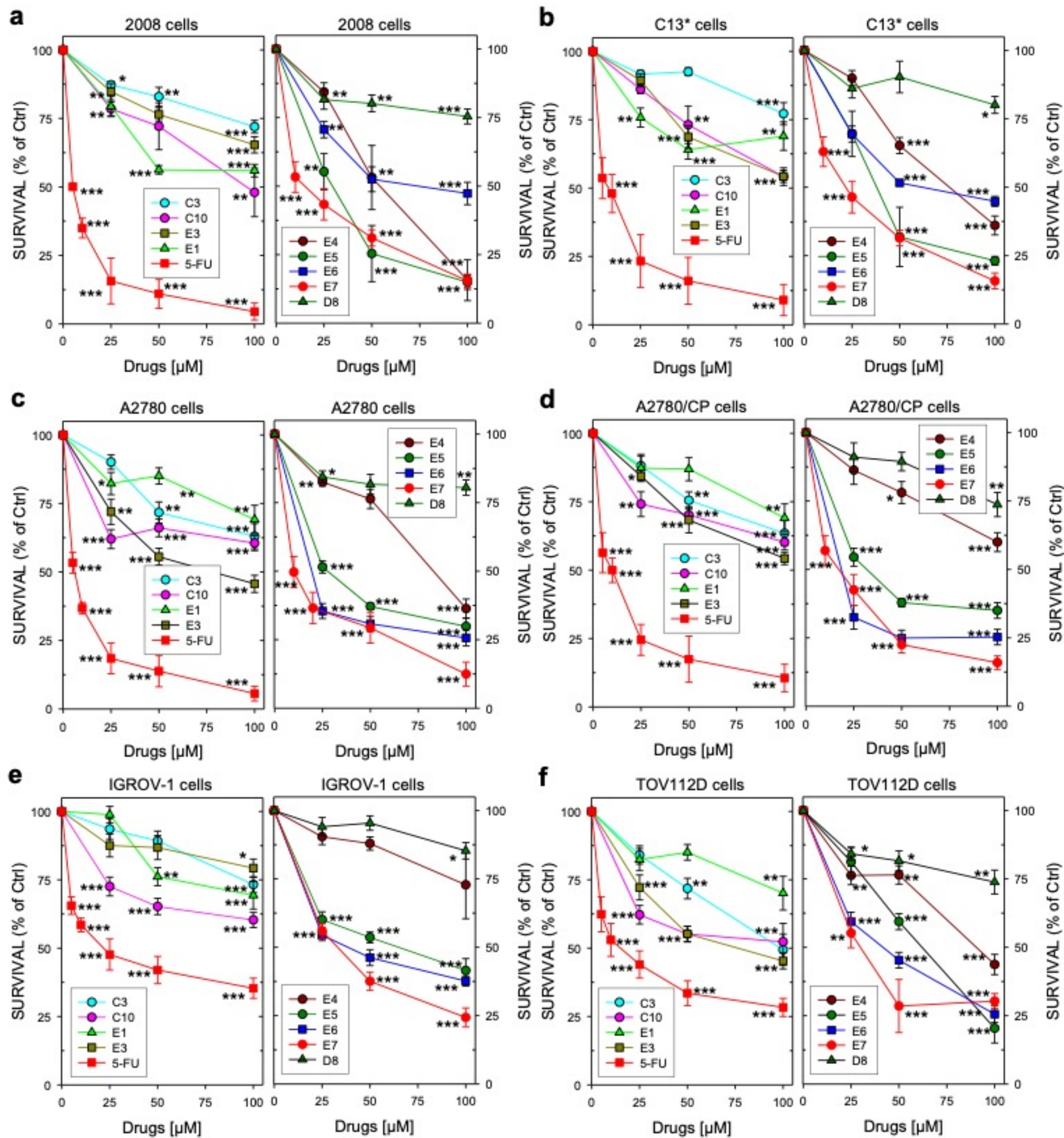




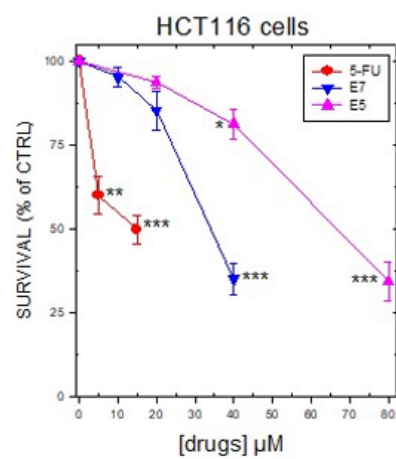




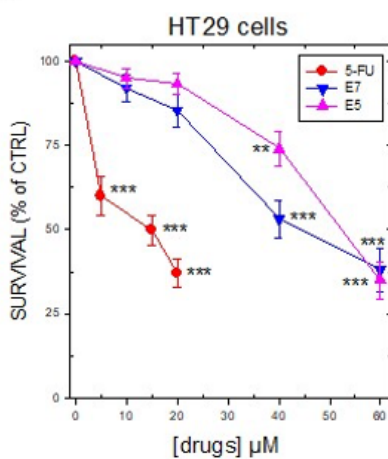




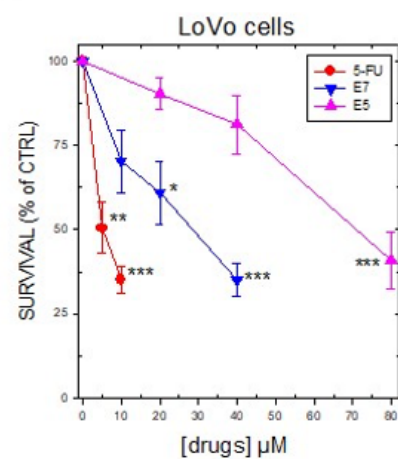
a

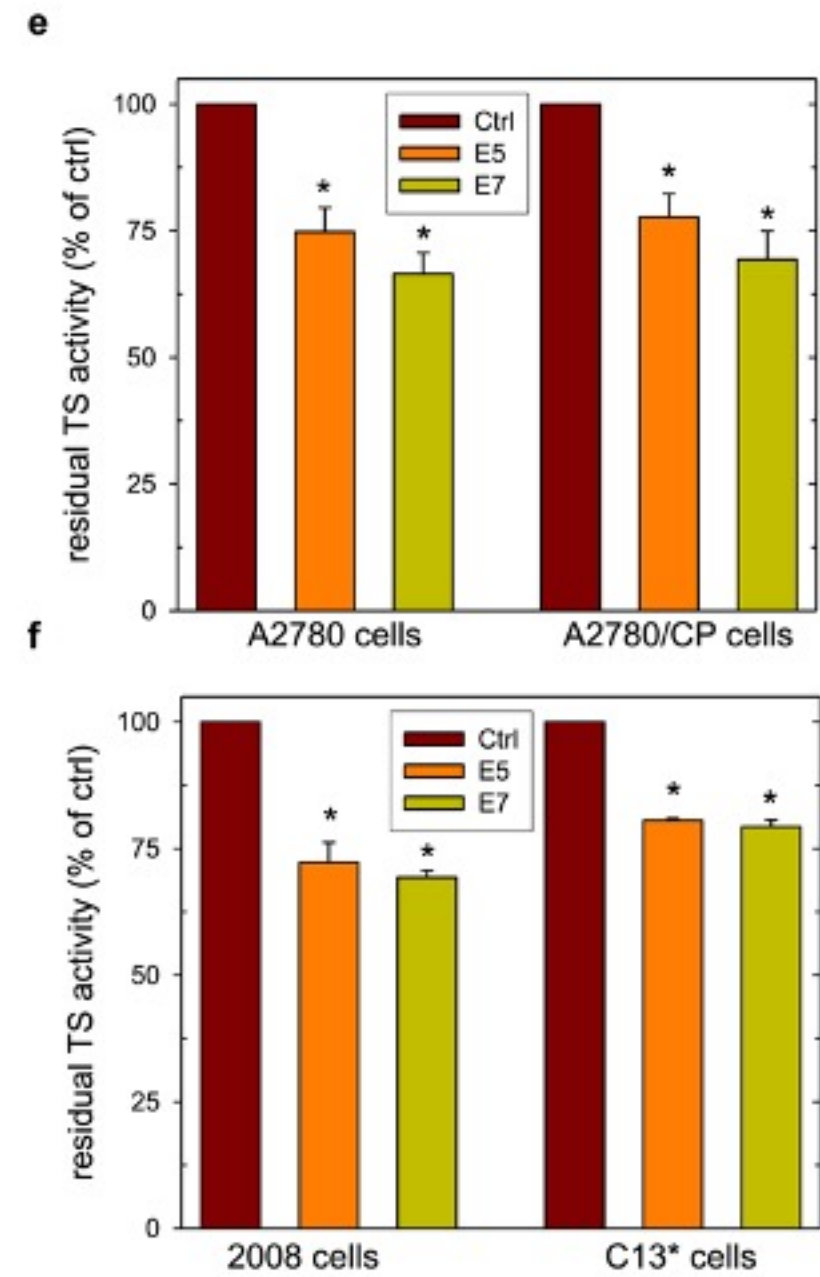
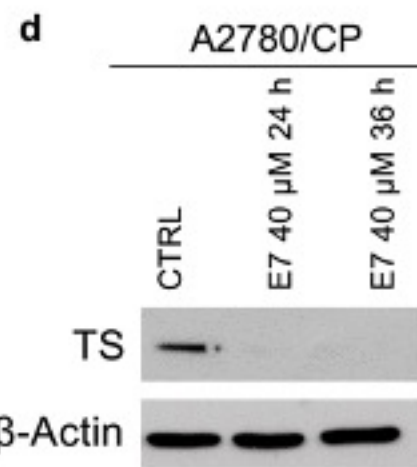
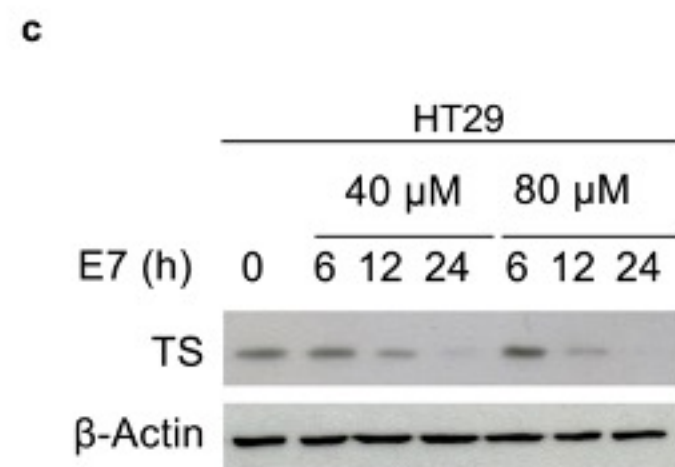
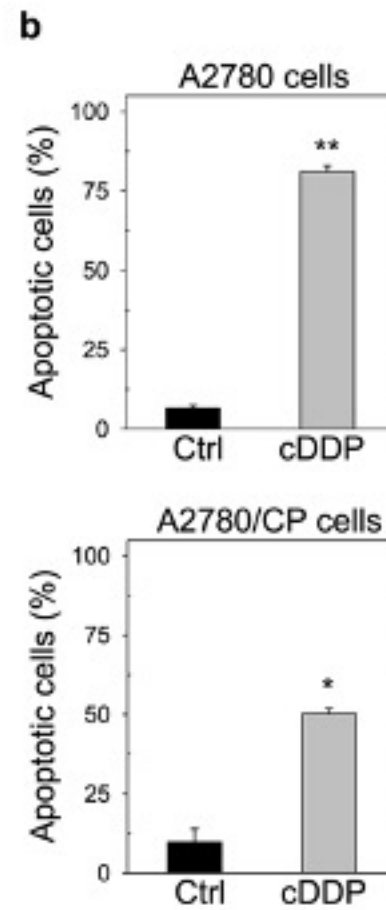
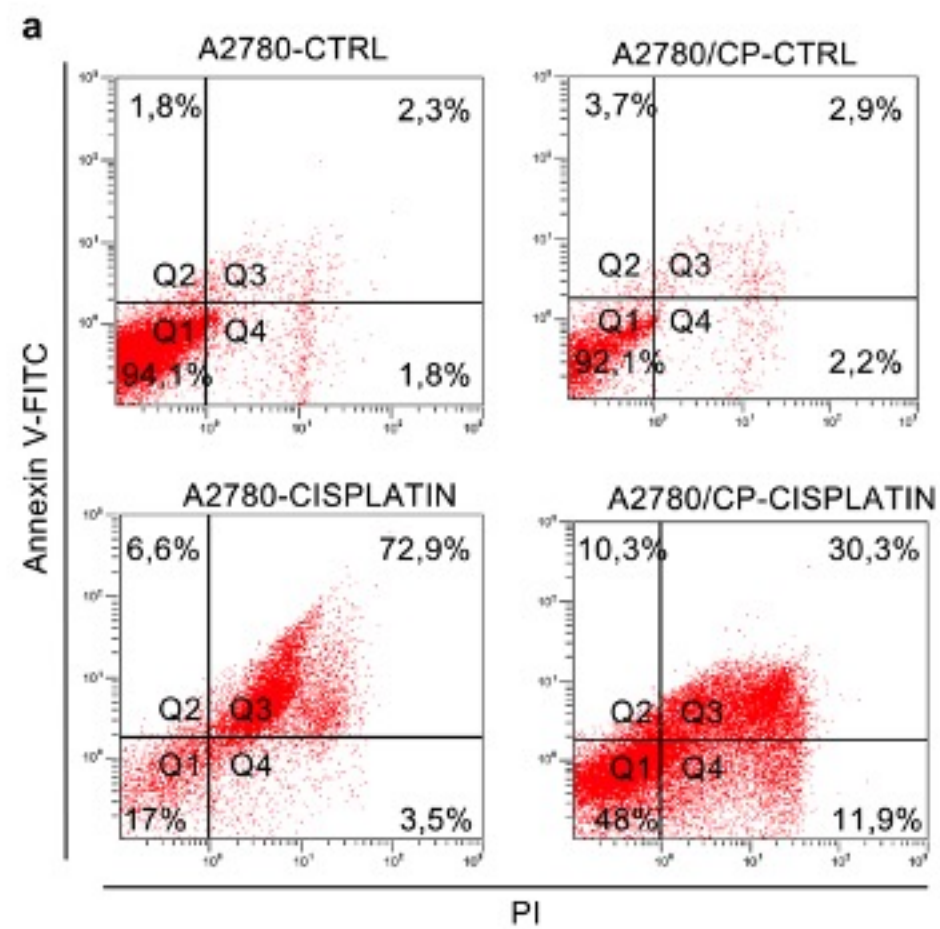


b

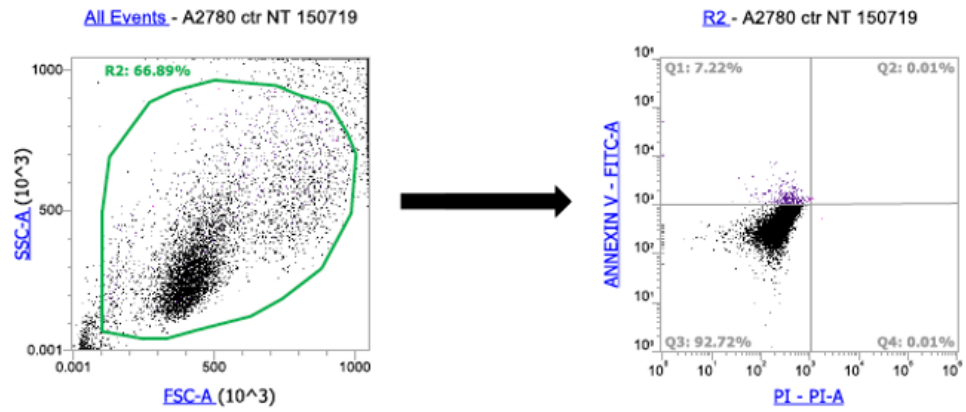


c





a



b

